DISS. ETH NO. 17168

The Formation of Excess Air in Groundwater Studied Using Noble Gases as Conservative Tracers in Laboratory and Field Experiments

A dissertation submitted to
ETH ZURICH

for the degree of
DOCTOR OF SCIENCES

presented by
STEPHAN RÜDIGER KLUMP
Dipl.-Geol., Clausthal University of Technology (Germany)
born March 17, 1977
citizen of Germany

accepted on the recommendation of
Prof. Dr. Dieter M. Imboden, examiner
Prof. Dr. Wolfgang Kinzelbach, co-examiner
Dr. Rolf Kipfer, co-examiner

2007

Chapter 4 has been published as:
Klump, S., Tomonaga, Y., Kienzler, P., Kinzelbach, W., Baumann, T., Imboden, D. M., and Kipfer, R. (2007). Field experiments yield new insights into gas exchange and excess air formation in natural porous media. *Geochim. Cosmochim. Acta.*, 71(6): 1385-1397.

Chapter 5 (5.2-5.3) has been published as:
Klump, S., Brennwald, M. S., and Kipfer, R. (2006). Comment on "Noble gases and stable isotopes in a shallow aquifer in southern Michigan: Implications for noble gas paleotemperature reconstructions for cool climates" by Chris M. Hall et al. *Geophys. Res. Lett.*, 33: L24403.

Chapter 7, except for section 7.2.5, has been published as:
Klump, S., Kipfer, R., Cirpka, O. A., Harvey, C. F., Brennwald, M. S., Ashfaque, K. N., Badruzzaman, A. B. M., Hug, S. J., and Imboden, D. M. (2006). Groundwater dynamics and arsenic mobilization in Bangladesh assessed using noble gases and tritium. *Environ. Sci. Technol.*, 40(1): 243-250.

Acknowledgments

I would like to express my gratitude to the referees of my dissertation: *Dieter Imboden*, *Wolfgang Kinzelbach*, and *Rolf Kipfer*. I have always appreciated my fruitful and pleasant discussions with Dieter Imboden, and his helpful, sound and critical reviews helped to improve my thesis considerably. I thank Wolfgang Kinzelbach for consenting to be co-referee on my thesis and for valuable discussions.

Very special thanks are due to my supervisor Rolf Kipfer, alias *RoKi*, who gave me the opportunity to work in Eawag's exciting and inspiring environment. I have always been impressed by his infectious enthusiasm for science, his unconventional ways of thinking, and his motivating and supportive character. Working with RoKi was a great professional and personal experience!

For the pleasant working atmosphere I would like to thank the members of the Eawag W+T department, and in particular my colleagues in the Environmental Isotopes Group: *Matthias Brennwald*, *Christian Holzner*, *Helena Amaral*, *Yama Tomonaga*, *Edi Hoehn*, *Thomas Jankowski*, *Yvonne Scheidegger*, and *Markus Hofer*. I especially thank *David Livingstone* who always did a great job in checking and correcting the English of my various drafts.

My thanks also go to those who collaborated with us in our joint SNF research project "Models and tracer methods for groundwater resource management": *Amsicora Onnis*, *Fritz Stauffer*, *Harrie-Jan Hendricks Franssen*, *Roland Purtschert*, and *Rolf Althaus*, who was a great friend and colleague during numerous sampling campaigns.

I am grateful to *Olaf Cirpka* for his unflagging and spontaneous help with all sorts of modeling and Matlab problems. His exhaustive knowledge of and enthusiastic devotion to numerics and equations is impressive (and frightening – at least from a geologist's point of view). *Frank Peeters* helped with some modifications of the KBD model.

Stephan Hug, *Michael Berg*, and *Olivier Leupin* (who was a great help in surviving Dhaka, especially its traffic) gave me the opportunity to work with them on their exciting projects on arsenic-contaminated groundwater in Bangladesh and Vietnam, which I very much enjoyed!

I would also like to thank *Thomas Baumann* and his group for giving me access to the "Münchner Loch", for their support during my field work, and of course, for the tasty Weißwurst lunch.

I thank *Heinz Surbeck* for providing the TDGP probes, and for many fruitful dis-

cussions. I have always enjoyed going to Neuchâtel.

Peter Kienzler made it possible to take part in his sprinkling experiment in Grüningen by providing a well-equipped field site – a necessary prerequisite for a successful experiment.

I am thankful to *Tim Grundl* for initiating the Wisconsin project and for all the interesting and pleasurable discussions.

Thanks are also due to the noble-gas group at ETH Zurich. I thank *Heiri Baur* and the workshop staff for their great work in keeping our noble-gas mass spectrometers running. I also thank my lab mates *Ansgar Grimberg*, *Philipp Heck*, and *Stefan Strasky* for making the long days in the lab a bit more pleasant.

For the financial support of this thesis, I want to thank the Swiss National Science Foundation.

Last but not least, I would like to thank *my family* for their never-ending support and care, and *my friends* just for being there.

Contents

Seite Leer /
Blank leaf

Abstract

The concentrations of atmospheric noble gases dissolved in groundwater mostly exceed their respective atmospheric equilibrium concentrations. In groundwater hydrology, this well-known phenomenon is usually referred to as the "excess air" phenomenon. The presence of excess air crucially affects the quantitative interpretation of environmental tracer concentrations in terms of paleo-environmental conditions and groundwater residence time, because a reliable determination of the atmospheric equilibrium component is required in such cases. In addition, excess air itself is potentially a tracer for paleo-recharge conditions. This represents an opportunity in the field of environmental tracer hydrology which has not yet been fully exploited.

The formation of excess air as a result of the dissolution of entrapped air within the quasi-saturated zone is still not thoroughly understood. Although knowledge of the physical processes governing the formation of excess air has been greatly enhanced during recent years, verification of the underlying conceptual ideas in natural systems is still lacking. In the work described here, both laboratory and field experiments were conducted in conjunction with numerical simulations, with the aim of obtaining a better understanding of the role of kinetic effects and flow direction in the dissolution of entrapped air. In addition, the conceptual ideas developed within the context of laboratory experiments and numerical investigations were upscaled and verified by field experiments.

A sand-column experiment, in combination with numerical simulations, indicates that kinetic effects on the dissolution of entrapped air in quasi-saturated porous media are negligible for the small water flow velocities usually found in natural systems. Only for large flow velocities are kinetic effects of significant importance. The assumption of local equilibrium between the water and entrapped gas phases is not valid in such a case. However, the flow direction (horizontal, vertically downward or vertically upward) crucially affects the bubble-mediated gas transfer, because the hydrostatic pressure gradient in the direction of the flow depends on flow direction.

Furthermore, laboratory experiments showed that apparently unfractionated excess air can be produced in the presence of a progressively dissolving entrapped gas phase. This finding contradicts the original conceptual idea of the formation of unfractionated excess air as being the result of complete bubble dissolution, and opens up new vistas for the interpretation of the presence of such apparently unfractionated excess air.

Field experiments confirmed that excess air results from the dissolution of en-

trapped air during infiltration. However, the experiments also suggest a strong dependence on soil properties, such as grain-size and pore-size distributions and hydraulic conductivity. Infiltration into a fine-grained sediment produced significant amounts of excess air in the seepage water, whereas infiltration into very coarse and highly conductive gravels did not. Moreover, the depth profile of the noble gas temperature – i.e., the temperature calculated from the noble gas concentrations in the seepage water – was identical to that of the soil temperature. This indicates that the infiltrating water was in equilibrium with the ambient soil air under atmospheric pressure, and that noble gas temperatures do indeed record the soil temperature during infiltration, an assumption which is implicitly made when noble gases are used as a proxy for paleotemperature at the time of recharge. Based on these results, explanations were found for a noble gas data set from an aquifer in Michigan in which the noble gas temperatures are consistently lower than the mean annual soil temperature. Because noble gases record the temperature at the time of recharge, the noble gas temperature can indeed be lower than the mean annual soil temperature if the unsaturated zone is shallow and recharge occurs predominantly during the cold season. Both of these seem to be the case in Michigan.

Since the amount and fractionation of excess air reflect the environmental conditions prevailing during groundwater recharge, they can, in principal, be used as a proxy for paleo-recharge conditions. Excess air amounts and their fractionation in Pleistocene groundwater from a deep aquifer in Wisconsin indicate the occurrence of changes in recharge conditions shortly before and at the beginning of the last glacial period, leading to an increase in the amount of excess air during this time period.

To summarize, the results presented in this thesis yield new insights into gas exchange in quasi-saturated porous media on very different scales. Based on the findings from well-controlled, small-scale laboratory experiments and numerical investigations, the conceptual model of the formation of excess air could be transferred to field experiments which confirmed the validity of this conceptual model in natural systems. Moreover, excess air in (paleo-)groundwater proved to be a promising tracer for past hydrological conditions, thus opening up an interesting field for future work.

Kurzfassung

Die Konzentrationen gelöster atmosphärischer Gase im Grundwasser übertreffen meistens die entsprechenden atmosphärischen Gleichgewichtskonzentrationen. Diese Luftüberschüsse werden in der Grundwasserhydrologie als "Excess Air" bezeichnet. Die Luftüberschüsse erschweren die quantitative Interpretation von Umwelttracerdaten hinsichtlich der Paläo-Umweltbedingungen und der Aufenthaltszeit des Grundwassers, da diese Anwendungen die zuverlässige Bestimmung der atmosphärischen Gleichgewichtskomponente an der Gesamtkonzentration der Gase voraussetzen. Ausserdem stellen die Luftüberschüsse selbst einen potenziellen Tracer für die Bedingungen während der Grundwasserneubildung dar – eine Möglichkeit, die in der Tracerhydrologie bis heute erst wenig Anwendung fand.

Die Entstehung der Luftüberschüsse als Folge der Auflösung von eingeschlossenen Luftblasen in der quasigesättigten Zone ist bis heute noch nicht vollständig verstanden. Obwohl das Verständnis der physikalischen Prozesse, die die Bildung der Luftüberschüsse kontrollieren, in den letzten Jahren deutlich erweitert werden konnte, fehlt die Übertragung der Konzepte auf natürliche Systeme. In der vorliegenden Arbeit wurden sowohl Labor- und Feldexperimente, als auch numerische Simulationen mit dem Ziel durchgeführt, die Relevanz kinetischer Effekte und den Einfluss der Fliessrichtung auf die Auflösung eingeschlossener Gasblasen zu untersuchen. Ausserdem wurden die konzeptuellen Modelle, die im Zusammenhang mit Laborexperimenten entwickelt wurden, in Feldexperimenten überprüft und verifiziert.

Ein Sandsäulenexperiment hat in Kombination mit numerischen Simulationen gezeigt, dass kinetische Effekte bei der Auflösung eingeschlossener Gasblasen in der quasigesättigten Zone bei kleinen Strömungsgeschwindigkeiten, die typisch sind für natürliche Systeme, vernachlässigbar sind. Nur für sehr hohe Strömungsgeschwindigkeiten sind kinetische Effekte von signifikanter Bedeutung und die Annahme von lokalem Lösungsgleichgewicht ist in solchen Fällen nicht zulässig. Hingegen beeinflusst die Richtung der Strömung, d.h. horizontal, vertikal abwärts oder vertikal aufwärts, die Gasblasenauflösung deutlich, weil der Gradient des hydrostatischen Druckes unterschiedlich ist für verschiedene Strömungsrichtungen.

Darüber hinaus zeigten die Laborexperimente, dass scheinbar unfraktionierte Luftüberschüsse trotz Anwesenheit einer sich auflösenden Gasphase gebildet werden. Diese Beobachtung widerspricht der ursprünglichen Erklärung für die Entstehung von unfraktionierten Luftüberschüssen durch die vollständige Auflösung eingeschlossener Luftblasen. Damit eröffnen sich neue Möglichkeiten zur Interpretation scheinbar un-

fraktionierter Luftüberschüsse.

Die Ergebnisse der durchgeführten Feldexperimente bestätigen das konzeptuelle Modell zur Entstehung der Luftüberschüsse durch die Auflösung von eingeschlossenen Luftblasen während der Infiltration. Die Experimente zeigen eine starke Abhängigkeit der Bildung der Luftüberschüsse von Bodeneigenschaften, wie der Korn- und Porengrössenverteilung und der Durchlässigkeit. Während die Infiltration in einen feinkörnigen Boden zur Produktion von Luftüberschüssen im Wasser führte, wurden bei der Infiltration in grobkörnige, gut durchlässige Sedimente keine Luftüberschüsse gebildet.

Das Tiefenprofil der Edelgastemperatur, d.h. der Temperatur, die aus den im Sickerwasser gemessenen Edelgaskonzentrationen berechnet wurde, stimmt sehr gut mit dem Profil der Bodentemperatur überein. Das deutet darauf hin, dass das Wasser im Lösungsgleichgewicht mit der umgebenden Bodenluft unter Atmosphärendruck war und die Edelgastemperatur tatsächlich die Bodentemperatur während der Infiltration wiedergibt – eine Annahme, die bei der Verwendung von Edelgasen als Indikator für Paläotemperaturen implizit gemacht wird. Basierend auf diesen Ergebnissen konnten neue Erklärungen für einen Edelgasdatensatz aus einem Grundwasserleiter in Michigan gefunden werden, in dem die Edelgastemperaturen durchweg niedriger sind, als die mittlere Jahresbodentemperatur. Da Edelgase die Bodentemperatur zum Zeitpunkt der Neubildung repräsentieren, kann die Edelgastemperatur tatsächlich niedriger sein als die mittlere Jahresbodentemperatur, falls die ungesättigte Zone geringmächtig ist und die Grundwasserneubildung vorwiegend während der kalten Jahreszeit stattfindet. Beide Voraussetzungen scheinen in Michigan erfüllt zu sein.

Da die Bildung der Luftüberschüsse von den Umweltbedingungen während der Infiltration abhängt, können sie im Prinzip selbst als Proxy für die Bedingungen während der Grundwasserneubildung verwendet werden. Luftüberschüsse in pleistozänem Grundwasser aus einem tiefen Grundwasserleiter in Wisconsin zeigen Änderungen in der Grundwasserneubildung, die zu einem Anstieg der Luftüberschüsse kurz vor und zu Beginn der letzten Vereisungsphase führten.

Die Resultate der vorliegenden Arbeit gewähren neue Einblicke in den Gasaustausch in quasigesättigten porösen Medien auf sehr unterschiedlichen Grössenskalen. Aufbauend auf den Erkenntnissen aus Laborversuchen, durchgeführt unter gut kontrollierbaren Bedingungen, und numerischen Untersuchungen liefern die Feldexperimente Informationen über die Entstehung von Luftüberschüssen in natürlichen Systemen. Weiterhin stellte sich der Luftüberschuss als viel versprechender Tracer für paläohydrologische Verhältnisse heraus und es eröffnet sich somit ein interessantes Feld für künftige Arbeiten.

Part I

Introduction and theoretical background

Chapter 1

Introduction

1.1 Atmospheric gas partitioning and excess air formation

Atmospheric gases dissolved in groundwater are mostly found to be supersaturated with respect to atmospheric solubility equilibrium. Since more than 50 years, this so-called excess air has been a known phenomenon in almost all groundwater systems. Oana (1957) first reported Ar supersaturation in groundwater samples from Japan. The term "excess air" was introduced by Heaton and Vogel (1981) because the composition of the excess air component is often similar to that of atmospheric air. However, many groundwater samples show excess air which is fractionated with respect to atmospheric air – a fact that is very important regarding the interpretation of gaseous environmental tracer concentrations.

Although excess air is a common feature of almost all groundwater samples, its formation has only seldom been assessed systematically. The main reason for this is the fact that the most widely investigated dissolved gas species in groundwater is oxygen. Since oxygen is consumed rather quickly in natural systems due to soil respiration and biogeochemical oxidation processes, supersaturation of oxygen in groundwater samples is rarely found. Most studies of this phenomenon have therefore been conducted within the context of environmental tracer applications.

Only recently, Holocher et al. (2002) were able to generate excess air in laboratory experiments using sand columns. In addition, Holocher et al. (2003) introduced a numerical model that describes the formation of excess air based on a sound understanding of the relevant physical processes. Holocher et al. (2002) confirmed the hypothesis of Heaton and Vogel (1981) that the dissolution of entrapped air bubbles within the quasi-saturated zone is responsible for the formation of excess air in groundwater systems. Gas exchange between seepage water and soil air within the quasi-saturated zone is fundamentally different from gas exchange across a free boundary layer; e.g., in surface water bodies. The quasi-saturated groundwater zone includes the zone above the fully water-saturated soil zone which is temporarily saturated with water when the groundwater table rises. Since the water does not remove

the soil air entirely when the groundwater table rises, air bubbles are entrapped in the soil matrix and are dissolved partially or completely, depending on the increase in hydrostatic pressure.

Although Holocher et al. (2002) were able to produce excess air in laboratory experiments and successfully developed a physical model that describes the dissolution of entrapped air bubbles, the verification of these concepts in natural and semi-natural laboratory systems is still lacking. The aim of the present work is to assess gas exchange by laboratory experiments using sand columns and in natural aquifers, making use of noble gases as conservative tracers for gas/water partitioning.

Atmospheric noble gases are widely used as environmental tracers in subsurface hydrology. Noble gases are chemically inert and all alterations of their concentrations in groundwater are the result of well-known physical processes such as advection, dispersion, diffusion, and production. In addition, noble gases are preeminently suitable to investigate gas/water partitioning between groundwater and the soil air or atmosphere because of the absence of non-physical interactions and because atmospheric input is well-defined. Hence, dissolved atmospheric noble gases are well-suited for studying the formation and fractionation of excess air in groundwater systems that result from gas exchange between groundwater and entrapped air bubbles within the quasi-saturated zone (Figure 1.1).

The formation of excess air is also likely to be controlled by the characteristics of the soil matrix and by the hydraulic conditions prevailing during groundwater recharge. Excess air in groundwater therefore represents a potential proxy for the (climatic) conditions prevailing during infiltration and/or for the physical properties of the aquifer matrix; e.g., grain-size distribution and hydraulic conductivity. However, this promising potential of excess air as a further (paleo-)environmental proxy has only been exploited to a very small extent (e.g., Beyerle et al., 2003), and has so far been widely neglected in subsurface hydrology.

A further aspect of gas exchange in groundwater is the gas loss into a free gas phase that arises within the aquifer. Degassing of groundwater severely hampers the interpretation of gaseous environmental tracers, for instance in terms of groundwater residence times and the reconstruction of past environmental conditions. In the recent past, this problem has become increasingly apparent, especially within the context of degassed groundwater samples taken from very reducing aquifers; e.g., in south and southeast Asia.

1.2 Outline

The thesis is comprised of two parts. The first part deals with gas exchange in porous media, especially with regard to the formation of excess air in groundwater, and presents the results of laboratory and field experiments set up to study air/water partitioning in quasi-saturated porous media. In addition to these experimental investigations, numerical simulations of the dissolution of entrapped air bubbles were performed that yield new insights into the underlying physical processes. In the second

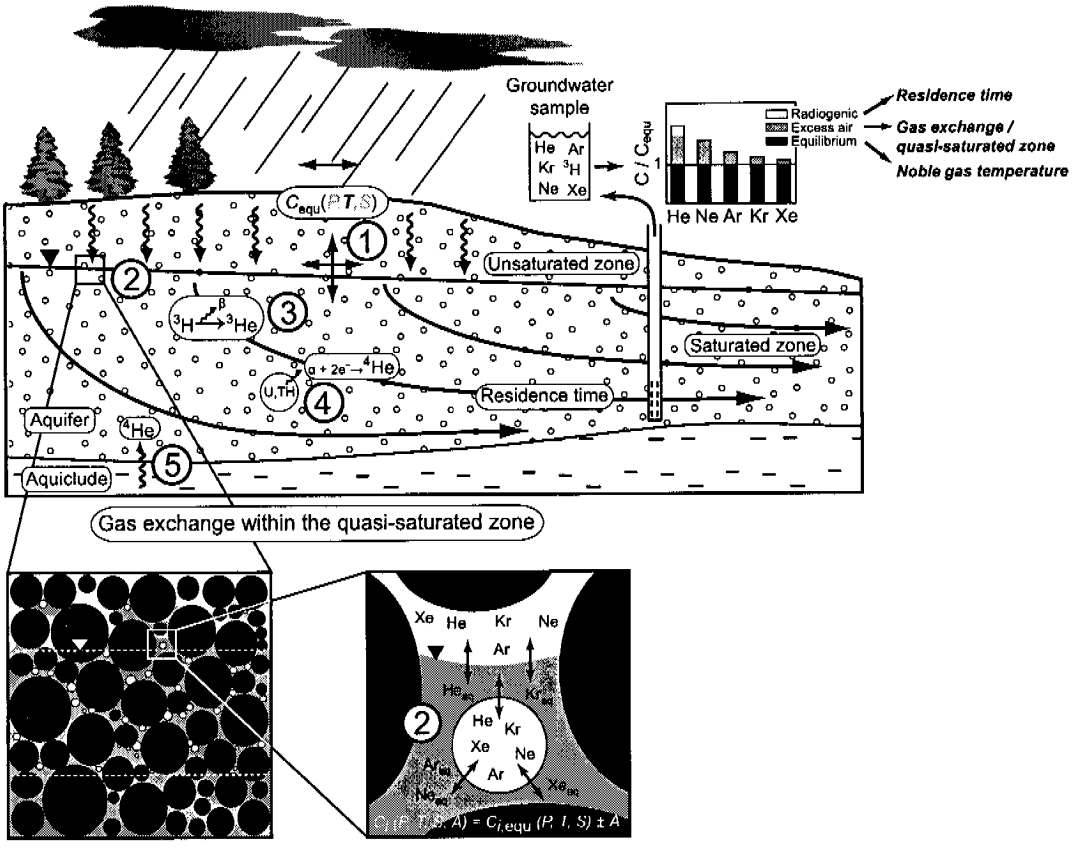

Figure 1.1: Conceptual picture to illustrate the different physical processes, affecting the occurrence of dissolved noble gases in groundwater. (1) Air/water partitioning; (2) gas exchange in the quasi-saturated zone and formation of excess air; (3) radioactive decay of ^{3}H to ^{3}He; (4) radioactive decay of U and Th producing ^{4}He; (5) external ^{4}He flux.

part of the thesis, case studies are presented in which gas exchange in groundwater plays an important role for the interpretation of environmental tracer data.

The thesis is structured as follows:

Noble gases as environmental tracers in subsurface hydrology (Chapter 2). This chapter provides the necessary background information on the use of noble gases dissolved in groundwater as conservative tracers. It describes the different sources of noble gases, and demonstrates the physical principles of gas dissolution in groundwater. In addition, an overview of the available excess air models is given, including both lumped-parameter models for the interpretation of dissolved noble gases in groundwater and numerical models that describe gas exchange in quasi-saturated porous media.

Laboratory experiments (Chapter 3). Based on the experimental results of Holocher et al. (2002), further laboratory experiments were conducted to study gas exchange and excess air formation in sand-column experiments. These experiments aim to provide a better understanding of the physical processes governing the formation of

excess air, and address specific open questions which could not be answered by the experiments of Holocher et al. (2002).

Field experiments (Chapter 4). In this chapter, the results of two field experiments to study the formation of excess air in natural porous media are presented. The aim of these experiments was to verify the validity of the physical concepts to explain the formation of excess air – which were derived from laboratory experiments – in natural systems. Two field sites with differing soil characteristics were chosen to assess these issues.

Noble gas temperature and soil temperature in Michigan (Chapter 5). As was shown in the field experiments described in chapter 4, the noble gas temperature is virtually identical to the in-situ soil temperature of the unsaturated zone. However, the noble gas temperature does not necessarily have to be identical to the mean annual soil temperature in shallow unsaturated zones, although this assumption is often implicitly made if noble gases are used to reconstruct past soil temperatures. Such a discrepancy between noble-gas temperature and the mean annual soil temperature has been observed in shallow groundwater in Michigan by Hall et al. (2005). However, their interpretation is incomplete and debatable, and additional explanations for their data set are provided here.

Paleogroundwater in Wisconsin (Chapter 6). Excess air is a promising proxy for environmental change – especially in paleogroundwater which archives pronounced climatic and hydraulic changes in the past. This is the case for Pleistocene groundwater from a deep aquifer in Wisconsin. Excess air in this groundwater in conjunction with noble gas paleo-thermometry and ^{14}C dating can be used to assess environmental changes in the past. However, the application of excess air as a (paleo-)environmental tracer requires a sound physical understanding of the underlying physical processes. The experimental investigations described in chapters 3 and 4 contribute substantially to obtaining such an understanding.

Geogenic arsenic in groundwater from Bangladesh (Chapter 7). Contamination of groundwater with naturally occurring arsenic is a severe problem in many countries, especially in south and southeast Asia, and is currently the subject of extensive research. Groundwater dynamics are likely to be an important aspect in understanding the mechanisms controlling the mobilization of arsenic in these aquifers, although groundwater hydraulics has only rarely been incorporated into recent arsenic studies. Noble gases and tritium were used to assess the groundwater dynamics of an arsenic contaminated aquifer in Bangladesh. Gas loss due to secondary gas exchange turned out to be a crucial factor in interpreting the environmental tracer data from these aquifers.

Chapter 2

Noble gases as environmental tracers in groundwater hydrology

Noble gases make excellent environmental tracers to study physical processes in groundwater and surface water because of their chemical inertness. Because of this, noble gas concentrations in natural water systems can only be altered by physical processes and do not undergo biogeochemical transformations. Noble gases dissolved in groundwater originate from different sources. The main reservoir for all stable noble gases found in groundwater (He, Ne, Ar, Kr, Xe) is the atmosphere. With the exception of He and Rn (and to a lesser extent Ar), there is no other source in meteoric groundwater than the atmosphere for all noble gases. He also originates from the solid earth and water-bound tritium (^{3}H) by radioactive production. Degassing of primordial He from the earth's mantle can be a further source of He, especially in tectonically active regions. Rn isotopes are formed in the natural decay series of U and Th. The Ar isotope ^{40}Ar is also a product of the radioactive decay of ^{40}K, but accumulates on very large time scales and is very seldom found to exceed the atmospheric fraction in groundwater. The non-atmospheric noble gases are usually referred to as either radiogenic or terrigenic. For an extensive review of the use of noble gases as environmental tracers in aquatic systems see Kipfer et al. (2002).

In summary, noble gases dissolved in groundwater originate from different sources and are incorporated into groundwater by different gas exchange processes that are explored in detail in the following sections. The measured concentration C_i of the noble gas i in groundwater can usually be separated into its components as follows:

$$C_i = C_i^{\mathrm{equ}} + C_i^{\mathrm{exc}} + C_i^{\mathrm{rad}} + C_i^{\mathrm{ter}} \tag{2.1}$$

The atmospheric fraction consists of the atmospheric equilibrium C_i^{equ} and the excess air fractions C_i^{exc}. The non-atmospheric component includes the radiogenic (C_i^{rad}) and terrigenic (C_i^{ter}) fractions.

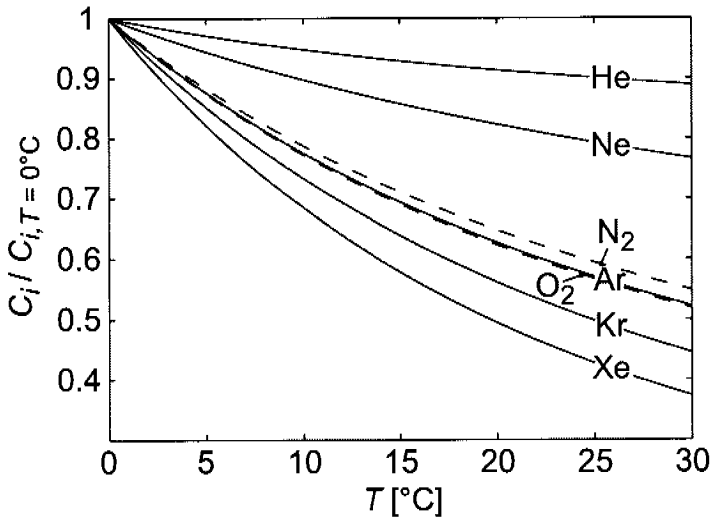

Figure 2.1: Temperature dependence of the solubilities of the noble gases He, Ne, Ar, Kr, and Xe, and those of the two main atmospheric air constituents O_2 and N_2.

2.1 Atmospheric noble gases

With the exception of He, the atmospheric inventory of all noble gases can be assumed to have been constant since the formation of the earth's atmosphere, and because atmospheric mixing is fast all noble gases can be assumed to be uniformly distributed in the atmosphere. He isotopes, in contrast to the heavier noble gases Ne, Ar, Kr, and Xe, escape from the atmosphere into space. However, on time scales of less than about 10^6 yr the partial pressure and isotopic composition of He in the atmosphere is fairly constant because He loss into space and He emanation from the earth's crust and mantle are in equilibrium on that time scale (Ozima and Podosek, 1983).

Atmospheric gases are incorporated into (ground)water as a result of gas exchange between the atmosphere and (seepage) water. The atmospheric equilibrium concentration, as a function of the physical conditions that prevail during gas exchange, can reasonably be approximated by Henry's Law (cf. chapter 4, Eq. (4.1)).

In the present work, the Henry coefficients are calculated according to the empirical solubility data recommended and compiled by Kipfer et al. (2002). That is, the solubility data for He and Ne are those given by Weiss (1971), those for Ar, N_2 and O_2 by Weiss (1970), those for Kr by Weiss and Kyser (1978), and those for Xe by Clever (1979). The Henry coefficients and molecular diffusivities of the noble gases and those of the two main atmospheric air constituents N_2 and O_2 are summarized in Tables 2.1 and 2.2. Figure 2.1 shows the temperature-dependence of the solubilities of the different gases.

In addition to the equilibrium fraction, further noble gases of atmospheric origin are incorporated into groundwater by the (partial or complete) dissolution of entrapped air bubbles within the quasi-saturated zone. This process leads to the formation of excess air and will be discussed in detail below.

Table 2.1: Non-dimensional Henry coefficients for various gases at different water temperatures ($S = 0$ g/kg, $P = 1$ atm; Weiss, 1970, 1971; Weiss and Kyser, 1978; Clever, 1979).

	0 °C	5 °C	10 °C	15 °C	20 °C	25 °C	30 °C
	$K_{H,i}$ [(mol/L)$_{gas}$/(mol/L)$_{water}$]						
He	107	108	109	109	109	109	108
Ne	80.8	84.1	86.9	89.4	91.5	93.4	95.0
Ar	18.8	21.0	23.3	25.6	27.9	30.2	32.4
Kr	9.2	10.6	12.1	13.6	15.2	16.9	18.6
Xe	4.52	5.40	6.37	7.41	8.52	9.69	10.9
N_2	42.4	47.2	51.9	56.5	61.0	65.4	69.6
O_2	20.5	23.0	25.6	28.1	30.7	33.2	35.6

Table 2.2: Molecular diffusivities of various gases in water at different water temperatures (Jähne et al., 1987).

	0 °C	5 °C	10 °C	15 °C	20 °C	25 °C	30 °C
	D_i [10^{-9} m^2/s]						
He	4.74	5.19	5.68	6.19	6.73	7.29	7.88
Ne	2.34	2.63	2.94	3.28	3.65	4.04	4.46
Ar	1.44	1.65	1.87	2.11	2.38	2.67	2.98
Kr	0.877	1.03	1.20	1.39	1.61	1.85	2.11
Xe	0.664	0.788	0.929	1.09	1.27	1.47	1.70
N_2	1.01	1.19	1.39	1.62	1.87	2.15	2.47
O_2	1.11	1.30	1.52	1.77	2.05	2.36	2.70

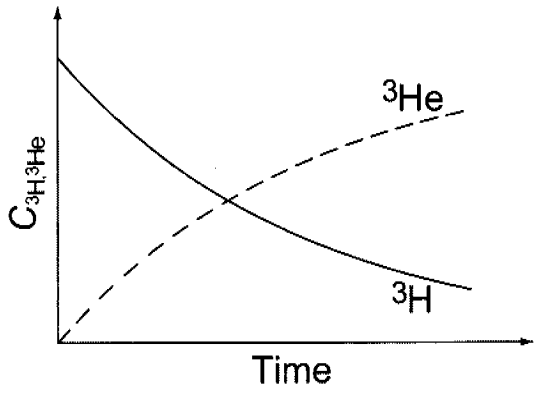

Figure 2.2: ^{3}H and ^{3}He$_{tri}$ concentrations in an isolated water parcel as a function of time.

2.2 Non-atmospheric noble gases

Non-atmospheric noble gases comprise terrigenic and radiogenic noble gases. These terms are often used synonymously although they do not necessarily describe the same source of non-atmospheric noble gases. The most important terrigenic (and radiogenic) noble gas isotope is ^{4}He, which is produced by the α-decay of natural U and Th. The most relevant radiogenic (but not terrigenic) isotope is tritiogenic ^{3}He; i.e., ^{3}He that is produced by the decay of ^{3}H. In this thesis, the term 'terrigenic ^{4}He' is used for ^{4}He produced by the radioactive decay of U and Th. Non-radiogenic, terrestrial He (i.e., primordial He from the earth's mantle) is irrelevant for this work and will not be considered further.

^{3}H decays to ^{3}He with a half-life of 4500 d (Lucas and Unterweger, 2000): $^3\text{H} \overset{\beta}{\rightsquigarrow} {}^3\text{He}_{tri}$. In an isolated water parcel, the concentration of ^{3}He$_{tri}$ increases to the same degree as the concentration of ^{3}H decreases (Figure 2.2). Therefore, the ratio of the concentration of the decay product ^{3}He$_{tri}$ to that of ^{3}H can be used to determine the residence time of the isolated water parcel, defined as the time since gas exchange between the water parcel and the gas reservoir ceased (Eq. (7.1); Torgersen et al., 1977, 1979). A more detailed description of the ^{3}H/^{3}He dating method is given in section 7.2.4.

Terrigenic ^{4}He (^{4}He$_{ter}$) accumulates in groundwater due to the radioactive α-decay of U and Th present in the aquifer sediments or due to its influx from deeper strata. He accumulation rates can differ over a broad range of magnitudes, depending on the U and Th content of the aquifer matrix. He fluxes from the deeper crust and mantle are also strongly spatially variable. Aquifers in tectonically active regions can be especially subject to high ^{4}He accumulation, which, however, often show high spatial variability, as well. Since the local ^{4}He$_{ter}$ accumulation rate is usually unknown, ^{4}He$_{ter}$ only represents a qualitative tracer for groundwater residence time. However, it has also been used quantitatively when it can be calibrated by other appropriate dating methods (e.g., ^{14}C). ^{4}He$_{ter}$ usually accumulates on time scales of 10^2 years or greater, so that it does not occur in significant concentrations in young groundwa-

ter which contains considerable amounts of ^{3}H, unless it indicates the admixture of an older groundwater component. In such cases, $^{4}He_{ter}$ can be an useful tracer for groundwater mixing.

A further important non-atmospheric noble gas which can be used as an environmental tracer in aquatic systems is Rn. All Rn isotopes are radioactive and are formed in the decay chains of ^{238}U (^{222}Rn, half-life: 3.8 d), ^{232}Th (^{220}Rn, half-life: 56 s), and ^{235}U (^{219}Rn, half-life: 4 s). ^{222}Rn has been employed in surface water studies as a tracer for mixing processes in lakes and oceans (e.g., Imboden, 1977; Imboden and Emerson, 1978; Imboden and Joller, 1984), and in groundwater studies (for a review see, for example, Cecil and Green, 2000). Due to its short half-life, ^{222}Rn is especially suitable for studying physical processes on very short time scales, for instance for dating groundwater having a residence time of only a few days. ^{222}Rn can also be used to study surface-water (river bank) infiltration or groundwater discharge into rivers or lakes. The use of Rn as a natural tracer will not be further discussed in this work.

2.3 Excess air models

Several conceptual and mathematical models have been developed to describe gas exchange and excess air formation quantitatively. These models can be classified as either lumped-parameter models or numerical gas-exchange models. In this thesis, models which parameterize the amount and fractionation of excess air in order to separate the different gas fractions – i.e., equilibrium, terrigenic, radiogenic, and excess air fractions – are referred to as lumped-parameter models. These models are routinely applied in the interpretation of the concentrations of dissolved noble gases as environmental tracers in groundwater. Several lumped-parameter models have been developed in order to reliably quantify the excess air component in groundwater samples. However, these lumped-parameter models only parameterize the excess air component rather than describe the physical processes involved in the formation of excess air. By contrast, models have been developed to study gas exchange and excess air formation in quasi-saturated porous media on a sound physical basis. These models are here referred to as numerical gas-exchange models.

2.3.1 Pure excess air (UA) model

The simplest excess air model assumes the complete dissolution of an additional air volume. The pure excess air model (unfractionated excess air, UA model) follows the conceptual idea that air bubbles entrapped in the soil matrix are dissolved completely owing to an increase in hydrostatic pressure. The composition of the resulting excess air component is therefore the same as that of the atmosphere; i.e., the excess air component is isotopically and elementally unfractionated with respect to atmospheric

air. Pure excess air is parameterized as follows (e.g., Heaton and Vogel, 1981):

$$C_i(T,S,P,A_{\mathrm{ua}}) = C_i^{\mathrm{equ}}(T,S,P) + A_{\mathrm{ua}} \cdot z_i \tag{2.2}$$

The concentration C_i of the gas i in water is given by the sum of the atmospheric equilibrium concentration C_i^{equ} (expressed as a function of temperature T, salinity S, and pressure P) and the additionally dissolved dry air volume A_{ua}, with z_i being the volume fraction of the gas i in dry air.

2.3.2 Closed-system equilibration (CE) model

Because the excess air component is often fractionated – i.e., the elemental (and isotopic) composition of the gas excess does not exactly coincide with the composition of atmospheric air – additional excess air models have been developed to allow fractionated samples to be interpreted reliably. The most common and physically most appropriate model for fractionated excess air is the closed-system equilibration model (CE model, Aeschbach-Hertig et al., 2000). The CE model assumes equilibration of a finite water volume with a finite air volume under increased hydrostatic pressure. For a more detailed description of the CE model see section 4.2.2.

2.3.3 Partial re-equilibration (PR) model

The partial re-equilibration model (PR model) is a further model explaining the fractionation of excess air (Stute et al., 1995b). The conceptual idea of the PR model is the complete dissolution of the entrapped air volume followed by a secondary diffusive gas loss across the groundwater table. The model equation is given by:

$$C_i(T,S,P,A_{\mathrm{pr}},F_{\mathrm{pr}}) = C_i^{\mathrm{equ}}(T,S,P) + A_{\mathrm{pr}} \cdot z_i \cdot \exp\left(-F_{\mathrm{pr}}\frac{D_i}{D_{\mathrm{Ne}}}\right) \tag{2.3}$$

where A_{pr} is the amount of initially entrapped and dissolved air, F_{pr} is the fractionation factor and D_i is the molecular diffusion coefficient of gas i in water. According to the PR model, the fractionation – in contrast to the CE model – is controlled by the different diffusivities of the respective atmospheric gases. Hence, the composition of both the remaining gas phase and the dissolved excess air component is fractionated elementally and isotopically relative to atmospheric air. The isotopic fractionation is an important feature of that model and, in practice, often allows this model to be rejected because isotope ratios in groundwater samples, e.g., $^{20}Ne/^{22}Ne$ and $^{36}Ar/^{40}Ar$, are usually identical to those in air-equilibrated water.

Assuming a one-step process of dissolution and subsequent diffusive gas loss, the required initial entrapped air volume must often be unrealistically large. This problem can be overcome conceptually by multi-step partial re-equilibration; that is, by a continuous series of cycles of air dissolution and degassing steps (Kipfer et al., 2002).

2.3.4 Capillary pressure model

In addition to the lumped-parameter models, which assume the formation of excess air as a result of the dissolution of entrapped air bubbles due to the increase in hydrostatic pressure, Mercury et al. (2004) propose a different mechanism of excess air formation based on increasing gas equilibrium concentrations due to increasing capillary pressure. The internal water pressure of capillary water in the unsaturated zone decreases with decreasing soil air humidity, resulting in an increase in (noble) gas equilibrium and mass fractionation in favor of the heavier noble gases. This mechanism may lead to the formation of excess air in the capillary water of very fine-grained sediments. The capillary pressure is given by the fundamental equation of capillarity (Laplace's Law):

$$\Delta P = \frac{2 \cdot \sigma \cdot \cos \alpha}{r_{\mathrm{p}}} \tag{2.4}$$

where ΔP is the pressure difference between water and air, σ is the surface tension between liquid water and water vapor in air, r_{p} is the pore radius (negative for a capillary), and α is the contact angle between the dry solid wall and the capillary ($r_{\mathrm{p}}/\cos\alpha$ corresponds to the radius of the meniscus).

The solubility of gas i changes due to the change in internal water pressure. For constant T, the change in the Henry coefficient $K_{\mathrm{H},i}$ is given by the following equation (Mercury et al., 2004):

$$\ln \frac{K_{\mathrm{H},i}(T,P)}{K_{\mathrm{H},i}(T,1)} = -\frac{1}{RT} \cdot \int_1^P \Delta V \cdot \mathrm{d}P \tag{2.5}$$

with ΔV being the volume change and $\mathrm{d}P$ being the negative pressure change related to capillarity. If the ratio $K_{\mathrm{H},i}(T,P)/K_{\mathrm{H},i}(T,1)$ decreases, the solubility of the gas increases, and vice versa.

However, according to the capillary pressure model the formation of excess air is only possible under very specific circumstances: First, the soil air humidity must be low because capillary pressure decreases strongly with increasing soil air humidity and hence with water saturation. Therefore, the capillary effect is not expected to occur under the quasi-saturated conditions that prevail near the groundwater table. Second, the capillary water must be transported into the saturated zone without any significant further gas exchange or gas loss.

2.4 Numerical gas-exchange models

As the lumped-parameter models described above only yield a parameterization for excess air, additional, more sophisticated models are necessary to study the formation of excess air, taking into account the relevant physical processes. Several numerical models have been developed to describe gas exchange in quasi-saturated porous media between a mobile water phase and an immobile, entrapped gas phase.

2.4.1 Local equilibrium model

In contrast to the KBD model (see below), the local equilibrium model assumes local solubility equilibrium to exist between the immobile gas phase and the mobile water phase (Cirpka and Kitanidis, 2001). Therefore, kinetic effects are neglected, and gas exchange is controlled solely by the different gas solubilities and not by the molecular diffusivities. As in the KBD model, the entrapped air bubbles consist of the noble gases He, Ne, Ar, Kr, and Xe, and the two main air constituents N_2 and O_2.

Governing equations for the local equilibrium model. The transport of the gas i is described by:

$$\Theta\frac{\partial C_{i,\mathrm{tot}}}{\partial t} + \nabla\cdot(\mathbf{q}C_i) - \nabla\cdot(\Theta\mathbf{D}\nabla C_i) = 0 \tag{2.6}$$

with porosity Θ, total concentration $C_{i,\mathrm{tot}}$ of gas i, specific-discharge vector $\mathbf{q}$, aqueous-phase concentration C_i, and dispersion tensor $\mathbf{D}$.
The continuity equation is given by:

$$\Theta\frac{\partial(1-S_\mathrm{g})}{\partial t} + \nabla\cdot\mathbf{q} = 0 \tag{2.7}$$

with S_g being the gas-filled porosity (gas saturation).
The total concentration $C_{i,\mathrm{tot}}$ is defined as

$$C_{i,\mathrm{tot}} = S_\mathrm{g}C_i^\mathrm{g} + (1-S_\mathrm{g})C_i \tag{2.8}$$

with C_i^g being the concentration of gas i in the gas phase.
Substitution of Eq. (2.8) into Eq. (2.6) yields:

$$\Theta(1-S_\mathrm{g})\frac{\partial C_i}{\partial t} + \Theta\frac{\partial(S_\mathrm{g}C_i^\mathrm{g})}{\partial t} + \mathbf{q}\cdot\nabla C_i - \nabla\cdot(\Theta\mathbf{D}\nabla C_i) = 0 \tag{2.9}$$

Equilibrium between aqueous and gaseous phases is given by Henry's Law:

$$C_i^\mathrm{g} = K_{\mathrm{H},i}C_i \tag{2.10}$$

with the Henry coefficient $K_{\mathrm{H},i}$ being subject to a pressure constraint:

$$P_\mathrm{g} = RT\sum_i C_i^\mathrm{g} \tag{2.11}$$

where R is the ideal gas constant, T is the absolute temperature, and P_g is the gas pressure:

$$P_\mathrm{g} = P_\mathrm{aq} + \frac{2\sigma}{r} \tag{2.12}$$

where P_aq is the pressure in the aqueous phase, σ is surface tension, and r is the bubble radius.

The bubble radius is related to the bubble volume V_b by:

$$V_b = \frac{4\pi}{3} r^3 \tag{2.13}$$

The gas saturation S_g is related to the bubble volume by:

$$S_g = \frac{n_b V_b}{V_{por}} = \frac{n_b}{V_{por}} \frac{4\pi}{3} r^3 \tag{2.14}$$

where n_b/V_{por} is the number of gas bubbles per pore volume.
The bubble radius can now be formulated as a function of the gas saturation:

$$r = \left(\frac{V_{por}}{n_b} \frac{3S_g}{4\pi} \right)^{1/3} \tag{2.15}$$

The resulting gas pressure is given by:

$$P_g = P_{atm} + \rho g h + 2\sigma \left(\frac{V_{por}}{n_b} \frac{3S_g}{4\pi} \right)^{-1/3} \tag{2.16}$$

in which P_{atm} is the atmospheric pressure and $\rho g h$ is the hydrostatic pressure at depth h below the water surface.

2.4.2 Kinetic bubble dissolution (KBD) model

Holocher et al. (2003) developed the kinetic bubble dissolution (KBD) model to describe the dissolution of entrapped air bubbles in quasi-saturated porous media. The mass transfer between the spherical air bubbles and the water phase is modeled assuming rapid equilibration between the two phases according to Henry's Law (Eq. (4.1)) and using a water-side boundary-layer gas-exchange approach. The composition of the bubbles is assumed to consist of the noble gases He, Ne, Ar, Kr, Xe, and the two main air constituents N_2 and O_2.

Governing equations for the KBD model. The inter-phase mass flux is proportional to the concentration gradient between the gas and water phases. The mass flux J of gas i is given by:

$$J_i = k_i \cdot \left(C_{w,i} - \frac{P_i}{RTK_{H,i}} \right) \tag{2.17}$$

where $C_{w,i}$ is the aqueous concentration of gas i, P_i is the partial pressure of gas i, R is the universal gas constant, T is water temperature, and $K_{H,i}$ is the Henry coefficient of gas i. The mass transfer coefficient k_i is defined as follows (Epstein and Plesset, 1950):

$$k_i = D_{w,i} \cdot \left(\frac{1}{r} + \sqrt{\frac{v}{2\pi r D_{w,i}}} \right) \qquad [LT^{-1}] \tag{2.18}$$

where $D_{w,i}$ is the molecular diffusion coefficient of gas i in water, r is the bubble radius, and v is flow velocity.

The rate of change of dissolved total mass is given by the sum of those for all gases in each spherical air bubble:

$$\frac{dn_{tot}}{dt} = \sum_i \frac{dn_i}{dt} = -4\pi r^2 \sum_i k_i \left(C_{w,i} - \frac{x_i}{RTK_{H,i}} \left(P_{atm} - P_w + \rho gh + \frac{2\sigma}{r} \right) \right) \quad (2.19)$$

with $i = \mathrm{He, Ne, Ar, Kr, Xe, N_2, O_2}$.

where n_i is the exchanged number of moles of gas i, x_i is the mole fraction of gas i, P_{atm} is the atmospheric pressure, P_w is the water vapor pressure in the bubble, ρgh is the hydrostatic pressure at depth h below the water surface, and $2\sigma/r$ is the surface-tension pressure due to the curvature of the bubble surface, with surface tension σ. The resulting change in bubble radius with time is given by:

$$\frac{dr}{dt} = \frac{3RT}{4\pi r} \left(\frac{1}{6\sigma + 3r(P_{atm} - P_w + \rho gh)} \right) \frac{dn_{tot}}{dt} \quad (2.20)$$

The temporal change in the dissolved gas concentration for gas i is:

$$\frac{dC_{w,i}}{dt} = \frac{n_{bubble} \cdot A_{int}}{V_w} \cdot J_i = \frac{n_{bubble}}{\frac{V_{tot}\Theta}{1+r_{a-w}}} \frac{dn_i}{dt} \quad (2.21)$$

where n_{bubble} is the number of bubbles, A_{int} is the surface area of the bubble, V_w is the water-filled pore volume, V_{tot} is the total volume of the column, Θ is the total porosity, and r_{a-w} is the air/water ratio (V_a/V_w).

In addition to the mass transfer between air bubbles and the water phase, the KBD model includes an advection-dispersion transport model. The one-dimensional flow is given by:

$$\frac{\partial(\Theta_w C_{w,i})}{\partial t} = \frac{\partial}{\partial t} \left(\Theta_w D_x \frac{\partial C_{w,i}}{\partial x} - \Theta_w v C_{w,i} \right) + B = \frac{\partial}{\partial x} \left(\Theta_{w,i} D_x \frac{\partial C_{w,i}}{\partial x} - q C_{w,i} \right) + B \quad (2.22)$$

where Θ_w is the water-filled porosity, D_x is the hydrodynamic dispersion coefficient in the direction x of the flow, and q is the Darcy velocity (specific discharge). B represents a source term that results from the mass transfer between the water and entrapped gas phases (cf. Eq. (2.21)). For a more detailed description of the KBD model see Holocher et al. (2003).

2.5 Excess air as a paleo-hydrological tracer

As the formation of excess air most likely depends on the physical conditions prevailing during groundwater recharge – including the infiltration mechanism, climatic

conditions, recharge dynamics, soil properties, etc. – excess air can itself be viewed as a potential proxy for the environmental conditions that prevailed during infiltration. The amount of excess air, as well as the degree of fractionation of the excess air component, is likely to contain information on, for example, the extent of groundwater table fluctuations and the recharge area. Up to now, the potential of excess air as a paleo-hydrological tracer has very seldom been exploited, and have hardly ever been applied to field studies. Stute and Talma (1998) link large amounts of excess air in groundwater from Namibia to wetter climate in the past, and Aeschbach-Hertig et al. (2002a), in an analysis of paleo-groundwater from several semi-arid regions, argue that the large amounts of excess air found are associated with higher precipitation in the past. Beyerle et al. (2003) used the excess air in paleo-groundwater from the Niger Sahel to identify differences in the recharge dynamics occurring during periods of cooler and wetter climate in the past. Beyerle et al. (2003) found a correlation between excess Ne and the stable isotopic composition of the groundwater which indicates stronger formation of excess air during past wet periods. Similar conclusions were drawn by Kulongoski et al. (2004) for excess air in groundwater from the Kalahari desert in Botswana.

Although there are those few studies in which excess air has been used as a proxy for past environmental conditions, the conclusions drawn are rather qualitative and sometimes ambiguous to a certain extent. One of the main reasons for this is that the formation of excess air has been only poorly understood in sound physical terms. As long as the relevant physical mechanisms for the formation of excess air are not fully understood, it is not possible to reliably relate amount and fractionation of the excess air qualitatively and quantitatively to recharge dynamics and soil properties. The experiments and numerical investigations conducted in this work to study the formation of excess air (cf. chapters 3 and 4) aim at obtaining a better understanding of the formation of excess air, which will also improve the physical basis for the application of excess air as an environmental tracer. In chapter 6, a further case study in which excess air is used as a proxy for environmental change during the last glacial maximum and Holocene in North America will be described.

Part II

Gas exchange and formation of excess air in porous media

Chapter 3

Laboratory experiments and numerical investigations

3.1 Introduction

Holocher et al. (2002, 2003) investigated gas exchange and the formation of excess air in quasi-saturated porous media using sand-column experiments in conjunction with numerical simulations of solute transport coupled to gas bubble dissolution. Based on their results, further sand-column experiments were conducted. My work will address several questions which were posed by Holocher (2002) and which have not yet been answered sufficiently. These questions concern: (i) the role of kinetic effects on the dissolution of entrapped air; (ii) the effect of the direction of the water flow (vertical or horizontal); and (iii) the formation of apparently unfractionated excess air despite evidence of incomplete bubble dissolution.

(i) As described in section 2.4, there are different gas-exchange models available which either consider kinetic effects on the dissolution of entrapped gas bubbles (KBD model) or assume local equilibrium between the water and gas phases (local equilibrium model). For a description of these models see section 2.4. To choose the appropriate model describing the dissolution of entrapped air in porous media, the role of kinetic effects and their characteristic time scales have to be explored. This is of special interest because the local equilibrium model is much less demanding than the KBD model in terms of computing time.

(ii) Holocher et al. (2002) performed all their experiments in systems characterized by one-dimensional vertically downward flow. Because hydrostatic pressure is the main factor controlling the gas equilibrium in quasi-saturated porous media, horizontal flow (with quasi-constant hydrostatic pressure in the direction of the flow) is conceptually different from vertical flow (with a positive or negative pressure gradient in the direction of the flow). As the natural flow direction of groundwater is mostly horizontal, or at least has a significant horizontal flow component, the differences between vertical and horizontal water flow are of great importance for understanding gas exchange in porous media.

(iii) In his sand-column experiments, Holocher et al. (2002) observed the formation of apparently unfractionated excess air in the presence of partially dissolved gas bubbles. This finding is in agreement with modeling results based on the KBD model. However, Holocher et al. (2002) was able to provide neither systematic experimental evidence nor a convincing explanation for this puzzling phenomenon, which remains unresolved. The observation of apparently unfractionated excess air by Holocher et al. (2002) in experiments and its occurrence in model calculations are interesting because they contradict the original conceptual assumption that unfractionated excess air is produced as the result of the complete dissolution of entrapped air. The observation is also of importance for the interpretation of excess air in terms of recharge dynamics (cf. section 2.5).

3.2 Experimental methods

3.2.1 Experimental set-up

In this thesis, the laboratory experiments were conducted using a packed sand column. The experimental set-up is shown in Figure 3.1. The acrylic glass column had a length of 1 m and an inner diameter of 5.2 cm, and was equipped with sampling ports at both the inflow and outflow of the column. The column was packed with clean, well-sorted quartz sand with a grain size of 1.6 to 2.5 mm (Dorsilit®Nr. 5 G, Dorfner). The column was installed horizontally. As a boundary condition, a constant head of 1.855 m was applied to the inflow, and 1.845 m to the outflow, resulting in a hydraulic gradient of 0.01.

The sand column was filled vertically from the bottom to the top with air-equilibrated water. During the filling process, air bubbles were entrapped in the column. After the column had been filled completely, it was turned to a horizontal position. To allow re-equilibration of the water and the entrapped gas phase, the through flow experiment was started 3 h after filling the column.

Local tap-water was used which had been equilibrated with the atmosphere by slowly stirring it in an open reservoir (~100 L) for about one week. To ensure full equilibration, the water was analyzed for dissolved noble gases prior to the experiment. Biological consumption of oxygen was prevented by adding about 10 mg/L chlorine dioxide. The experiment was conducted in a climatized room with a constant air temperature of 20 °C and a constant relative humidity of 90 %. The mean atmospheric pressure was 0.956 atm. Water samples for the analysis of dissolved noble gases were taken both from the inflow and outflow of the column during the experiment, which lasted about 46 h. Water samples (22.5 mL) were put into copper tubes, which were then sealed gas-tight by pinch-off clamps, following the standard sampling procedure (Beyerle et al., 2000).

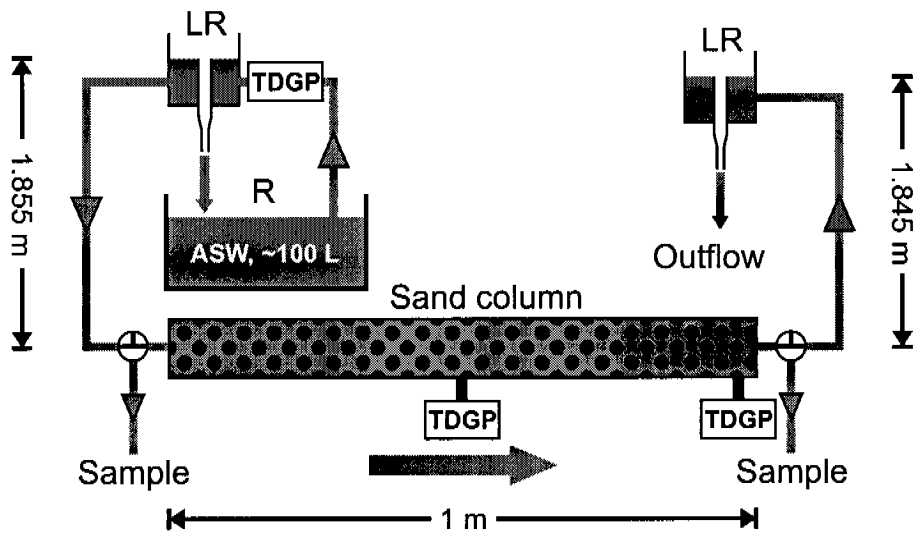

Figure 3.1: Experimental set-up for the sand-column (length: 1 m, diameter: 5.2 cm) experiment. About 100 L of air-saturated water (ASW) was prepared in an open reservoir (R). The hydraulic heads at both ends of the column were kept constant making use of leveling reservoirs (LR). Water samples for the analysis of dissolved noble gases could be taken at both inflow and outflow of the column. Total dissolved gas pressure (TDGP) was measured in the inflowing water, in the middle, and at the end of the column.

3.2.2 Transport parameter identification

In order to determine the transport parameters of the sand, a tracer experiment was conducted using sodium chloride as a conservative tracer. The tracer was injected continuously into the inflow of the column, while the tracer breakthrough was detected at the outflow by measuring the electrical conductivity every minute. The tracer dosage corresponded to an increase in electrical conductivity from about 800 μS/cm to about 1150 μS/cm. The occurrence of density-driven flow could be avoided by this relatively small increase in electrical conductivity, i.e., total dissolved solids are <1 g/L after tracer injection. The tracer transport is described by the one-dimensional transport equation:

$$D_L \frac{\partial^2 C_t}{\partial x^2} - v\frac{\partial C_t}{\partial x} = \frac{\partial C_t}{\partial t} \tag{3.1}$$

which has the following analytical solution for the case of continuous tracer injection (Kreft and Zuber, 1978):

$$\frac{C_t(x,t)}{C_{t,0}} = \frac{1}{2}\cdot \mathrm{erfc}\left(\frac{x-vt}{\sqrt{4D_L t}}\right) + \frac{1}{2}\cdot \exp\left(\frac{vx}{D_L}\right)\cdot \mathrm{erfc}\left(\frac{x+vt}{\sqrt{4D_L t}}\right) \tag{3.2}$$

where C_t is the tracer concentration, D_L is the longitudinal dispersion coefficient, v is the mean flow velocity, and x is the spatial coordinate in the direction of the flow. The mean flow velocity v and the longitudinal dispersion coefficient D_L were determined from Eq. (3.2) using unconstrained nonlinear optimization implemented in Matlab

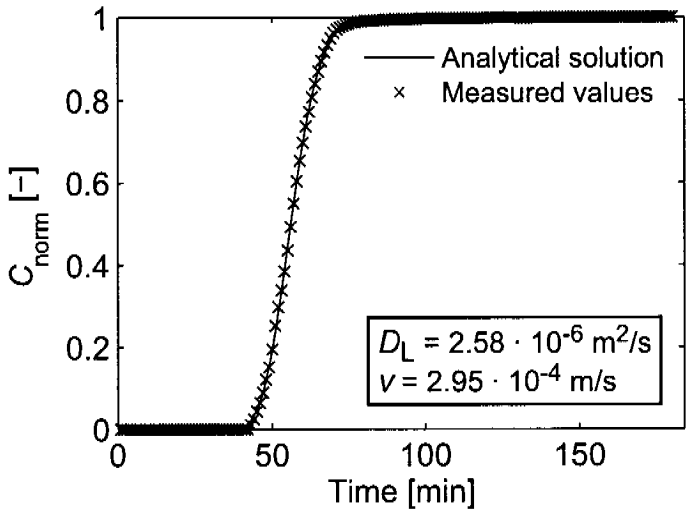

Figure 3.2: Breakthrough curve of the tracer experiment. The transport parameters were identified using the analytical solution of the 1-dimensional transport equation (Eq. (3.1)) for the case of continuous tracer injection (see Eqs. (3.2), (3.3), and (3.4)).

(Lagarias et al., 1998).

The porosity Θ can be determined according to:

$$\Theta = \frac{q}{v} = \frac{Q}{v \cdot A_{\text{col}}} \tag{3.3}$$

where q [L/T] is the Darcy velocity (specific discharge), Q [L^3/T] is the flow measured during the experiment, and A_{col} is the cross-sectional area of the column.

The hydraulic conductivity K can be computed as follows:

$$K = \frac{Q}{A_{\text{col}} \cdot I} \tag{3.4}$$

with $I = 0.01$ being the hydraulic gradient adjusted during the experiment, making use of leveling reservoirs at both the inflow and the outflow of the sand column (see Figure 3.1).

Figure 3.2 shows the tracer breakthrough curve which was detected at the outflow of the sand column. The parameter values for the longitudinal dispersion coefficient D_{L} and the mean flow velocity v were deduced from the tracer experiment according to Eq. (3.2) (Figure 3.2). The hydraulic conductivity of $K = 1.18 \cdot 10^{-2}$ m/s and the porosity of $\Theta = 0.4$ were determined using Eqs. (3.3) and (3.4).

3.2.3 Total dissolved gas pressure (TDGP) probes

In addition to the analysis of dissolved noble gases, total dissolved gas pressure (TDGP) probes[1] were used to investigate gas exchange and the formation of excess air during the column experiment. The TDGP probe consists of a gas-permeable silicone-rubber tube (length: 10 cm, inner diameter: 1 mm) with a pressure transducer attached at one end. The other end of the tube is knotted tightly to close it off. Two tubes are rolled up in a spiral and installed directly into the sand at the middle and at the outflow of the column. The pressure transducer is connected to the silicone-rubber tubes via short stainless-steel cannulas (length: 1 cm) which are fitted through the acrylic glass wall of the column. In addition, a third TDGP probe was installed in the inflow of the column to measure the TDGP in the inflowing water.

The gas volume inside the silicone-rubber tube's void is in gas exchange with the surrounding water phase, and the total gas pressure inside the tube is measured relative to the ambient atmospheric pressure. If the sum of the partial pressures of the dissolved gases in the water exceeds the atmospheric solubility equilibrium pressure, the total pressure inside the tube must exceed the atmospheric pressure. As the partial pressures of N_2 and O_2 amount to about 99 % of the total pressure in atmospheric air, the TDGP signal in water is usually given essentially by the sum of the partial pressures of these two gases.

The main advantage of the TDGP probe is its ability to measure quasi-continuously the total dissolved gas content of the water. During the experiment, the TDGP of the water was measured in the inflow to the column, at the middle of the column, and in the outflow of the column at intervals of 30 min.

The response time of the TDGP probes can be estimated from Fick's first law of diffusion (Manning et al., 2003):

$$t_e = -\frac{V_t \delta}{A_t D_i^{sil}} \cdot \ln\left(1 - \frac{E}{100}\right) \tag{3.5}$$

where V_t is the void of the silicone-rubber tube, δ is the thickness of the tube wall, A_t is the surface area of the tube, D_i^{sil} is the diffusion coefficient of the gas i in silicone rubber, and E is the percent equilibrated, which is defined as:

$$E = \left(\frac{P_i^t - P_i^0}{P_i - P_i^0}\right) \cdot 100 \tag{3.6}$$

where P_i is the partial pressure of gas i after complete equilibration, P_i^0 is the initial partial pressure of gas i in the tube's void, and P_i^t is the partial pressure of gas i in the tube's void at time t.

The response time of the TDGP probe is shown in Figure 3.3 for the molecular diffusivity of N_2 in silicone rubber at 20 °C of $D_{N_2}^{sil} \approx 4 \cdot 10^{-10}$ m^2/s (http://www.

[1] The TDGP probes were produced and provided by Heinz Surbeck, Centre of Hydrogeology, University of Neuchâtel.

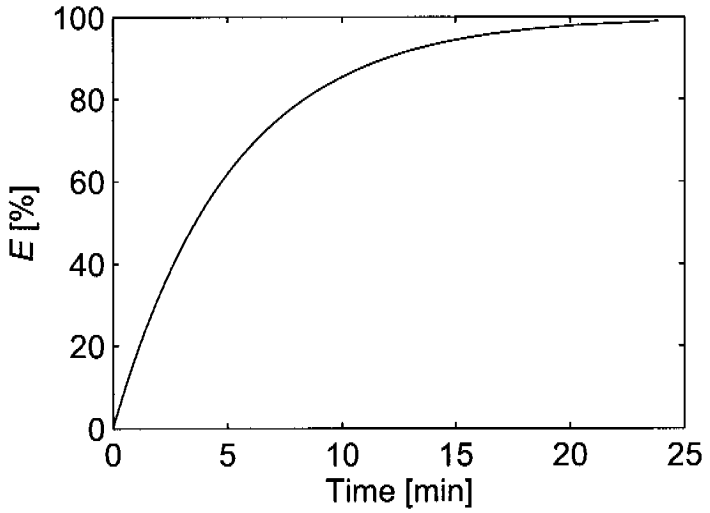

Figure 3.3: Response time for N_2 of the TDGP probes calculated applying Eq. (3.5).

goodfellow.com).

3.3 Results and discussion

3.3.1 Noble gases

The concentrations of noble gases in the samples taken during the sand-column experiment are summarized in Table 3.1. The closed-system equilibration (CE) model of Aeschbach-Hertig et al. (2000) was used to calculate the noble gas temperature (NGT) T, the amount of entrapped air A, and the fractionation factor F of the excess air component from the measured dissolved noble gas concentrations (cf. section 4.2.2, Table 3.2). The model results demonstrate that the dissolved concentrations of noble gases in the samples from the water reservoir, which contains the water that is injected into the column, are indeed very close to atmospheric solubility equilibrium and are approximately constant during the entire experiment (Table 3.1). The mean NGT ($20.0 \pm 0.2\,°C$) of the inflow samples is identical to the constant ambient air temperature of $20\,°C$.

Figure 3.4 shows the evolution of the noble gas concentrations during the column experiment. After filling the column at $t = -3\,h$, the initially air-equilibrated water dissolved part of the entrapped air, leading to the supersaturation observed at $t = 0\,h$. After initiation of the water flow at $t = 0\,h$, the concentrations of the light noble gases He and Ne continued to increase, whereas the concentrations of the heavy noble gases Ar, Kr, and Xe decreased. This is because Ar, Kr, and Xe have significantly higher solubilities than He and Ne. With respect to atmospheric air, the entrapped air therefore became enriched in He and Ne, and depleted in Ar, Kr, and Xe. Later, at about $t = 15\,h$, all noble gas concentrations decreased due to the progressively

Table 3.1: Noble gas concentrations and isotope ratios in the water samples from the sand column experiment. All noble gas concentrations are given in cm^3_{STP}/g. The overall measurement errors (1σ errors) are $\pm 1\%$ for He, Ne, and Ar, $\pm 1.5\,\%$ for Kr, $\pm 2\,\%$ for Xe, $\pm 0.7\,\%$ for $^3He/^4He$, $\pm 0.3\,\%$ for $^{22}Ne/^{20}Ne$, and $\pm 0.2\,\%$ for $^{40}Ar/^{36}Ar$.

No.	Time [h]	He $[10^{-8}]$	Ne $[10^{-7}]$	Ar $[10^{-4}]$	Kr $[10^{-8}]$	Xe $[10^{-9}]$	$^3He/^4He$ $[10^{-6}]$	$^{22}Ne/^{20}Ne$ [–]	$^{40}Ar/^{36}Ar$ [–]
					Inflow				
I1	0.00	4.36	1.78	3.01	6.62	9.14	1.38	0.1023	295.3
I2	20.00	4.34	1.77	2.99	6.57	9.19	1.36	0.1021	296.1
I3	46.00	4.35	1.77	2.98	6.55	9.05	1.38	0.1020	296.2
					Outflow				
1	0.00	5.13	2.09	3.42	7.38	9.97	1.37	0.1022	295.7
2	5.25	5.53	2.23	3.26	6.93	9.45	1.37	0.1020	295.9
3	11.50	5.82	2.25	3.20	6.86	9.40	1.38	0.1019	295.5
4	15.00	5.63	2.19	3.17	6.78	9.36	1.37	0.1021	295.5
5	17.50	5.39	2.11	3.13	6.69	9.00	1.37	0.1023	295.8
6	22.50	4.95	1.98	3.08	6.68	9.29	1.36	0.1019	296.0
7	27.50	4.51	1.83	3.01	6.59	9.26	1.37	0.1020	295.1
8	34.00	4.36	1.78	3.00	6.56	9.22	1.37	0.1019	295.2
9	42.25	4.33	1.75	2.99	6.60	9.15	1.36	0.1021	295.1

dissolving gas phase. After about 35 h, the entrapped air was virtually completely dissolved by the water flowing through the column, and concentrations in the outflow were approximately identical to those in the inflow.

The NGTs of the samples taken from the outflow of the column during the experiment also agree with the ambient air temperature of 20 °C (mean NGT: 20.5 ± 0.6 °C), although most NGTs are slightly higher than the real water temperature of 20 °C.

Figure 3.5 shows the evolution of the He and Ar concentrations during the experiment. The first two samples 1 and 2 taken at $t = 0$ h and $t = 5.25$ h (see Figures 3.4 and 3.5) contain excess air components which are fractionated with respect to pure atmospheric air; i.e., the best fit was achieved by fitting the model parameters T, A, and $0 < F < 1$ using the CE model (Table 3.2). All other samples (3 – 9; see Figures 3.4 and 3.5) contain pure, unfractionated excess air, yielding the best fits for $F = 0$.

The observation that the excess air component is fractionated during the early stage of bubble dissolution and unfractionated during the latter part of the experiment is in good agreement with the results of Holocher et al. (2002), who made the same observation in previous investigations, although the experimental data basis was weak and theoretical understanding was lacking. Importantly, these findings contradict the classical interpretation of the formation of unfractionated excess air as being the result of the complete dissolution of entrapped air. Since the samples containing apparently unfractionated excess air were taken in the presence of a dissolving gas phase, this

Table 3.2: Noble gas temperature T, amount of entrapped air A, and fractionation factor F of the water samples from the sand-column experiment. The parameter values were obtained from the measured noble gas concentrations using the CE model of Aeschbach-Hertig et al. (2000).

No.	Time [h]	T [°C]	A [cm^3_{STP}/kg]	F [–]
		Inflow		
I1	0.00	20.2±0.1	0.16±0.03	0±0
I2	20.00	19.8±0.1	0.15±0.03	0±0
I3	46.00	20.0±0.1	0.13±0.03	0±0
		Outflow		
1	0.00	22.0±0.9	311±268	0.82±0.00
2	5.25	20.1±0.4	7.55±2.32	0.52±0.08
3	11.50	20.5±0.2	2.90±0.04	0±0
4	15.00	20.5±0.2	2.54±0.04	0±0
5	17.50	20.9±0.2	2.12±0.04	0±0
6	22.50	20.2±0.2	1.29±0.04	0±0
7	27.50	20.1±0.1	0.44±0.03	0±0
8	34.00	20.0±0.1	0.18±0.03	0±0
9	42.25	19.9±0.1	0.07±0.03	0±0

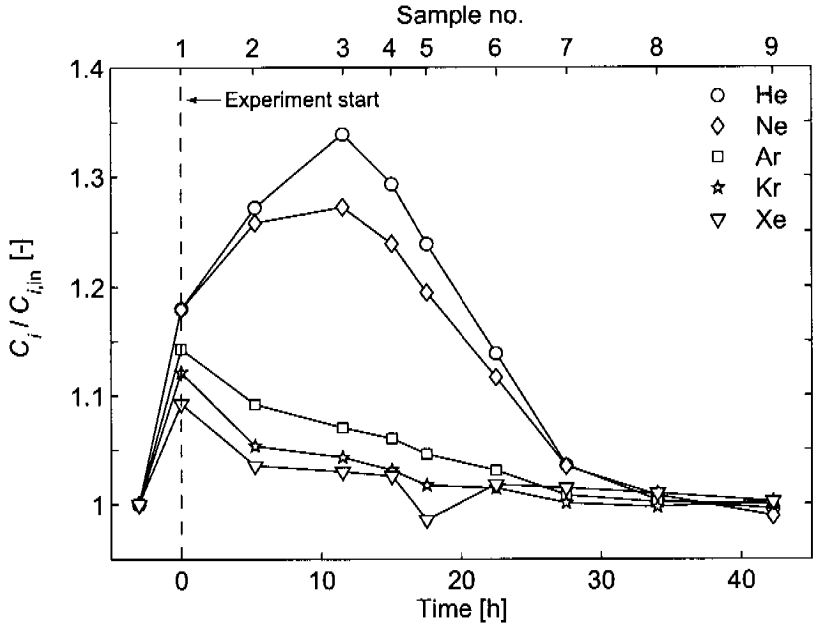

Figure 3.4: Measured dissolved noble gas concentrations during the column experiment. All concentrations are normalized to their respective initial concentration.

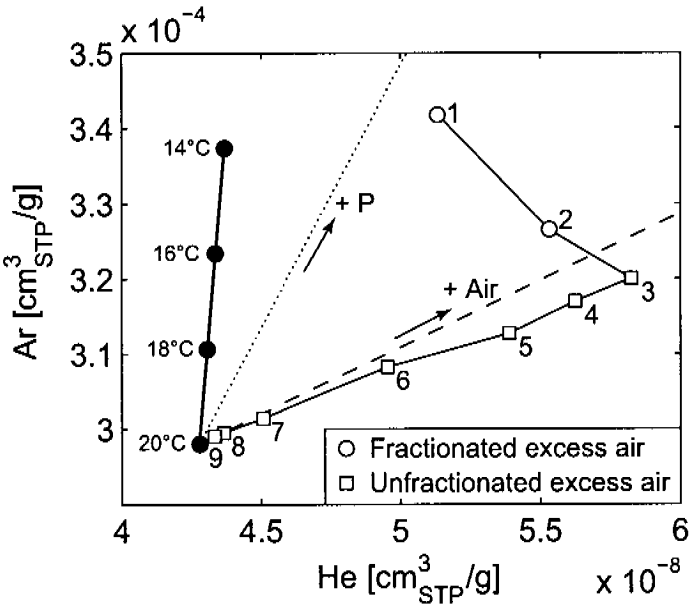

Figure 3.5: Measured He and Ar concentrations during the sand-column experiment. The circles represent atmospheric solubility equilibrium at different temperatures. The dashed line indicates the addition of unfractionated air, and the dotted line denotes solubility equilibrium at increasing pressure. The first two samples (1, 2), which plot between the lines for pure excess air and pressure enhancement, are fractionated with respect to the composition of atmospheric air. All other samples (3 – 9) contain unfractionated excess air, which is indicated by them plotting close to the unfractionated excess air line.

finding casts severe doubt on the validity of the original interpretation of the formation of unfractionated excess air. This astonishing finding will be further elucidated in combination with numerical simulations (see below).

3.3.2 Total dissolved gas pressure

The TDGP was measured during the experiment, starting at time $t = -3$ h, when the sand column was filled with air-equilibrated water (Figure 3.6). The increase in TDGP from $t = -3$ h to the start of the experiment at $t = 0$ h – while the water stagnated in the column and re-equilibrated with the entrapped gas phase – probably represents both the typical response time of the TDGP probes, which is in the order of ~15 min (Figure 3.3), and the delay due to the kinetically controlled gas exchange between the initially air-equilibrated water and the entrapped air. Starting at time $t = 0$ h, when the water flow was initiated, the TDGP at the outflow of the column was quasi-constant, lasting until about $t = 20$ h, when the TDGP decreased rapidly – most likely due to the complete dissolution of the entrapped gas phase. The time of this rapid decrease in TDGP corresponds reasonably well to the time of decrease in the noble gas supersaturations (see Figure 3.4), but with a slight delay. Possible reasons for this delay will be discussed below. The maximum TDGP relative to the atmospheric

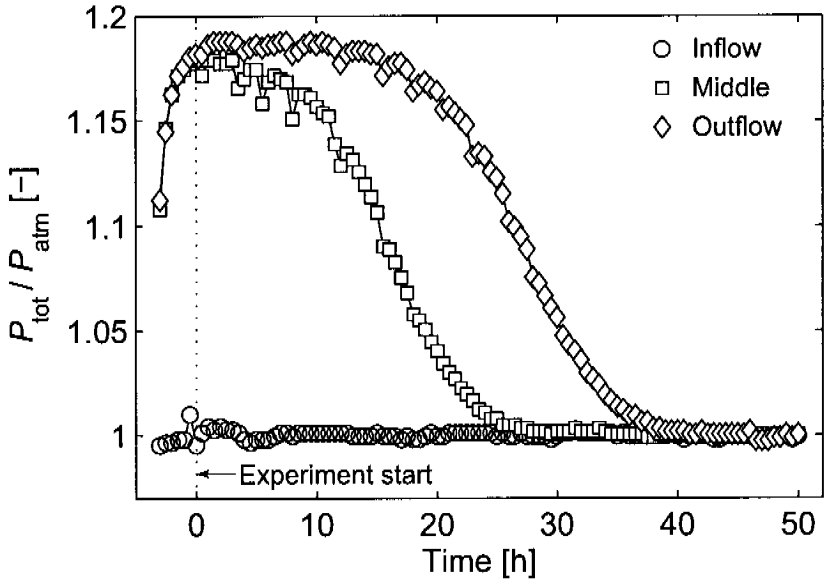

Figure 3.6: Total dissolved gas pressure (TDGP) measured in the inflow to the column, at the middle of the column, and in the outflow of the column during the sand-column experiment.

pressure of about 1.18 agrees very well with the hydrostatic pressure imposed on the column, corresponding to the hydraulic head above the sand column of 1.85 m.

3.3.3 Modeling

To gain a better understanding of the underlying physical processes and the role of kinetic effects on the formation of excess air, the dissolution of entrapped air was simulated using both the KBD model of Holocher et al. (2003) and the local equilibrium model of Cirpka and Kitanidis (2001) (see also section 2.4). All parameter values used for the KBD and local equilibrium models are summarized in Table 3.3 ("Sand column"). Figures 3.7 and 3.8 show the results of the simulations of gas dissolution using the KBD and local equilibrium models.

The noble gas concentrations simulated by the KBD model (Figure 3.7) agree very well with those measured in the water samples from the outflow of the column.

The results of the local equilibrium model (Figure 3.8) obviously fail to match the measured noble gas concentrations. The temporal evolution of the dissolved gas concentrations cannot be reproduced by the local equilibrium model – not even qualitatively. This is especially true of the abrupt decrease in supersaturation at the time when all bubbles are near to complete dissolution. It can therefore be concluded that kinetic effects, which are included in the KBD model but not in the local equilibrium model, play an important role during the gas dissolution process in the column experiment. Under such conditions and at such time scales, the assumption of local equilibrium between the water and entrapped air bubbles is not valid.

Table 3.3: Model parameter values used in the KBD and local equilibrium model simulations. The simulation 'sand column' refers to the experiment conducted in this work. The simulation 'sand filter' is based upon reprocessed data of Holocher et al. (2003). The parameter values used for different scenarios to compare the KBD and local equilibrium models are summarized under 'model comparison'.

Simulation			Sand column	Sand filter	Model comparison
Model parameter				Value	
Flow direction			H[a]	VD[b]	H, VD, VU[c]
h	Hydraulic head	[m]	1.85[d]	0.2[e]	1[d] (H), 0[e] (VD), 1[e] (VU)
L	Column length	[m]	1	1	1
r	Initial bubble radius	[mm]	1.5	0.35	0.5
Θ	Total porosity	[-]	0.4	0.4	0.4
r_{a-w}	Air-water ratio	[-]	0.074	0.2	0.05
T	Water temperature	[°C]	20	8	10
P_{atm}	Atmospheric pressure	[atm]	0.9564	0.9615	1
S	Salinity	[‰]	0	0	0
q	Darcy velocity	[m/s]	$1.18 \cdot 10^{-4}$	$2.78 \cdot 10^{-5}$	10^{-4}, 10^{-5}, 10^{-6}
D_L	Dispersion coefficient	[m^2/s]	$2.58 \cdot 10^{-6}$	10^{-6}	0
Initial concentrations					
$C_{He,in}$	He	[$\cdot C_{He,equ}$]	1.02	1.09	1
$C_{Ne,in}$	Ne	[$\cdot C_{Ne,equ}$]	1.01	1.07	1
$C_{Ar,in}$	Ar	[$\cdot C_{Ar,equ}$]	1.01	1.02	1
$C_{Kr,in}$	Kr	[$\cdot C_{Kr,equ}$]	0.99	1.01	1
$C_{Xe,in}$	Xe	[$\cdot C_{Xe,equ}$]	1.01	1.01	1
$C_{N_2,in}$	N_2	[$\cdot C_{N_2,equ}$]	1	1.04	1
$C_{O_2,in}$	O_2	[$\cdot C_{O_2,equ}$]	1	1.02	1

[a] H: Horizontal, [b] VD: Vertically downward, [c] VU: Vertically upward
[d] Above center of column, [e] Above top of column

The calculated TDGP also agrees qualitatively with the corresponding measured values (Figure 3.9), although the timing of the decrease in TDGP is delayed with respect to both the model prediction and the observed decrease in measured noble gas concentrations. The increase in TDGP before the actual start of the experiment ($t < 0\,\mathrm{h}$) seems to be faster than the increase proposed by the KBD model. Furthermore, the maximum measured TDGP values are significantly higher than the simulated values. The following may explain at least part of these discrepancies:

(i) Diffusion of the gases through the silicone-rubber tube might be significantly slower than expected (see Eq. (3.5)); i.e., the diffusivity of N_2 in silicone rubber might be lower than the value given above ($D^{\mathrm{sil}}_{N_2} = 4 \cdot 10^{-10}\,\mathrm{m^2/s}$). However, the experimental data of Manning et al. (2003) and H. Surbeck (pers. comm.) indeed show that the typical equilibration time for N_2 is about 15 min or less. Other authors report even larger diffusivities for N_2 in silicone rubber (e.g., Merkel et al., 2000). Also, the increase in TDGP in the time interval before the flow started was too fast for slow mass transfer to occur through the tube wall.

(ii) Gas sorption in the silicone-rubber tube could be a further possible explanation for the observed delay. However, solubility data for atmospheric gases in silicone rubber are rare in the literature. Merkel et al. (2000) report a solubility of N_2 in silicone of about $0.1\,\mathrm{cm^3_{STP}/(cm^3 \cdot atm)}$. Gas sorption in the silicone rubber might therefore cause a delay in the response time of the TDGP probes. However, the experimental data of Manning et al. (2003) and H. Surbeck (pers. comm.) to determine the response time of the TDGP probe contradict this hypothesis. Like hypothesis (i), this second hypothesis cannot explain the fast increase in TDGP at $t < 0\,\mathrm{h}$ with respect to the prediction of the KBD model.

(iii) Since silicone rubber is hydrophobic – i.e., the contact angle between silicone and water is greater than 100° for most kinds of silicone rubber – it is likely that entrapped gas bubbles concentrate at the surface of the silicone-rubber tube. This accumulation of gas bubbles attached to the tube's surface would have two major effects on the TDGP measurements. First, gas exchange between the tube void and the attached gas bubbles would probably be much faster than the kinetically slowed gas exchange occurring between the water, the gas bubbles, and the tube void. This would explain why the increase in TDGP at $t < 0\,\mathrm{h}$ is faster than predicted by the KBD model. Second, the accumulation of gas bubbles at the surface of the tube increases the local gas saturation, and hence increases the time that elapses until all gas bubbles in the immediate vicinity of the tube are completely dissolved. This could explain the observed time lag between the decrease in TDGP and the calculated TDGP values based on the KBD model. The difference in the maximum values of TDGP could also be explained by this hypothesis. Since kinetic effects are much less significant for the direct gas exchange between the tube void and attached gas bubbles, the maximum TDGP would be higher than the values calculated by the KBD model. This is indicated by the results of the simulation using the local equilibrium model (see Figure 3.8), which shows considerably higher supersaturations, especially for the light noble gases and N_2.

In conclusion, the third hypothesis of an increase in gas saturation at the surface of the silicone-rubber tube due to its hydrophobic nature seems to be the most likely explanation for the observed discrepancies between measured and modeled TDGP. However, to really pin down the (in)validity of the above mentioned hypotheses, further experiments would be necessary to determine exact values for the contact angle, and for the diffusivities and solubilities of atmospheric gases in the silicone rubber used here.

Comparison of the KBD and local equilibrium models

Although the results of the sand-column experiment reveal that kinetic effects are significant under the conditions pertaining during the experiment, it remains unclear under which conditions the simulated gas concentrations of the KBD and local equilibrium models would become essentially identical. From a conceptual point of view, kinetic effects should be insignificant for small flow velocities, because the flow velocity, and hence the residence time of the water in the quasi-saturated porous medium, determines the contact time between the mobile water and the immobile gas bubble. However, the flow velocity also influences the mass transfer coefficient (cf. Eq. (2.18)), and kinetic effects therefore increase with decreasing flow velocity. To investigate the difference between the KBD and local equilibrium models in relation to flow velocity, (i) the experimental data of Holocher et al. (2003) were reprocessed, and (ii) simulation results for different flow velocities were compared using both models.

From a more general point of view, the nondimensional Damköhler number Da can be used to estimate the degree of non-equilibrium between water and the entrapped gas phase; i.e., it can be used to judge whether the local equilibrium assumption is appropriate.

$$Da = \frac{\beta_i \cdot L}{v} \tag{3.7}$$

where L is the characteristic length (=column length), v is the water flow velocity, and β_i is the rate constant of mass transfer:

$$\beta_i = \left(\frac{A_b}{V_w}\right) \cdot k_i \tag{3.8}$$

k_i is the mass transfer coefficient (cf. Eq. (2.18)), and (A_b/V_w) is the specific interfacial contact area:

$$\left(\frac{A_b}{V_w}\right) = \frac{A_b}{V_b} \cdot \frac{V_b}{V_w} = \frac{3}{r} \cdot \frac{S_g}{1 - S_g} \tag{3.9}$$

where A_b is the bubble surface, V_b is the bubble volume, and V_w is the water volume. Substitution of Eqs. (2.18) and (3.9) into Eq. (3.8) yields:

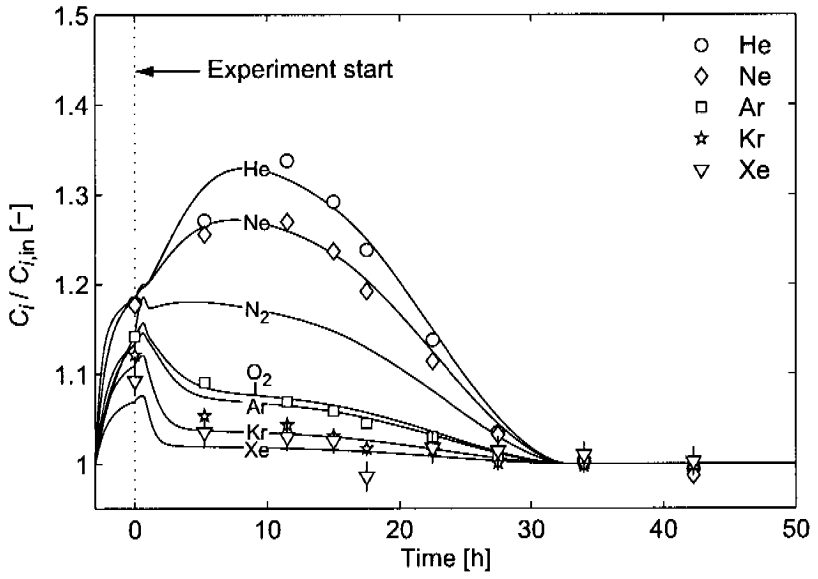

Figure 3.7: Measured (symbols) and modeled (solid lines) noble gas concentrations in the sand-column experiment calculated using the KBD model. All concentrations are normalized to the respective concentrations in the inflowing water. The dotted line denotes the start of the experiment at $t = 0$ h.

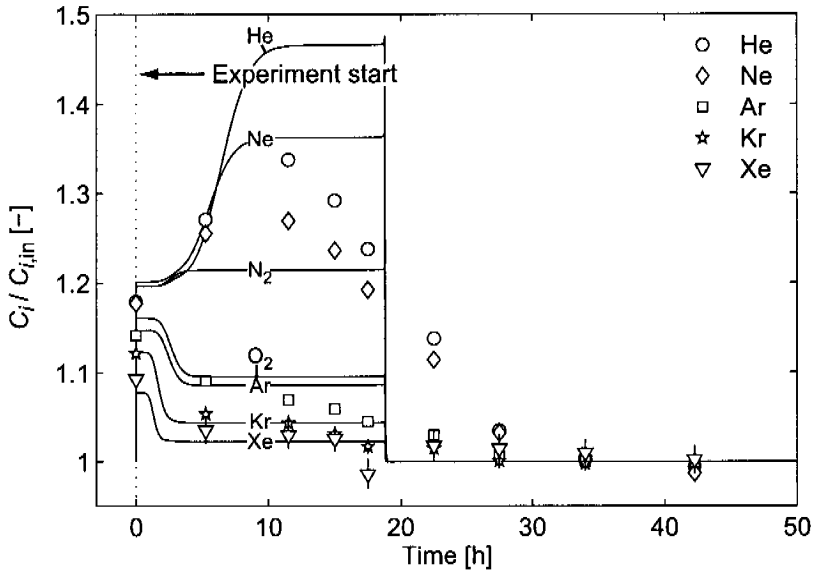

Figure 3.8: Measured (symbols) and modeled (solid lines) noble gas concentrations in the sand-column experiment calculated using the local equilibrium model. All concentrations are normalized to the respective concentrations in the inflowing water.

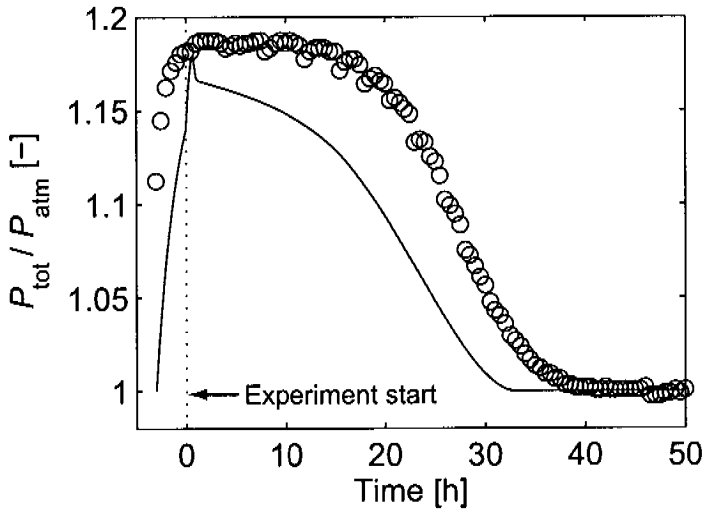

Figure 3.9: Measured (circles) and modeled (solid line) TDGPs in the sand-column experiment calculated using the KBD model. All TDGPs are normalized to the respective TDGP in the inflowing water, which is identical to the ambient atmospheric pressure. Three major differences between the measured and modeled TDGPs are obvious: (i) the increase in measured TDGP at $t < 0$ h is faster than the increase in calculated TDGP; (ii) the timing of the decrease in measured TDGP between $t \approx 20$ and $t \approx 35$ h is delayed substantially with respect to the calculated values; and (iii) the maximum measured TDGP is lower than the maximum modeled TDGP.

$$\beta_i = \frac{3S_g D_{w,i}}{r(1-S_g)} \left(\frac{1}{r} + \sqrt{\frac{v}{2\pi r D_{w,i}}} \right) \tag{3.10}$$

Both gas saturation S_g and bubble radius r change during the experiment. As a result, the Damköhler number also changes during the experiment, decreasing continuously with decreasing gas saturation and decreasing bubble radius. Therefore, all following results refer to the initial Damköhler number Da_{ini}, which is defined as:

$$Da_{ini} = \frac{\beta_i(t=0) \cdot L}{v} \tag{3.11}$$

Several authors report that the assumption of local equilibrium is valid for $Da > 100$ (Brusseau, 1992, and references therein). A Damköhler number of $Da < 10$, however, shows that mass transfer is controlled significantly by kinetics. In this case the assumption of local equilibrium would be inappropriate.

Holocher et al. (2003) conducted a large-scale column experiment using a sand filter in the waterworks of the city of Zurich. The initially dry quartz-sand filter, which is used for drinking water treatment, was filled with water from the bottom of the sand to the top. Air bubbles were entrapped during this process. Then, a downward water flow was initiated and the entrapped bubbles were progressively dissolved, resulting in the formation of excess air in the water flowing through the sand filter. Holocher

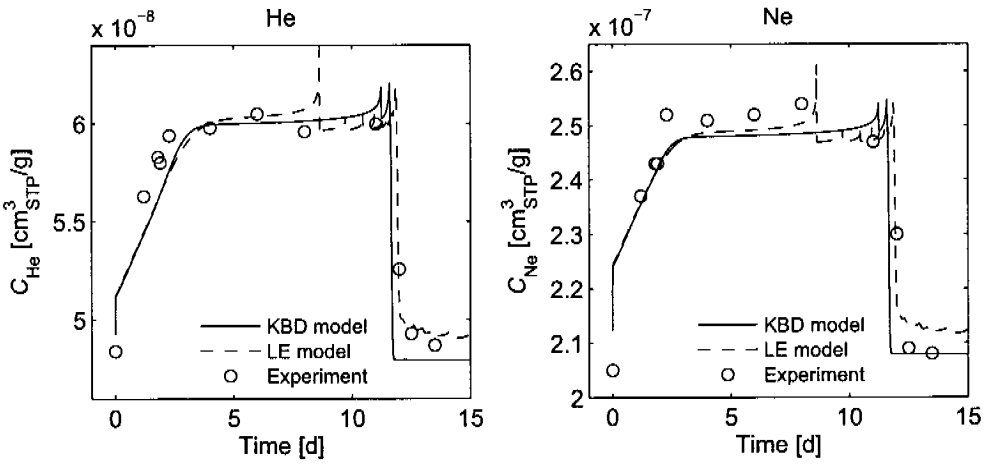

Figure 3.10: He and Ne concentrations in the large-scale sand-filter experiment measured (symbols) and modeled (lines) using the KBD and local equilibrium models (reprocessed data of Holocher et al., 2003).

et al. (2003) used the KBD model to simulate this experiment. The noble gas concentrations measured in the outflow of the sand filter agree well with the concentrations predicted by the KBD model. The model parameter values are given in Table 3.3 ("Sand filter"). The Darcy velocity during the experiment was $2.78 \cdot 10^{-5}$ m/s, which is about an order of magnitude smaller than the Darcy velocity used in the column experiment described above. Therefore, kinetic effects should be less significant in the experiment of Holocher et al. (2003). In addition to using the KBD model, the experiment was also simulated using the local equilibrium model. The results indeed show no significant differences between the results of the KBD and local equilibrium models (Figure 3.10). Kinetic effects are therefore negligible in the experiment of Holocher et al. (2003); i.e., the assumption of local equilibrium between the flowing water and the entrapped air bubbles is appropriate for the prevailing physical conditions.

The initial Damköhler number Da_{ini} for this experiment is 209; i.e., clearly greater than 100 (see above). This also suggests that the assumption of local equilibrium is valid in this case.

Additionally, reference simulations for three different Darcy velocities, and hence for three different values of Da_{ini}, for both horizontal and vertical flow in a column 1 m long were performed using the KBD and local equilibrium models (see Table 3.3, 'Model comparison'). For better comparability, all data are plotted against nondimensional pore volume.

$$\text{Pore Volume} = \frac{q \cdot t}{\Theta \cdot L} \tag{3.12}$$

with the Darcy velocity (= specific flux) q, porosity Θ, and column length L.

The values of Da_{ini} for the Darcy velocities of 10^{-4}, 10^{-5}, and 10^{-6} m/s are 14, 61, and 365, respectively. The local equilibrium assumption can therefore be expected to apply in the case of the latter simulation, with a Darcy velocity of 10^{-6} m/s, and

might still be a reasonable assumption for a Darcy velocity of 10^{-5} m/s. However, kinetic effects are expected to play an important role for a Darcy velocity of 10^{-4} m/s, and the local equilibrium assumption is probably not valid in this case. The results indeed show that the modeled noble gas concentrations for $Da_{\mathrm{ini}} = 14$ ($q = 10^{-4}$ m/s, water residence time $\tau \approx 1$ h in the sand column) differ significantly between the two models (Figure 3.11). By contrast, the results of the KBD and local equilibrium models are similar for $Da_{\mathrm{ini}} = 61$ ($q = 10^{-5}$ m/s, $\tau \approx 10$ h), and essentially identical for $Da_{\mathrm{ini}} = 365$ ($q = 10^{-6}$ m/s, $\tau \approx 100$ h). Therefore, one can conclude that kinetic effects are only of significant importance for $Da << 100$; i.e., kinetic effects play an important role for large flow velocities and short flow paths through the quasi-saturated porous medium, but not otherwise.

Figure 3.12 shows values of Da_{ini} for the three different Darcy velocities q applied in the simulations described above, and as a function of characteristic length L and gas saturation S_g. In the case of a Darcy velocity of 10^{-4} m/s, which would correspond to a high flow velocity in natural aquifers, the local equilibrium assumption is only valid for a large characteristic length and a large initial gas saturation S_g (see Figure 3.12). In contrast, for Darcy velocities of 10^{-5} or 10^{-6} m/s, which would be typical flow velocities in natural systems, the local equilibrium assumption is valid over a broad range of values of L and S_g.

System behavior

Neglecting dispersion, the coupled transport of the dissolved gases in the presence of an entrapped gas phase can be described by a system of hyperbolic equations. Each partitioning compound is characterized by its corresponding Henry coefficient. Therefore, variations of the composition are split into variations of each compound, each propagated with its characteristic velocity. In a system with n different gases, n waves travel through the system, each with its own characteristic velocity. Because the dissolved concentrations and the partial pressures of the noble gases in the gas phase are very small with respect to those of the main air constituents N_2 and O_2, variations in the noble gas concentrations have hardly any effect on the gas saturation, and therefore hardly affect the concentrations and partial pressures of the other gases. By contrast, changes in the concentrations of the main constituents N_2 and O_2 significantly affect the concentrations and partial pressures of all the other gases.

Since hydrostatic pressure dominates the solubility equilibrium between water and the entrapped gas phase, the dissolution of entrapped gas depends significantly on flow direction. If the direction of flow is horizontal, the hydrostatic pressure is almost constant along a short flow distance, and hence the gas equilibrium is also almost identical along the same distance. In contrast, in the case of vertical flow, there is a hydrostatic pressure gradient either in the direction of the flow (for vertically downward flow) or in the reverse direction of the flow (for vertically upward flow). As a result, the gas equilibrium also changes along the flow paths. The temporal characteristics of bubble dissolution are therefore different for horizontal, vertically downward, and vertically upward flow directions.

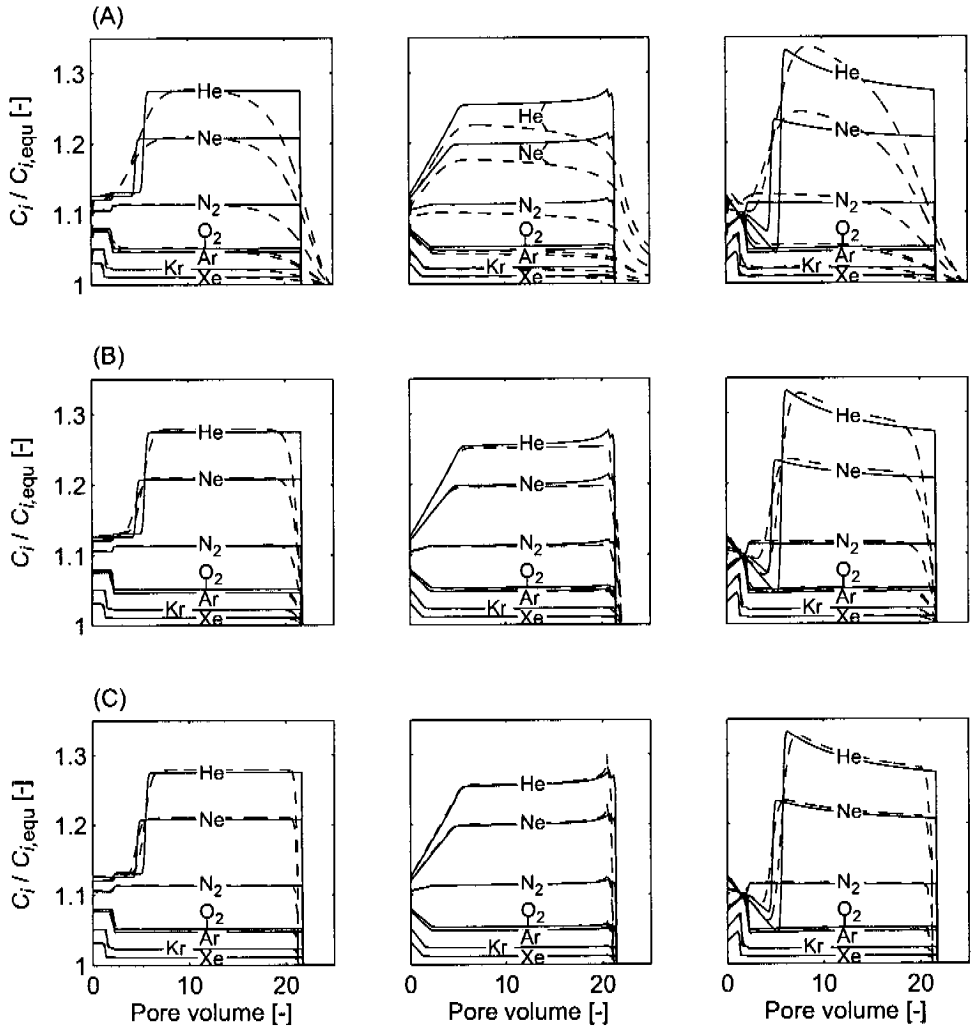

Figure 3.11: Comparison of the results of the KBD model (dashed lines) and the local equilibrium model (solid lines) at the outflow of the column 1 m long for three different values of Da_{ini}: (A) $Da_{\text{ini}} = 14$ ($q = 10^{-4}$ m/s, $\tau \approx 1$ h), (B) $Da_{\text{ini}} = 61$ ($q = 10^{-5}$ m/s, $\tau \approx 10$ h), (C) $Da_{\text{ini}} = 365$ ($q = 10^{-6}$ m/s, $\tau \approx 100$ h). Three different flow directions are compared: horizontal flow (left-hand panel), vertically downward flow (middle panel), and vertically upward flow (right-hand panel).

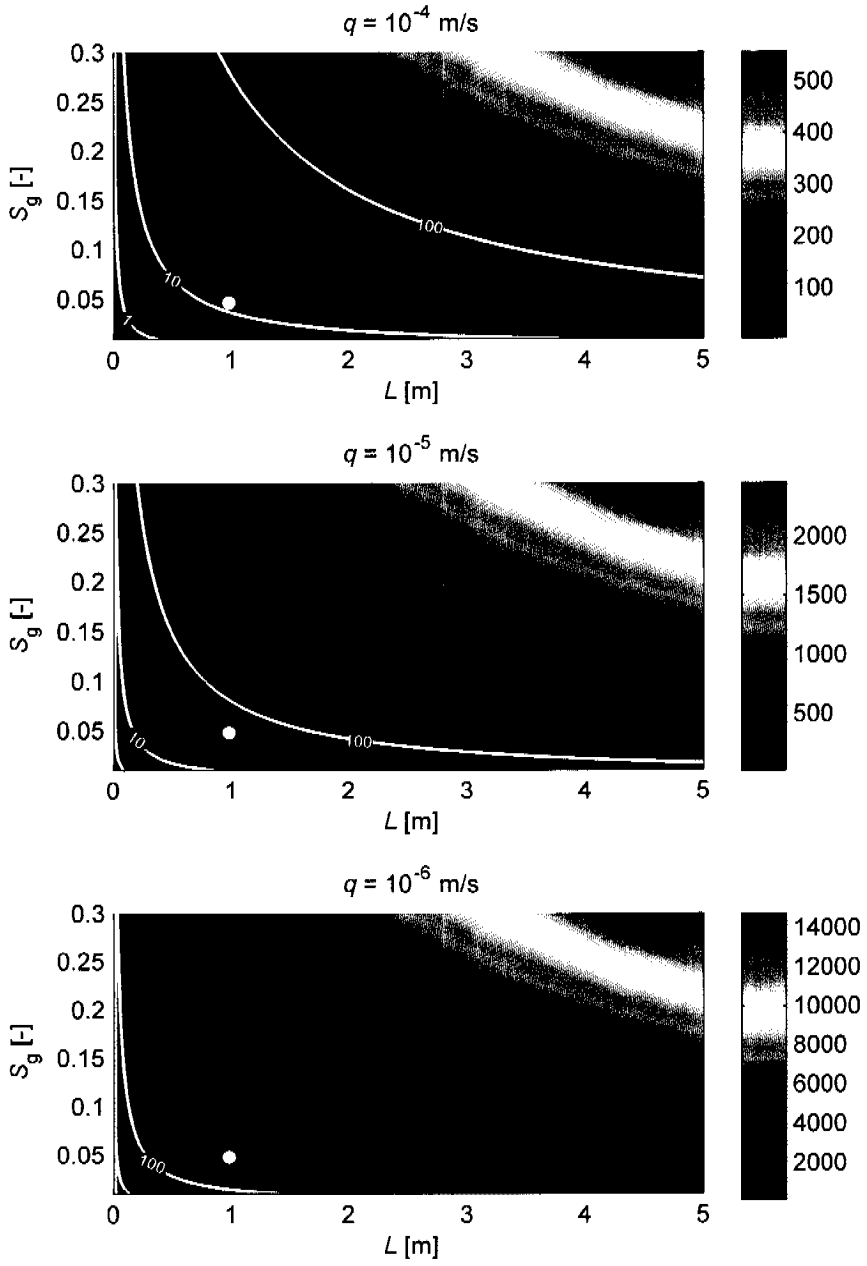

Figure 3.12: Initial Damköhler number Da_{ini} for three different Darcy velocities q, and as a function of characteristic length L and initial gas saturation S_g. The values of Da_{ini} for the three reference simulations described in the text are indicated by white dots.

Figure 3.13 shows the results of simulations using the KBD and local equilibrium models for horizontal, vertically downward, and vertically upward flow. All other model parameter values are identical for all simulations (see Table 3.3, "Model comparison"). Three main differences in the system behavior are obvious (see Figure 3.13):

(i) In all simulations the supersaturations evolve into a quasi-constant, plateau-like phase which lasts for a long time period during bubble dissolution. However, the behavior from the beginning of the simulation to that plateau phase is different for different flow directions. In the case of horizontal flow, there is a step-wise increase in the supersaturations of the lighter gases (He, Ne, N_2), and a step-wise decrease in the supersaturations of the heavier gases (Ar, Kr, Xe, O_2). In the case of vertically downward flow, by contrast, the supersaturations increase or decrease into the plateau phase, forming a ramp instead of a step. In the third case of vertically upward flow, the lighter gases first decrease and then increase to the plateau phase, and the heavier gases first increase and then decrease to the plateau phase.

(ii) The timing of the complete dissolution of the entrapped air also depends strongly on flow direction. If the flow direction is horizontal, the relationship between complete bubble dissolution in the flow direction and the distance traveled is linear. In the case of vertically downward flow, complete bubble dissolution takes place almost simultaneously throughout the column. Only very close to the inflow does the entrapped air dissolve significantly faster than in the rest of the column. In the case of vertically upward flow, the time of complete bubble dissolution increases more than linearly with distance.

(iii) The evolution of the gas saturation is also different for horizontal and vertical flow directions. In the case of horizontal flow, the gas saturation remains almost constant until abrupt, complete bubble dissolution. In the case of vertically downward flow, the gas saturation decreases linearly with time, whereas vertically upward flow leads to an increase in gas saturation close to the top of the column until instantaneous bubble dissolution occurs. This is because the gas equilibrium decreases with decreasing hydrostatic pressure in the direction of the flow, and the gas phase is therefore relocated and accumulates further downstream; i.e., further towards the top of the column.

Apparently unfractionated excess air

An unexpected finding of the present study is that all samples taken after $t \approx 6\,\mathrm{h}$ after the start of the sand-column experiment contain apparently unfractionated excess air (see above), although an entrapped and progressively dissolving gas phase was definitely present during that time. By contrast, unfractionated excess air is usually attributed to the complete dissolution of entrapped air. This observation is of crucial importance for the interpretation of environmental tracer data.

During the experiment, an entrapped gas phase was present and this gas phase must have been fractionated with respect to atmospheric air, because the composition of the dissolving gas phase changes relative to atmospheric air owing to the different

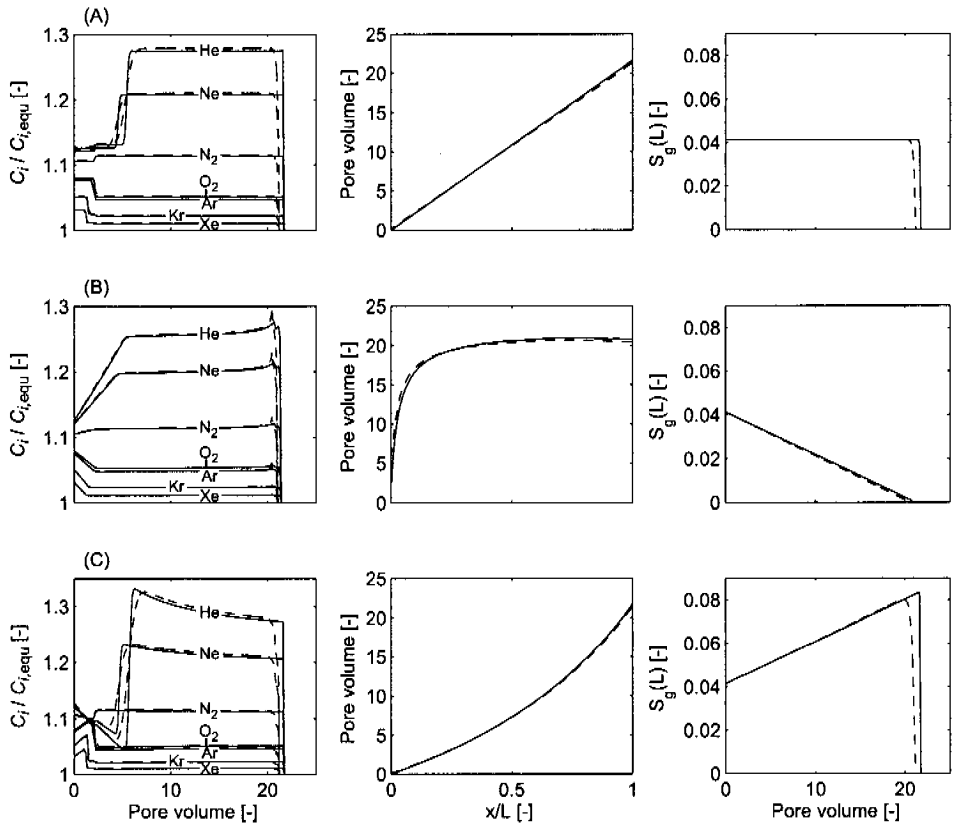

Figure 3.13: The effects of horizontal and vertical flow directions, simulated using the local equilibrium model (solid lines) and the KBD model (dashed lines): (A) horizontal flow, (B) vertically downward flow, and (C) vertically upward flow, for $Da_{\text{ini}} = 365$ ($q = 10^{-6}$ m/s, $\tau \approx 100$ h). The graphs in the middle panel show the pore volumes that are required until complete bubble dissolution is achieved as a function of flow distance x. The graphs in the right-hand panel show the gas saturation at the end of the column.

solubilities of the gases involved. The only reasonable explanation for the formation of apparently unfractionated excess air during the experiment is that the composition of the gas excess, and hence the composition of the gas flux from the entrapped gas bubbles in the water, is very similar to the composition of free atmospheric air. To verify this hypothesis, the elemental ratios of the gas excess component – defined as the difference between the measured concentration and the atmospheric equilibrium concentration of the gas considered – were calculated and compared them with the partial pressure ratios in atmospheric air (Figure 3.14A and B).

For less than about 6 pore volumes – phase 1 of the simulation (see Figure 3.14) – the elemental ratios of the gas excess vary strongly and are significantly different from the atmospheric partial pressure ratios, causing the formation of fractionated excess air. After about 6 pore volumes – phase 2 of the simulation – the elemental ratios in the gas excess are almost constant and are partly very similar to the partial pressure ratios in the atmosphere. The more similar the gases are in terms of solubility, the more similar are the elemental ratios of the gas excess to the partial pressure ratios in the atmosphere (e.g., He/Ne, Kr/Xe, Ar/O_2). The ratios of gases with more different solubilities differ considerably more from the atmospheric partial pressure ratios (e.g., He/Ar, Ne/Xe). Figures 3.14C and 3.14D show the fitted parameters T (noble gas temperature) and F (fractionation factor) obtained from the simulated noble gas concentrations, using the CE model. In phase 1, the CE model proposes the formation of fractionated excess air, indicated by $F > 0$. The fractionation then decreases until unfractionated excess air is formed in phase 2; i.e., the value of F decreases to 0 at the end of phase 1. The NGT (Figure 3.14C) also varies considerably during phase 1 in response to the variations in the elemental ratios of the gas excess. That is, a relative surplus of the more soluble and more temperature-dependent noble gases – e.g., a low ratio of Ne/Xe, or Kr/Xe – is compensated for by a low NGT, and vice versa. In phase 2, the NGT varies only slightly and remains almost constant with time. The relative surplus of the least soluble noble gases He and Ne (see Figure 3.14B) is compensated for by a NGT that is slightly above the real water temperature of 10 °C. Importantly, the excess air component seems to be unfractionated according to the parameter estimation using the CE model, adjusting the NGT to a value which is slightly above the real water temperature of 10 °C. This is the reason why the NGTs of the sand-column experiment described above are slightly higher than the real water temperature (see section 3.3.1). The difference between NGT and real water temperature, however, is smaller than the uncertainty in the NGT calculation using the CE model.

3.4 Conclusions

The sand-column experiments conducted in combination with simulations using the KBD and local equilibrium models show that kinetic effects on the dissolution of entrapped air bubbles play an important role for small values of $Da << 100$; i.e., in the case of large flow velocities or small travel distances through the quasi-saturated zone. For large values of $Da > 100$, both models yield very similar results; i.e., the

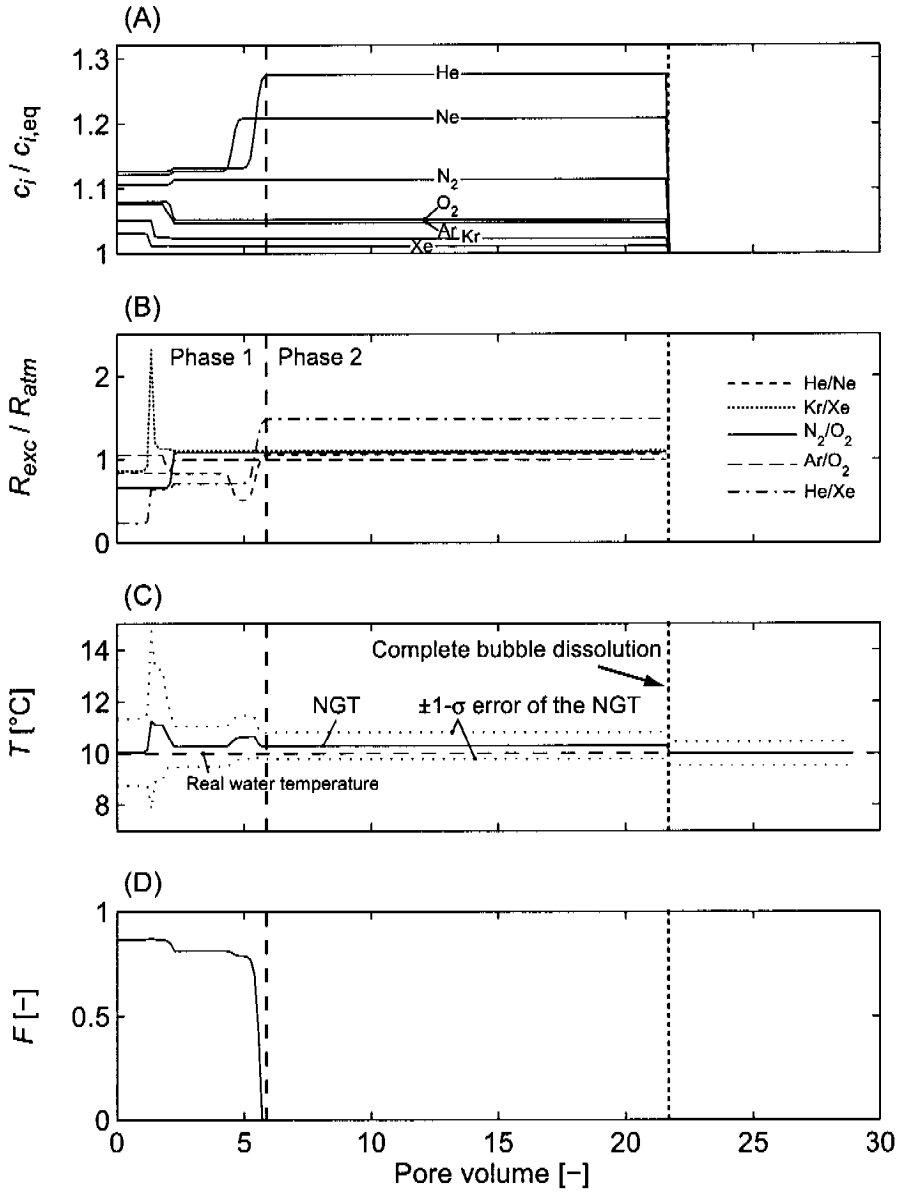

Figure 3.14: (A) Relative supersaturations during the dissolution of entrapped air calculated using the local equilibrium model. (B) Elemental ratios of the gas excess relative to the partial pressure ratios of atmospheric air. (C) Noble gas temperatures (NGT) calculated using the CE model. (D) Fractionation factor F determined using the CE model.

assumption of local solubility equilibrium between the water and gas phases is valid for low flow velocities and large distances.

Groundwater table fluctuations in temperate climate zones are usually within the range of a few meters at most, and the thickness of the quasi-saturated zone is therefore limited. Thus, for vertical flow, the characteristic length scale used in the calculation of the Damköhler number is limited. Under these conditions, flow velocities of 10^{-4} m/s or greater require that kinetic effects on gas dissolution be accounted for, whereas they may be neglected for velocities of 10^{-5} m/s or smaller. For horizontal flow, the travel distance in the quasi-saturated zone can be considerably greater, thus extending the range of applicability the local equilibrium model.

As groundwater flow velocities are usually on the order of several meters per day or less in natural aquifers, the comparison of the KBD and local equilibrium models suggests that kinetic effects are probably of minor importance in the field, and that the assumption of local equilibrium between the groundwater and entrapped air is often an appropriate one. The residence time of groundwater in the quasi-saturated zone of sandy aquifers is therefore very likely to be long enough for equilibrium between the groundwater and the entrapped gas phase to be reached; i.e., the corresponding value of Da is likely to be greater than 100. By contrast, gas exchange in the highly conductive hyporheic zone of a (mountain) torrent, for example, might be subject to very short water residence times, and therefore equilibrium between the water and gas phases would not be reached; i.e., corresponding values of Da are considerably smaller than 100. If the assumption of local equilibrium is valid, the dissolution of entrapped air can be simulated using the local equilibrium model, which has the advantage of being much faster than the KBD model in terms of computing time.

Although a majority of groundwater samples contain excess air which is fractionated with respect to the composition of free atmospheric air, unfractionated excess air is also frequently found in groundwaters and is usually attributed to the complete dissolution of entrapped air. However, it is also well known that the volume of entrapped air within the quasi-saturated zone is usually very large relative to the increase in hydrostatic pressure that is produced in response to only moderate groundwater table fluctuations; e.g., fluctuations that are on the order of a few meters in temperate climate regions, such as in Central Europe (Kipfer et al., 2002, and references therein). From a strict, physical point of view, the question of how unfractionated excess air can be produced despite the fact that the increase in hydrostatic pressure is quite limited therefore remains open.

The sand-column experiment, in combination with numerical simulations, indicates that apparently unfractionated excess air can be produced without the complete dissolution of entrapped air. Moreover, during the progressive dissolution of the entrapped gas phase, fractionated excess air is only produced during the beginning of the dissolution process. Apparently unfractionated excess air is generated during a predominant period of time over which the gas bubbles evolve in such a manner that the gas fluxes out of these bubbles show elemental ratios that are very similar to the partial pressure ratios in atmospheric air. In natural aquifers, the ratio of flow veloc-

ity (and hence the residence time within the quasi-saturated zone) to the frequency of water table fluctuations most likely determines whether fractionated or unfractionated excess air is produced. That is, if the flow velocity is high, the duration of phase 1 (cf. Figure 3.14), in which fractionated excess air is produced, is relatively short. In this case, fractionated excess air is produced primarily only when the frequency of the groundwater table fluctuations is high. By contrast, if the flow velocity is very low, phase 1 lasts longer, and fractionated excess air is also generated mainly when the frequency of the groundwater table fluctuations is low.

In conclusion, the presence of unfractionated excess air should not necessarily be attributed to the complete dissolution of entrapped air. Instead, the formation of excess air which, for the reasons described above, is only apparently unfractionated provides an alternative explanation. This explanation may apply for instance when the increase in hydrostatic pressure as indicated by groundwater table fluctuations is too small to cause complete dissolution of entrapped air, which is probably often the case in natural aquifers. In fact, as the classical pure excess air model has not been verified in the field, it is likely that this newly proposed mechanism involving the formation of apparently unfractionated excess air may apply much more often than even the original conceptual mechanism of complete bubble dissolution.

Chapter 4

Field experiments yield new insights into gas exchange and excess air formation in natural porous media

This chapter has been published in *Geochimica et Cosmochimica Acta* (Klump et al., 2007).

Abstract

Gas exchange between seepage water and soil air within the unsaturated and quasi-saturated zones is fundamentally different from gas exchange between water and gas across a free boundary layer, e.g., in lakes or rivers. In addition to the atmospheric equilibrium fraction, most groundwater samples contain an excess of dissolved atmospheric gases which is called "excess air". Excess air in groundwater is not only of crucial importance for the interpretation of gaseous environmental tracer data, but also for other aspects of groundwater hydrology, e.g., for oxygen availability in bioremediation and in connection with changes in transport dynamics caused by the presence of entrapped air bubbles. Whereas atmospheric solubility equilibrium is controlled mainly by local soil temperature, the excess air component is characterized by the (hydrostatic) pressure acting on entrapped air bubbles within the quasi-saturated zone. Here we present the results of preliminary field experiments in which we investigated gas exchange and excess air formation in natural porous media. The experimental data suggest that the formation of excess air depends significantly on soil properties and on infiltration mechanisms. Excess air was produced by the partial dissolution of entrapped air bubbles during a sprinkling experiment in fine-grained sediments, whereas similar experiments conducted in coarse sand and gravels did not lead to the formation of excess air in the infiltrating water. Furthermore, the experiments revealed that the noble gas temperatures determined from noble gases dissolved in seepage water at different depths are identical to the corresponding in-situ soil temperatures. This finding is important for all applications of noble gases as a paleotemperature indicator in groundwater since these applications are always based on the assumption that the noble gas temperature is identical to the (past) soil temperature.

4.1 Introduction

Atmospheric gases are incorporated into groundwater by gas exchange between seepage water and soil air during infiltration. The atmospheric solubility equilibrium is controlled by soil temperature and atmospheric pressure. However, the concentrations of atmospheric gases dissolved in groundwater are usually found to exceed their respective atmospheric equilibrium concentrations. Because the composition of the excess gas fraction is often similar to that of atmospheric air, Heaton and Vogel (1981) introduced the term "excess air" for this characteristic excess gas component of groundwater. Since the first observation of Ar supersaturation in Japanese aquifers (Oana, 1957), excess air in groundwater has been reported in numerous groundwater studies under different climatic and hydrogeological conditions, including studies in different climatic regions and on different aquifer types as well as studies on both young and old groundwaters (Mazor, 1972; Stute et al., 1995b; Wilson and McNeill, 1997; Aeschbach-Hertig et al., 1999, 2000; Kipfer et al., 2002). Thus, the presence of excess air is now known to be a fundamental property of almost all kinds of groundwater.

A widely accepted conceptual model of excess air formation is the partial dissolution of entrapped air bubbles within the quasi-saturated zone (Heaton and Vogel, 1981; Holocher et al., 2002, 2003). Due either to a rising groundwater table or to the formation of quasi-saturated lenses within the unsaturated zone during the infiltration process, the water phase does not completely remove the gas phase from the pore space of the soil matrix. Instead, air bubbles are entrapped by the surrounding water phase and are exposed to an increased hydrostatic pressure. As a result, the local solubility equilibrium exceeds that of the free atmosphere, and hence the air bubbles are forced to dissolve partly or completely in the water phase, depending on the degree of local pressure enhancement.

Excess air and its formation are of great importance in subsurface hydrology. Atmospheric trace gases – e.g., the noble gases, sulfur hexafluoride, and chlorofluorocarbons – are used as environmental tracers for investigating physical processes in groundwater, for reconstructing environmental conditions in the past, and for dating purposes (Cook and Herczeg, 2000; Kipfer et al., 2002). Most applications of gaseous environmental tracers require separation of the excess air component from the atmospheric equilibrium fraction. This is needed to interpret the tracer data in terms of the environmental conditions prevailing during water infiltration. In order to reliably identify and separate out the excess air component, different lumped-parameter models have been developed that are commonly used to correct noble gas concentrations of groundwater samples for the excess air component (Kipfer et al., 2002). These simplistic excess air models are clearly limited in a strict, physical sense, and yield a parameterization of the excess air rather than a mechanistic description of the processes controlling its formation.

Although the phenomenon of excess air in groundwater has been known for decades, a sound physical description of its formation in natural aquifer systems is still lacking. Recently, Holocher et al. (2003) developed the Kinetic Bubble Dissolution (KBD)

model, which gives a mechanistic description of the dissolution of entrapped air bubbles in quasi-saturated porous media based on physical principles. In addition, Holocher et al. (2002) were able to produce excess air in sand column experiments, the results of which were in accordance with the predictions of the KBD model and with observations in the field. These experiments confirm the validity of the conceptual model of the dissolution of entrapped air bubbles on the laboratory scale and yield some insight into the real physical processes that govern air/water partitioning within the quasi-saturated zone and which are parameterized by the lumped-parameter models. However, the validation of the concepts which describe the formation of excess air under natural conditions has up to now been addressed only poorly.

In this paper, we present the results of two field experiments conducted under different hydrological conditions to assess gas exchange and the formation of excess air in quasi-saturated soils under natural conditions, using dissolved noble gases as conservative tracers. We focused mainly on soil temperature and air entrapment, as these factors are presumed to exert a crucial control on gas exchange and excess air formation during infiltration.

4.2 Theory

4.2.1 Noble gases as environmental tracers

Noble gases are widely used as environmental tracers in subsurface hydrology. Atmospheric (noble) gases are incorporated into groundwater by gas exchange between rainwater and atmosphere, and between seepage water and soil air during infiltration. As soon as the water enters the saturated zone, no further gas exchange occurs. Since noble gases are chemically inert, the groundwater maintains the dissolved noble gas concentrations as a marker of the physical conditions (temperature, pressure, salinity) that prevailed during the infiltration process. This allows past climatic conditions to be reconstructed from atmospheric noble gases dissolved in groundwater (Aeschbach-Hertig et al., 2000; Beyerle et al., 1998, 1999b, 2003; Mazor, 1972; Stute et al., 1995a,b).

The noble gas temperature (NGT), which can be derived from the dissolved noble gas concentrations, is defined by the temperature that prevailed during the last gas exchange between the groundwater and the atmosphere. Since the last gas exchange usually occurs close to the groundwater table during infiltration, the NGT is assumed to be identical to the soil temperature prevailing during groundwater recharge (Stute and Sonntag, 1992; Stute and Schlosser, 1993). The soil temperature is a crucial factor controlling the gas exchange between seepage water and soil air. Numerous paleoclimate studies have been conducted using noble gases to determine past soil temperatures (reviewed by Kipfer et al., 2002). All these studies rely on the assumption that the NGT is equal to the mean annual soil temperature. The field experiments carried out gave us the opportunity to assess the validity of this assumption in addition to conducting the study on excess air formation.

4.2.2 Gas exchange in porous media

Atmospheric gases are incorporated into groundwater as a result of gas exchange between the water and the atmosphere or soil air. The dissolution of atmospheric (noble) gases in natural waters can be described according to Henry's Law:

$$C_i^{\mathrm{equ}} = \frac{C_i^{\mathrm{atm}}}{K_{\mathrm{H},i}(T,S)} = \frac{P_i}{R \cdot T \cdot K_{\mathrm{H},i}(T,S)} \tag{4.1}$$

The equilibrium concentration C_i^{equ} of the dissolved gas i is directly proportional to its local atmospheric concentration C_i^{atm}. Dalton's Law, in which R is the universal gas constant, relates the molar atmospheric concentration of gas i to its partial pressure P_i in the gas phase. The concentration proportionality is given by the nondimensional Henry coefficient $K_{\mathrm{H},i}$, the value of which depends on the physical conditions (e.g., temperature T and salinity S) prevailing during gas partitioning .

The solubilities of the noble gases increase with atomic mass from He to Xe (Weiss, 1970, 1971; Weiss and Kyser, 1978; Clever, 1979). The strongly temperature dependent solubilities of the heavy noble gases Ar, Kr, and Xe allow the temperature that prevailed during infiltration to be reconstructed. The least soluble light noble gases He and Ne react most sensitively to the presence of excess air, and they are therefore used to quantify the excess air component in groundwater samples. However, most groundwaters contain terrigenic He in addition to atmospheric He, and therefore Ne, which is of atmospheric origin only, is commonly used to determine the excess air component in groundwaters. Excess air is therefore often expressed in terms of relative Ne supersaturation (ΔNe); i.e., the Ne excess ($C_{\mathrm{Ne}}^{\mathrm{exc}}$) as a percentage of its atmospheric equilibrium concentration ($C_{\mathrm{Ne}}^{\mathrm{equ}}$).

$$\Delta\mathrm{Ne} = \frac{C_{\mathrm{Ne}}^{\mathrm{exc}}}{C_{\mathrm{Ne}}^{\mathrm{equ}}} \cdot 100\,[\%] \tag{4.2}$$

Whereas solubility increases with atomic mass, molecular diffusivity decreases. Hence, the light noble gases He and Ne react more sensitively to any diffusive alterations in the dissolved noble gas concentrations than do the heavier noble gases Ar, Kr and Xe.

Kinetic bubble dissolution (KBD) model

Holocher et al. (2003) developed the KBD model to describe the dissolution of entrapped air bubbles in quasi-saturated porous media. The bubbles are assumed to consist of the noble gases He, Ne, Ar, Kr, Xe, and the two main air constituents N_2 and O_2. The mass transfer between the spherical air bubbles and the water phase is modeled by assuming rapid local equilibration between the air bubbles and the surrounding water phase according to Henry's Law (equation 4.1) and by making use of a water-side boundary layer gas exchange approach (e.g., Schwarzenbach et al., 2003). The local pressure in the air bubbles has to be equal to the local total pressure, which is the sum of atmospheric, hydrostatic, and surface-tension pressures, the latter

being the result of the curvature of the bubble surface. In the case of flowing groundwater, the compositions of the gas and water phases change due to dissolution and due to the differing Henry coefficients of the gases, and the volumes of the gas bubbles shrink with time. As a result, gases from the gas phase are transferred to the water phase, yielding a typical excess air signal in the groundwater. Given the hydrological settings as boundary conditions, the KBD model was able to reproduce the amount as well as the elemental fractionation of excess air in laboratory experiments (Holocher et al., 2002). For a more detailed description of the KBD model, see Holocher et al. (2003).

Lumped-parameter models

For practical purposes, including the interpretation of dissolved noble gases in groundwater, simplified lumped-parameter models are commonly used for the parameterization of the amount of excess air in order to separate the measured gas concentrations into equilibrium and excess air components. Several conceptual excess air models have been developed. The simplest model assumes the excess air component to be unfractionated with respect to atmospheric air (Heaton and Vogel, 1981), whereas other models presume fractionated excess air (e.g., partial re-equilibration model, Stute et al., 1995b; closed-system equilibration model, Aeschbach-Hertig et al., 2000; capillary pressure model, Mercury et al., 2004).

According to the closed-system equilibration (CE) model, the formation of excess air is the result of the equilibration of a finite water volume with a finite air volume at increased hydrostatic pressure within the quasi-saturated zone:

$$C_i(T,S,P_{\mathrm{atm}},A,F) = C_i^{\mathrm{equ}}(T,S,P) + \frac{(1-F)\cdot A\cdot z_i}{1+F\cdot A\cdot z_i/C_i^{\mathrm{equ}}(T,S,P)} \tag{4.3}$$

The initial amount of entrapped air is given by A, whereas the fractionation parameter F describes the reduction of this initial gas volume due to dissolution and compression. The parameter z_i is the volume fraction of gas i in dry air.

If the entire volume of entrapped air is completely dissolved, the result is pure, unfractionated excess air. If the hydrostatic pressure is not sufficient for complete dissolution, the composition of both the dissolved gas and the remaining gas phase is fractionated; i.e., the elemental composition is fractionated relative to pure atmospheric air, whereas there is hardly any effect on the isotopic composition of any given element (e.g. Kipfer et al., 2002). Due to their high solubilities, the heavy noble gases Ar, Kr and Xe are enriched in the water phase relative to the poorly soluble, light noble gases He and Ne.

The degree of fractionation of the excess air component is described by the fractionation factor F:

$$F = \frac{V}{P_{\mathrm{r}}} \tag{4.4}$$

where $V = V_{\mathrm{g}}/V_{\mathrm{g}}^0$ is the ratio of the volume of entrapped air in the final state (V_{g}) to

that in the initial state (V_g^0), and $P_r = (P_{tot} - e_w)/(P - e_w)$ is the ratio of the dry gas pressure in the entrapped gas (P_{tot}) to that in the free atmosphere (P), with e_w being the saturation water vapor pressure. Typically, more air is entrapped in the soil matrix than can be dissolved at the prevailing pressure. Fractionation of the resulting excess air component is therefore similar to that described by the CE model, and its size, expressed as ΔNe (equation 4.2), is limited by the pressure acting on the entrapped air bubbles. The fractionation factor F ranges from 0 to 1; i.e., $F = 0$ implies complete dissolution of the entrapped air bubbles, yielding a pure, unfractionated excess air component, whereas $F = 1$ means that the bubbles are not being dissolved at all. Thus, low values of F imply only slightly fractionated excess air resulting from a high degree of dissolution of the entrapped air bubbles, whereas high values of F characterize highly fractionated excess air caused by their rather incomplete dissolution.

Usually, some of the free model parameters of the CE model are well constrained in groundwater studies. For example, S is commonly negligibly low in fresh groundwater and p_{atm} is defined by the altitude of the recharge area. The remaining unknown parameters T, A, and F can be determined from the measured Ne, Ar, Kr, and Xe concentrations using inverse techniques to solve equation (4.3) (Aeschbach-Hertig et al., 1999; Ballentine and Hall, 1999). Helium often cannot be used for this inversion because of the presence of non-atmospheric He due to the accumulation of radiogenic and terrigenic He isotopes.

In addition to the lumped-parameter models describing excess air formation as a result of the dissolution of entrapped air bubbles within the quasi-saturated zone, Mercury et al. (2004) propose a different mechanism for the formation of excess air based on increasing gas equilibrium concentrations due to increasing capillary pressure. The internal water pressure of capillary water in the unsaturated zone decreases with decreasing soil air humidity, resulting in an increase in (noble) gas equilibrium and mass fractionation in favor of the heavier noble gases. This mechanism may lead to the formation of excess air in the capillary water of very fine-grained sediments. However, capillary pressure decreases strongly with increasing soil air humidity and hence with increasing water saturation.

It is important to note that the capillary pressure model is different from the surface-tension pressure which is included in the KBD model. The latter is the result of the curvature of the bubble surface and contributes significantly to the total pressure in the bubble if the bubble radius is very small ($\lesssim$0.1 mm). In contrast, the capillary pressure model is related to the negative internal water pressure resulting from capillary forces.

4.3 Experiments and experimental methods

Sprinkling experiments at two different field sites were conducted to study gas exchange and the formation of excess air in natural porous media. The sprinkling experiments simulated intermediate to heavy rainfall events, forcing water to infiltrate into the soil matrix. Samples of this water were taken for dissolved noble gas analysis.

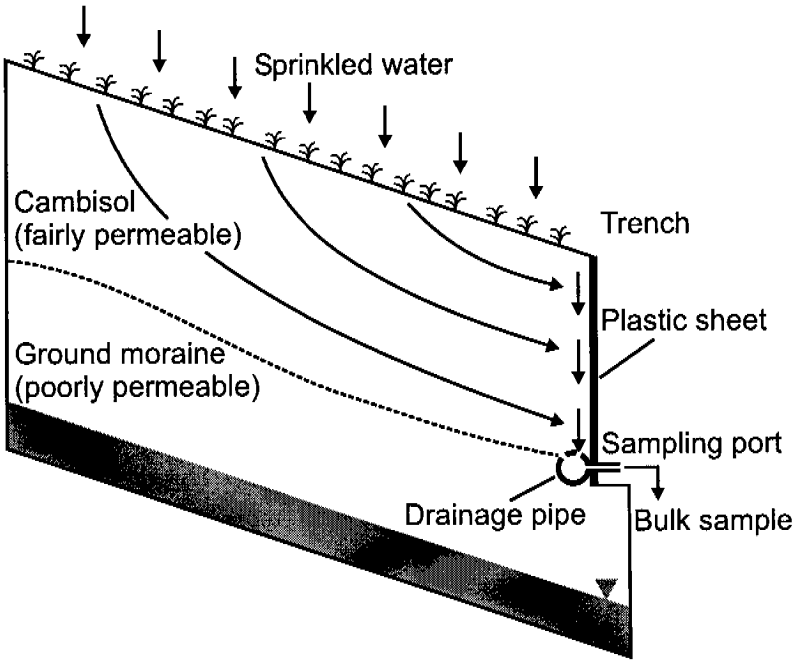

Figure 4.1: Schematic experimental set-up of the Schlüssberg site. The seepage water is collected by the plastic sheet (width: 9 m, height: 1.6 m) installed vertically on the trench wall facing the slope. The water drains to the sampling port via a drainage pipe which is inclined towards the center of the trench. It is important to note that the bulk samples represent a mixture of seepage water, integrated over a width of 9 m and a depth of 1.6 m.

Commercial water sprinklers were used to distribute the water over the soil surface at the experimental field sites.

4.3.1 Schlüssberg site (Switzerland)

A first field experiment was conducted close to the village of Grüningen, about 20 km south-east of the city of Zürich, Switzerland. The sprinkling experiment was carried out on June 10, 2004. The experimental site (Figure 4.1), which is situated on the slope of a drumlin (Schlüssberg) that was formed during the last ice age, is underlain by poorly permeable ground moraine sediments. The ground moraine is overlain by a cambisol 0.7 to 0.9 m thick, which has a higher hydraulic permeability due to its high macroporosity. The sediment is poorly sorted and consists of about equal proportions of clay, silt and sand (Oberrauch, 2003).

At the bottom of the slope, a trench 9 m wide and 1.6 m deep collects the lateral subsurface storm flow (Figure 4.1). The upper wall of the trench is sealed with a plastic sheet to collect all lateral subsurface storm flow, which is then drained into the trench, where it can be sampled. In contrast to the Munich site (see section 4.3.2), it is not possible to collect samples from distinct depths at the Schlüssberg site; instead, all samples represent bulk samples of the water discharging into the trench.

Water was sprinkled onto the catchment area ($\sim$110 m^2) of this trench for about

10 h at a mean rate of ~10 mm/h. The lateral subsurface runoff reached 4 mm/h (Kienzler and Naef, 2007). The first appearance of subsurface runoff water was observed in the trench 4 h after starting the sprinkling experiment. Subsequently, we collected samples for noble gas analysis for the next 4 h at intervals of 10 to 30 min.

4.3.2 Munich site ("Münchner Loch", Germany)

The "Münchner Loch" is a 10 m deep research shaft situated within the unsaturated zone of the Munich Gravel Plain, an important Pleistocene aquifer located south and west of the city of Munich (Figure 4.2A; Merkel et al., 1982). The sediment consists of glaciofluvial sands and sandy gravels (clay, silt: < 5 %, gravel: > 40 %) deposited during the last ice age (Kühnhardt, 1994). The thickness of the unsaturated zone is ~11 m. The coarse sand-gravel aquifer has a very high hydraulic permeability of up to 10^{-2} m/s.

The accessible, circular shaft has a diameter of 1.5 m and is equipped with devices for sampling seepage water and soil air at several depths. The seepage water collectors (SWCs) are comprised of stainless steel pipes of length 50 cm and diameter 7 cm that are open on the top to receive the seepage water (Figure 4.2B; Kühnhardt, 1994). Over the last 10 cm, the pipe is closed and filled with fine-grained gravel which is supported at the open part of the pipe and the outlet by screens with a mesh width of 1 mm. The SWCs are driven into the sediment and are inclined toward the shaft at an angle of 10-15°. Note that the open part of each SWC is filled with the original sediment. The outlet of the SWC is connected by a short silicone tube to a copper tube for noble gas sampling. In addition to water samples, soil air samples can be taken from stainless steel pipes of length 1.5 m and diameter 25 mm that are installed horizontally in the surrounding sediments.

To study the gas exchange between seepage water and soil air in the coarse sediments of the Munich Gravel Plain, we conducted two sprinkling experiments. The area adjacent to the shaft, defined as two thirds of its circumference at a distance of about 4 m, was sprinkled with water for 1.5 h (Exp. 1) and 3 h (Exp. 2) on two consecutive days (December 2 and 3, 2004). The mean water flux was about 35 mm/h. Seepage water samples for noble gas analysis were taken at depths of 0.5, 1, 2, and 3.5 m. Samples from greater depths could not be taken, because at these depths no water could be forced to flow during the experiments.

In addition to water sampling, we sampled the soil air immediately after the sprinkling experiments had been conducted. As a reference, two soil air profiles were sampled one month before and three months after the experiments.

4.3.3 Sampling and analytical methods

The water samples (~22.5 mL) for noble gas analysis were stored in copper tubes that can be sealed gas-tight by pinch-off clamps. Since degassing is always a critical factor during the sampling process, we exercised particular caution in order to avoid any gas loss that might have led to re-equilibration of the water during sampling.

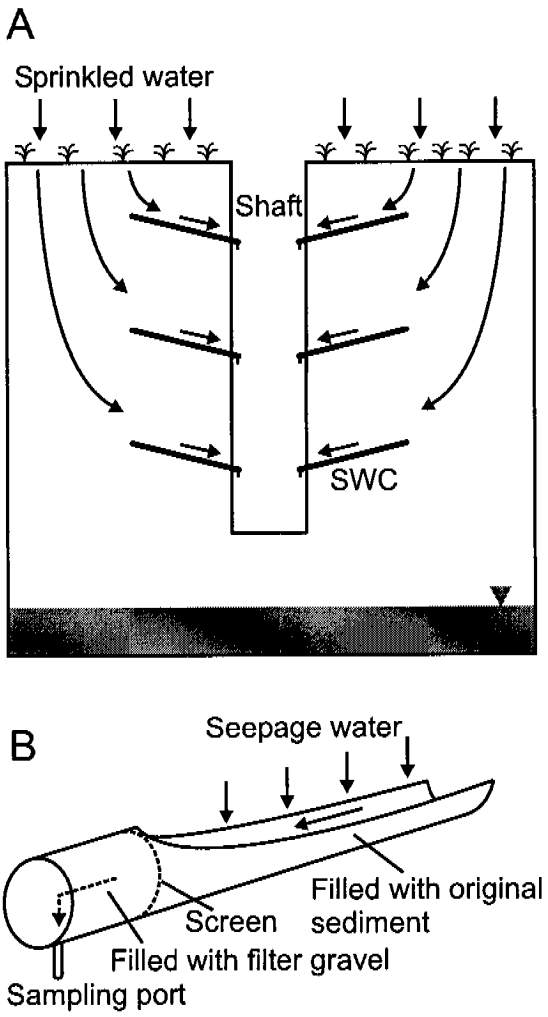

Figure 4.2: A: Schematic experimental set-up at the Munich site. Seepage water is sampled using seepage water collectors (SWC). Importantly, SWCs allow seepage water to be sampled without the need for negative pressure to suck water into the sample containers. This method therefore prevents the seepage water degassing owing to pressure reduction. B: Design of the SWCs (length: 50 cm, diameter: 7 cm).

At the Schlüssberg site, the subsurface runoff water was collected by the vertically installed plastic sheet, which drained the collected water toward the sampling port (Figure 4.1). The copper tube was connected to the sampling port by a short silicone tube. Air entrapment was prevented by tapping the sample container, and the absence of air bubbles was confirmed by visual check through the silicone tube. The copper tube was pinched off after flushing several times. Because the discharge rate was high (7 L/min), the copper tube could be filled and flushed quite rapidly.

At the Munich site, seepage water collectors (SWCs) were used to collect the infiltrating water (Figure 4.2). The copper tube was connected to the sampling port of the SWC using a short silicone tube. In addition to tapping the copper tube and conducting visual checks of the silicone tube, the copper tube was kept vertical in order to avoid air entrapment. The flow rate was low (a few mL/min) and sampling therefore lasted about 10 to 15 min per sample. The other end of the copper tube was connected to another silicone tube of about 50 cm length. The water column in this silicone tube acted as a diffusion barrier against the atmosphere and prevented (partial) re-equilibration of the water sample.

In the laboratory, the dissolved gases were extracted into an ultra-high vacuum extraction and purification line. Subsequently, the abundances of He, Ne, Ar, Kr, Xe, and the isotope ratios $^3He/^4He$, $^{20}Ne/^{22}Ne$, $^{36}Ar/^{40}Ar$ were measured using noble gas mass spectrometry in the Noble Gas Laboratory at ETH Zurich (Beyerle et al., 2000).

Samples of soil air were taken from stainless steel pipes (length: 1.5 m) driven from the shaft into the sediments at different depths. The soil air samples were transferred to 500 ml stainless steel cylinders (Whitey, 304L-HDF4-500, Arbor Inc.) equipped with two plug valves (Nupro, SS-4P4T1, Arbor Inc). Samples were taken with $\sim$3 bar overpressure using a diaphragm pump which pumped the air into the sample container. The sample container was closed after flushing the container several times with soil air. The noble gases (Ne, Ar, Kr, Xe) from the soil air samples were measured using GC-MS techniques. After passing through a drying agent (magnesium perchlorate, Merck Inc.) to remove water vapor, the air samples are injected through a 1 cm^3 gas sampling loop to the gas chromatograph (Finnigan TraceGC ultra, Thermo Inc.), and the gases are separated on a 4 m $\times$ 0.32 mm Carboxen 1010 Plot Capillary Column (Supelco Inc.) followed by a 30 m $\times$ 0.32 mm $\times$ 25 μm HP-Molsiv column. The carrier gas is He at 1.5 cm^3/min with a split ratio of 75. The oven temperature is programmed from 40 to 220 °C. The noble gases are quantified using a quadrupole mass spectrometer (Finnigan TraceDSQ, Thermo Inc.). The analytical errors deduced from the reproducibility of our air standard (dry compressed atmospheric air) are $\sim$2 % for Ne, Ar, and Kr, and $\sim$3 % for Xe. The blanks are below the detection limit for all noble gases.

4.4 Results and discussion

4.4.1 Schlüssberg site

Noble gases

When a water droplet from the sprinkler nozzle hits the soil surface and infiltrates into the soil, it is assumed to be in solubility equilibrium with the local atmosphere. This assumption is plausible because the water is sprinkled in the form of small drops and remains at the soil surface for several minutes as a thin water film before infiltrating. The diffusion distance z_i of noble gas i with effective diffusivity D_i can be approximated by the Einstein-Smoluchowski relation:

$$z_i = \sqrt{2D_i t} \tag{4.5}$$

Assuming that the water is in contact with the atmosphere for at least 10 min, and that the noble gases exhibit typical diffusivity values (Jähne et al., 1987), their diffusion distance, i.e., the characteristic length over which equilibration between water and air phases occurs, is in the range of at least several millimeters in all cases.

We applied the CE model to calculate NGTs and excess air contents. It is important to note that the aim of this work is not to verify or reject one or more of the available lumped-parameter models. We decided to use the CE model because it yields the best fit to the measured data, and because it has the most solid physical basis and extended experimental validation of all the lumped-parameter models that propose excess air formation to be the result of the dissolution of entrapped air (Kipfer et al., 2002). We did not use the capillary pressure model for two main reasons (see also further below in this section). First, the water saturation level of the subsurface zone increased to almost 100 % during the sprinkling experiment (Kienzler and Naef, 2007), calling into question whether the physical boundary condition for the application of the capillary pressure model, i.e., a high capillary pressure due to low relative soil air humidity, is realized at the Schlüssberg site. Second, changing mixing ratios of event and pre-event water, which were subject to different capillary pressures due to changing water saturation, do not cause any detectable change in the amount or elemental composition of the observed excess air.

The NGT reflects the temperature which prevailed during gas exchange. We used the mean NGT of $(15.5 \pm 1.3)\,^{\circ}\mathrm{C}$ to determine the atmospheric solubility equilibria which were established at the soil surface and during infiltration through the unsaturated zone. The mean NGT agrees with the measured temperatures of the water ($(15.0 \pm 0.5)\,^{\circ}\mathrm{C}$) that drained into the trench during the sprinkling experiment. Thus, the gas exchange between the infiltrating water and the (soil) air is controlled by the in-situ water temperature.

The noble gas concentrations in all samples from the sprinkling experiment were found to exceed significantly their respective atmospheric solubility equilibrium concentrations, which were calculated using the mean NGT (Tables 4.1 and 4.2). Values of ΔNe increase from 4 % at the beginning of the experiment to 6 % at the end (Fig-

ure 4.3). According to the CE model, the mean entrapped air volume A is about $100\,cm^3_{STP}/kg$, indicating that significant amounts of air are entrapped in the soil matrix. The excess air component is found to be strongly fractionated, indicating incomplete dissolution of the entrapped gas phase. The fractionation factor F is about 0.9 for all samples, suggesting that only a few percent of the entrapped air volume is actually dissolved in the water. This is because of the small increase in pressure, and the large, available entrapped air volumes (Aeschbach-Hertig et al., 2000). Hence, the Schlüssberg experiment, as the first field experiment ever, was able to provide evidence for the formation of excess air during groundwater infiltration in a natural soil under quasi-saturated conditions.

The $^4He/^{20}Ne$ elemental ratios for all samples are slightly below the value for air-saturated water, indicating either diffusive gas loss or elemental fractionation due to multi-step equilibration (Figure 4.4; Kipfer et al., 2002). However, for all samples, the values found for the $^3He/^4He$, $^{20}Ne/^{22}Ne$ and $^{36}Ar/^{40}Ar$ isotope ratios correspond closely to those found in the atmosphere, and show no fractionation within the limits of analytical error. As a result, diffusively controlled gas loss, as proposed by the partial re-equilibration model, can be excluded as a cause of the observed fractionation (Kipfer et al., 2002; Brennwald et al., 2005). The observed pattern might be caused by multi-step equilibration, i.e., the equilibration of a finite water volume with a finite gas volume, followed by the separation of the water and gas phases and the subsequent equilibration with another finite gas volume, and so forth. In this case, the secondary gas loss is controlled by the solubilities of the different gases rather than by their diffusivities. Hence, such a multi-step process, which is controlled by equilibrium partitioning governed by the Henry coefficients, would yield an elemental fractionation similar to that indicated by the measured $^4He/^{20}Ne$ ratio, but would yield no detectable isotopic fractionation for any given noble gas.

The concentrations of the heavy noble gases, especially Xe, show greater fluctuations than those of the light noble gases. These changes can be explained by a mixture of water that infiltrated during the experiment (event water) with water that was already present in the subsurface (pre-event water). If we suppose that these two types of water equilibrated at slightly different temperatures, varying mixing ratios in the water samples will affect the heavy noble gases mainly because of their strongly temperature-dependent solubilities. The same mixing would scarcely affect the light noble gas concentrations because their solubilities depend only weakly on temperature. Dye tracer tests using naphthionate which were conducted during the sprinkling experiment clearly indicate a contribution of pre-event water to the runoff (Figure 4.3). Based on dye tracer concentrations, mixing ratios of pre-event and event waters in the samples can be quantified. Most of the time the fraction of pre-event water varied only slightly about a constant value, but two to three hours after the water had entered the trench, the fraction of pre-event water decreased abruptly. However, this change in the fractions of event and pre-event water was not reflected in the light noble gas concentrations (Figure 4.3). The excess air component therefore seems to be independent of the occurrence and extent of the mixing of event and pre-event wa-

Table 4.1: Noble gas concentrations and isotope ratios in the water samples from the sprinkling experiments. All noble gas concentrations are given in cm^3_{STP}/g.

Time [h]	He $[10^{-8}]$	Ne $[10^{-7}]$	Ar $[10^{-4}]$	Kr $[10^{-8}]$	Xe $[10^{-8}]$	R_{He} [a] $[10^{-6}]$	R_{Ne} [b] [–]	R_{Ar}^{-1} [c] [–]
				Schlüssberg				
0.0	4.42	1.89	3.49	8.00	1.13	1.34	9.775	296.3
0.3	4.43	1.89	3.36	7.58	1.05	1.35	9.767	295.7
0.7	4.46	1.91	3.45	7.89	1.11	1.42	9.780	296.1
1.3	4.45	1.89	3.41	7.65	1.06	1.38	9.777	294.9
1.8	4.43	1.90	3.33	7.50	1.05	1.36	9.780	295.9
2.8	4.45	1.88	3.30	7.41	1.02	1.38	9.790	295.5
3.2	4.52	1.92	3.32	7.43	1.03	1.36	9.781	296.0
3.7	4.48	1.91	3.39	7.61	1.08	1.35	9.797	295.6
4.3	4.52	1.93	3.35	7.55	1.04	1.34	9.779	295.6
Depth [m]				**Munich**				
				Experiment 1				
0.5	4.57	2.02	4.02	9.62	1.42	1.36	9.786	296.0
1	4.51	1.96	3.92	9.36	1.41	1.42	9.803	295.8
2	4.44	1.93	3.78	8.95	1.33	1.40	9.787	295.9
3.5	4.47	1.90	3.39	7.79	1.12	1.36	9.808	294.6
				Experiment 2				
0.5	4.54	1.99	3.97	9.42	1.38	1.37	9.800	295.8
1	4.62	2.02	3.99	9.63	1.43	1.40	9.797	296.1
1	4.53	1.97	3.98	9.48	1.42	1.37	9.782	295.2
1	4.45	1.93	3.82	9.04	1.37	1.39	9.797	296.0
2	4.56	1.99	3.88	9.29	1.37	1.37	9.802	296.9
2	4.45	1.89	3.78	8.96	1.34	1.40	9.781	295.6
2	4.53	1.97	3.88	9.23	1.38	1.38	9.792	295.4
3.5	4.49	1.91	3.67	8.64	1.26	1.38	9.765	295.3
				Uncertainty				
	0.8 %	1.3 %	0.5 %	1.0 %	1.9 %	1.2 %	0.2 %	0.1 %

(a) $^3He/^4He$, (b) $^{20}Ne/^{22}Ne$, (c) $^{36}Ar/^{40}Ar$

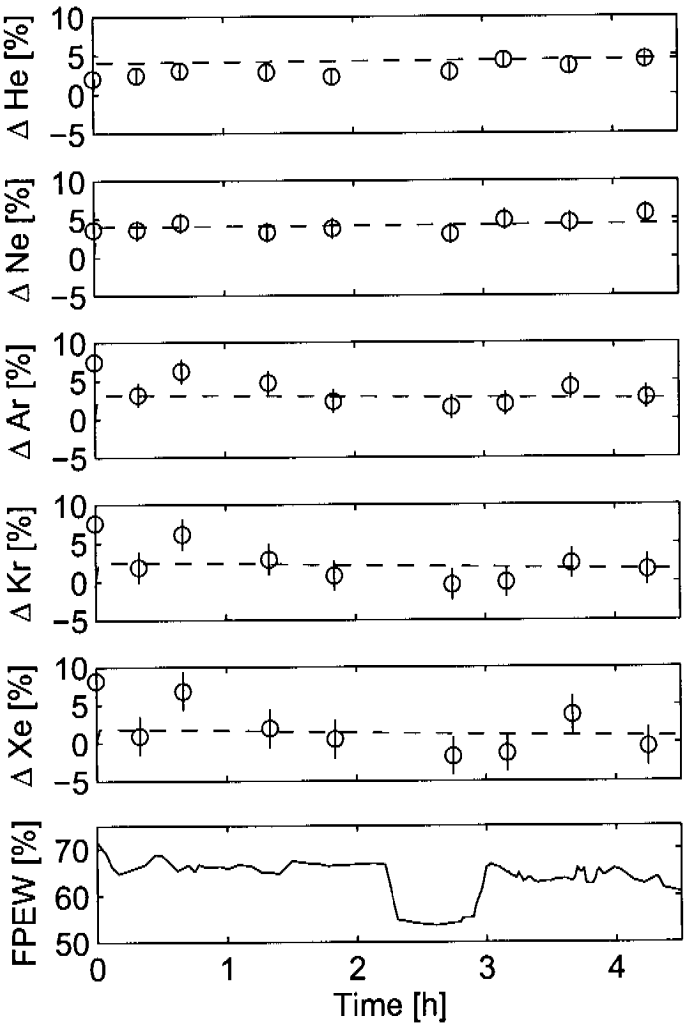

Figure 4.3: Measured (circles) and modeled (dashed lines) relative supersaturations of the noble gases and the fraction of pre-event water (FPEW, solid line in the lower panel) from the sprinkling experiment at the Schlüssberg site. The error bars represent 1σ-errors.

Table 4.2: NGTs and relative supersaturations in the water samples from the sprinkling experiment at the Schlüssberg site.

Time [h]	NGT [°C]	ΔHe [%]	ΔNe [%]	ΔAr [%]	ΔKr [%]	ΔXe [%]
0.0	13.5±3.7	2.1	3.6	7.4	7.5	8.1
0.3	15.9±3.5	2.5	3.6	3.2	1.9	0.9
0.7	14.0±1.7	3.0	4.5	6.2	6.1	6.8
1.3	15.5±3.7	2.9	3.3	4.8	2.9	1.9
1.8	15.1±0.6	2.3	3.8	2.3	0.8	0.5
2.8	16.8±3.0	2.9	3.0	1.6	-0.4	-1.8
3.2	16.7±1.0	4.4	4.9	2.0	-0.1	-1.3
3.7	15.0±0.5	3.6	4.5	4.2	2.4	3.7
4.3	17.3±2.4	4.4	5.7	2.9	1.5	-0.5
				Uncertainty		
		0.8	1.3	1.6	2.0	2.5

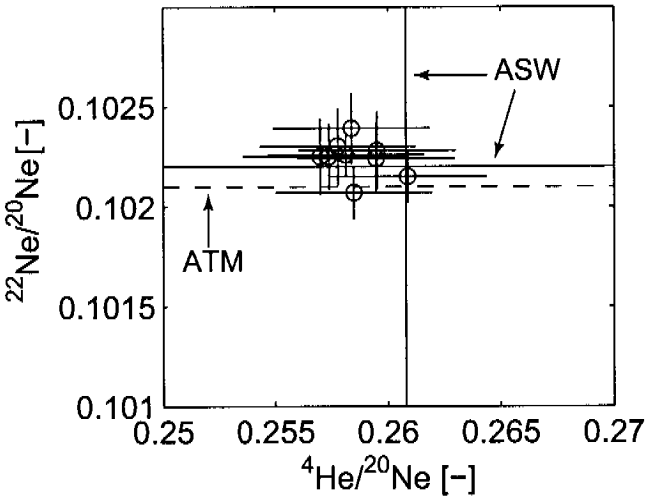

Figure 4.4: Plot of $^{22}Ne/^{20}Ne$ against $^{4}He/^{20}Ne$ for the water samples from the sprinkling experiment at the Schlüssberg site (ASW – air-saturated water; ATM – atmosphere). The error bars represent 1σ-errors.

ter, indicating that the excess air formation occurred during the sprinkling experiment in both event and pre-event water. Thus, excess air is generated in the discharging water due to hydraulic changes induced by the sprinkling experiment, i.e., by increasing water saturation, air entrapment, and partial dissolution of the air bubbles. The fact that excess air is produced in both event and pre-event waters favors the conceptual model – i.e., that excess air is produced by dissolution of entrapped air – and calls into question the validity of the capillary pressure model. Because the water saturation changed due to infiltration during the sprinkling experiment, the capillary pressure also changed, and is different for pre-event and event water. However, these possible changes in capillary pressure obviously do not affect the excess air content, and hence seem not to influence the formation of excess air significantly.

The experimental data show that a significant amount of excess air was generated during the sprinkling experiment. After sprinkling, the water infiltrated vertically along preferential flow paths. Parts of the previously unsaturated porous medium became quasi-saturated during the experiment, and lateral subsurface water flow occurred along (lateral) preferential flow paths (Figure 4.5A; Kienzler and Naef, 2007). The formation of the perched quasi-saturated zone is probably due to reduced hydraulic permeability at the moraine surface. Air bubbles were entrapped in the quasi-saturated sediment matrix, and the entrapped gas phase was then partially dissolved in the flowing water, which had initially been in atmospheric solubility equilibrium. A similar behavior has been observed in soil column experiments by Holocher et al. (2002). As put forward by Holocher et al. (2002, 2003), the dissolution of the entrapped gas bubbles is controlled and limited by the prevailing total pressure, and not by the amount of entrapped air available.

KBD model results

The sprinkling experiment was simulated using the KBD model. The parameter values defining the soil and flow characteristics of the sediment column are given in Table 4.3. The modeled noble gas concentrations agree reasonably well with the measured concentrations (Figure 4.3).

The hydrostatic pressure corresponding to a water column of about 0.2 m (see Table 4.3) seems to be hardly sufficient to cause the observed supersaturations of up to 6 % ΔNe. However, due to the small grain size of the sediment and the correspondingly small pore space, the entrapped air bubbles might be so small that surface-tension pressure could become relevant for the local solubility equilibrium. This is the case for bubble radii smaller than about 0.1 mm. A radius of 0.1 mm corresponds to a surface-tension pressure (P_{st}) of about 15 hPa, i.e., the surface-tension pressure is $\sim$1.5 % of the atmospheric pressure (P_{atm}). Bubble radii of about 0.01 mm ($P_{st} \approx 150$ hPa, $P_{st}/P_{atm} \approx 16\,\%$) to 0.05 mm ($P_{st} \approx 30$ hPa, $P_{st}/P_{atm} \approx 3\,\%$) would be small enough to explain the observed supersaturation without any significant hydrostatic overpressure. However, since we do not know the exact bubble radii, the contribution of the surface-tension pressure to the observed supersaturations remains speculative.

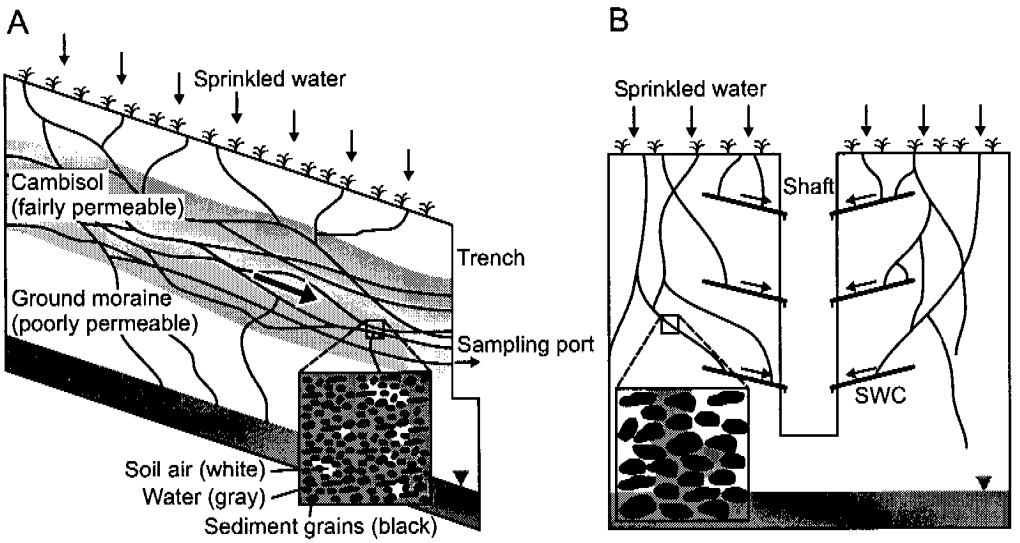

Figure 4.5: Schematic cross sections showing the conceptual models of the sprinkling experiments at the Schlüssberg and Munich sites. At the Schlüssberg site (A), the sprinkled water infiltrates into the soil and lateral subsurface flow is generated by partial saturation of the fine-grained unsaturated zone due to the reduced hydraulic permeability at the moraine surface. Vertical and lateral flow occurs along preferential flow paths (Kienzler and Naef, 2007). Air is entrapped in the quasi-saturated zone and partly dissolved due to the increased hydrostatic (and surface-tension) pressure. In contrast, during the sprinkling experiment in Munich (B), the water infiltrates along preferential flow paths into the seepage water collectors (SWC) without saturating large zones of the coarse soil. Soil air is still in contact with the free atmosphere, and gas exchange between the soil air and the infiltrating water is controlled by atmospheric pressure. Therefore, hardly any excess air is generated in the infiltrating water.

4.4.2 Munich site ("Münchner Loch")

Sprinkling Experiments

Again, it is reasonable to assume that the sprinkled water is in atmospheric solubility equilibrium before it infiltrates (see section 4.4.1). The noble gas concentrations measured in the seepage water from the shaft (Table 4.1) indicate that all samples contained little or no excess air. The ΔNe values range from -2.3 % to 3.5 %, and the corresponding volumes of entrapped air are very small (<0.35 cm^3_{STP}/kg; Figure 4.6, Table 4.4). For most of the samples, ΔNe is 0 % within the limits of analytical error. In all samples, the heavy noble gases are in atmospheric solubility equilibrium. Further, there is no significant relationship between the amount of excess air and either sampling depth or sampling time.

The fact that the samples contain virtually no excess air suggests that gas exchange between seepage water and soil air occurred at atmospheric pressure or at only marginally enhanced pressure. Further, the almost complete absence of detectable excess air indicates that hardly any air was entrapped in the quasi-saturated zone of the soil matrix during the infiltration experiment, and that capillary pressures are negligi-

Table 4.3: Model parameters for the KBD simulation of the Schlüssberg experiment.

Model parameter	Value	Parameter estimation
Column length	0.2 m	Best fit to measured data
Initial bubble radius	0.1 mm	Rough estimate from mean grain size
Total porosity	0.4	Typical value of fine-grained sand and silt deposits
Air-water ratio	0.1	Estimated from CE model results
Water temperature	15.5 °C	Mean NGT
Atmospheric pressure	954.6 hPa	Estimated from measurements at meteorological stations close to the study site
Salinity	0 ‰	Fresh water
Filter velocity	$8 \cdot 10^{-6}$ m/s	Estimated from volume of sprinkling water applied
Dispersion coefficient	$8 \cdot 10^{-7}$ m^2/s	Estimated from filter velocity, assuming a dispersivity of 0.1 m
Initial noble gas concentrations	C_i^{equ}	The water from the sprinklers is in atmospheric solubility equilibrium before infiltration (see section 4.4.1)

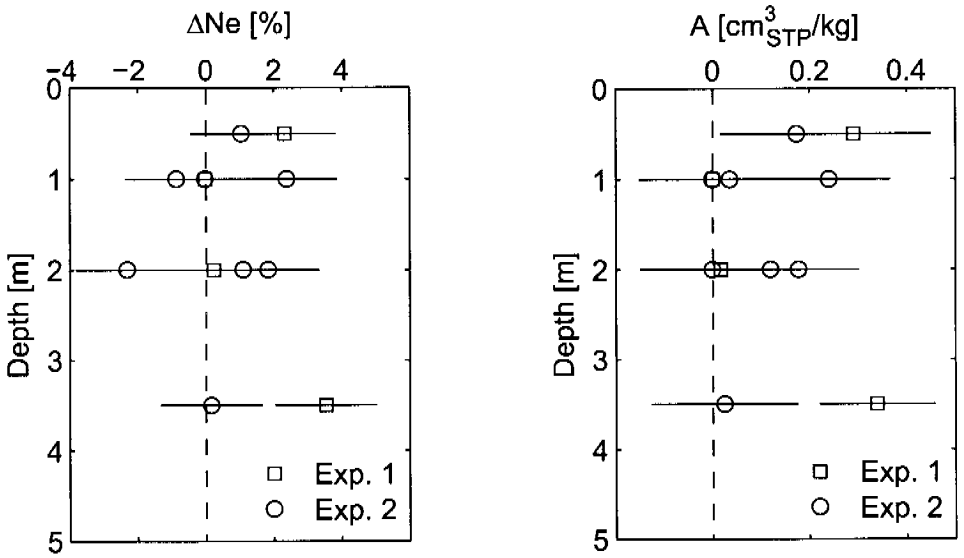

Figure 4.6: Depth profiles of ΔNe and dissolved excess air volumes (A) resulting from the sprinkling experiments (Exp. 1 and Exp. 2) in Munich. The error bars represent 1σ-errors.

Table 4.4: ΔNe, excess air (A), and NGTs of the water samples from the sprinkling experiments in Munich.

Depth [m]	ΔNe [%]	A [cm^3_{STP}/g]	NGT [°C]
	Experiment 1		
0.5	2.3	0.29	6.0
1	0.0	0.00	6.7
2	0.2	0.02	8.2
3.5	3.5	0.34	13.3
	Experiment 2		
0.5	1.1	0.17	6.7
1	2.4	0.24	6.3
1	0.0	0.04	6.4
1	-0.9	0.00	7.9
2	1.8	0.18	7.5
2	-2.3	0.00	8.3
2	1.1	0.12	7.5
3.5	0.2	0.02	9.7
	Uncertainty		
	1.5	0.14	0.2

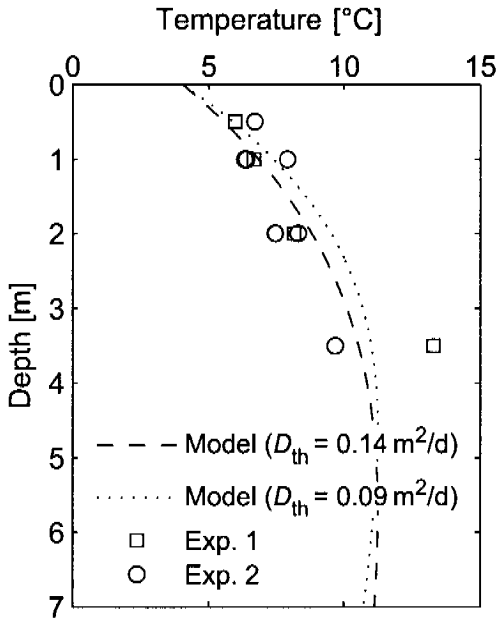

Figure 4.7: Comparison of NGTs (circles/squares) and modeled soil temperatures (dashed/dotted lines) based on two different values of thermal diffusivity (D_{th}) resulting from the sprinkling experiments (Exp. 1 and Exp. 2) in Munich. All samples – with one exception (Exp. 1, depth: 3.5 m) which gives an unrealistically high NGT – agree with the modeled soil temperature profile for the date of sampling. All errors of the NGTs are 0.2 °C.

bly small, as would be expected in coarse sediments.

The atmospheric solubility equilibria are mainly controlled by the temperature prevailing during gas exchange, which is reflected in the NGT. Remarkably, the NGT exhibits a continuous significant increase with depth (Figure 4.7, Table 4.4). Usually, the NGT is assumed to correspond to the mean annual soil temperature (Stute and Sonntag, 1992; Stute and Schlosser, 1993). The application of noble gases as a paleothermometer depends crucially on this basic assumption. Unfortunately, direct measurements of soil temperature at the study site were not available. We therefore applied a soil temperature model to reconstruct the local soil temperature at the field site as a function of soil depth and time.

The soil temperature profile can be described by the following partial differential 'thermal conduction' equation (e.g., Hillel, 2003):

$$\frac{\partial T(z,t)}{\partial t} = D_{\text{th}} \frac{\partial^2 T(z,t)}{\partial z^2} \tag{4.6}$$

with D_{th} being the thermal diffusivity. Equation (4.6) is solved for the following boundary conditions:

1. At the soil surface ($z = 0$) an annual sinusoidal temperature variation is assumed

around the annual mean soil temperature T_a:

$$T(0,t) = T_a + A_0 \sin\left(\frac{2\pi(t-t_0)}{365} - \frac{\pi}{2}\right) \tag{4.7}$$

A_0 is the annual amplitude of the surface soil temperature and t_0 is the time lag from an arbitrary starting date (taken as January 1 here) to the time of occurrence of the annual minimum.

2. As $z \to \infty$ the soil temperature tends to the (constant) annual mean soil temperature. The geothermal heat flux is negligible in comparison with the exchange fluxes to and from the atmosphere.

3. The thermal diffusivity D_{th} is constant throughout the soil profile and throughout the year.

The resulting temperature model is described by the following sinusoidal function:

$$T(z,t) = T_a + A_0 \exp(-z/d) \cdot \sin\left(\frac{2\pi(t-t_0)}{365} - \frac{z}{d} - \frac{\pi}{2}\right) \tag{4.8}$$

with damping depth $d = (2D_{th}/\omega)^{1/2}$ and angular frequency $\omega = 2\pi/365\,\mathrm{d}^{-1}$. The parameter values $T_a = 9.65 \pm 0.03\,^{\circ}\mathrm{C}$, $A_0 = 9.38 \pm 0.07\,^{\circ}\mathrm{C}$, $t_0 = 24.0 \pm 0.4\,\mathrm{d}$, and $D_{th} = 0.09 \pm 0.01\,\mathrm{m^2 d^{-1}}$ were determined from time series of daily mean soil temperatures measured at 0.05, 0.20, and 0.50 m depths in 2004. The soil temperature measurements were performed at the Roggenstein meteorological station about 20 km north-west of the study site (data are available at http://www.lfl.bayern.de, Bayerische Landesanstalt für Landwirtschaft). The climatic characteristics of the station are similar to those of our study site. Since the thermal diffusivity D_{th} depends on local soil properties, we also determined D_{th} from older soil temperature measurements at our study site. The value $D_{th} = 0.14 \pm 0.03\,\mathrm{m^2 d^{-1}}$ was obtained from a calibration based on soil temperature measurements from the shaft at depths of 0.2 to 9 m (data given in Freitag et al., 1987). The climate-related parameters T_a, A_0, and t_0 were calculated from more recent data that comprise temperature measurements from the year in which the sprinkling experiments were performed. We employed the Gauss-Newton method to determine the parameters.

Figure 4.8 shows the comparison of the measured and simulated soil temperatures for the Roggenstein station. The model reproduces the measured values well, and can therefore be assumed to be adequate to calculate the soil temperature profile at our study site. The NGTs determined from concentrations of noble gases in the seepage water agree fairly well with the modeled soil temperature depth profile (Figure 4.7).

The infiltration of pre-event water, which would have equilibrated under different temperatures prior to the experiment, could offer a further possible explanation for the observed increase in NGTs with depth if pre-event water formed larger perched saturated zones that prevented the water from re-equilibration with soil air. However,

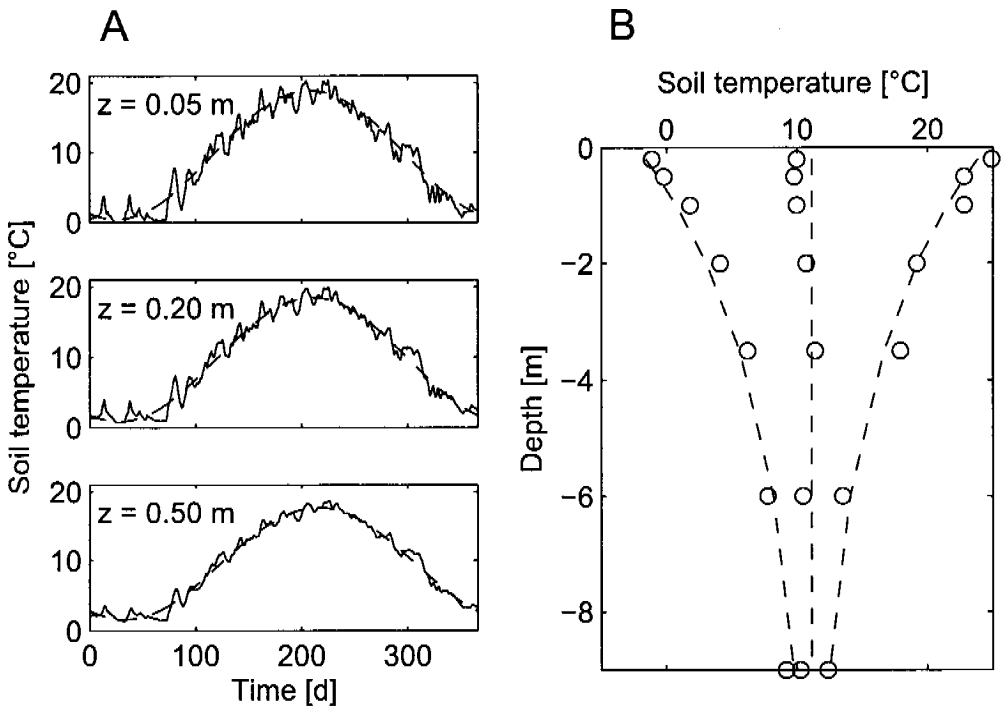

Figure 4.8: (A) Comparison of measured (solid lines), and modeled (dashed lines) soil temperatures at three different depths z at the Roggenstein station in 2004. The modeled soil temperatures were obtained by applying the thermal conduction equation (4.6). (B) Measured (circles) and modeled (dashed lines) soil temperatures at the Munich site. The circles represent minimum, maximum, and mean values of 1000 soil temperature measurements conducted during the 1980s.

there are two reasons to doubt the validity of this hypothesis. (i) The $^3He/^4He$ ratios do not indicate any significant accumulation of tritiogenic ^3He, excluding the presence of water with residence times of several months. (ii) As is known from previous studies at the same site (Freitag et al., 1987), the soil water content is about 5 to 10 %. This is owing to the small field capacity and the high hydraulic permeability of the coarse sediments. Therefore, the formation of larger perched saturated zones which prevent gas exchange between water and the local soil air is unlikely.

Thus, we conclude that the NGTs indeed reflect the soil temperature of the unsaturated zone, and that the water from the sprinkling experiments, which is assumed to have infiltrated along preferential flow paths, continuously exchanged gases with the soil air under atmospheric pressure conditions. In contrast to the Schlüssberg field site, a quasi-saturated zone did not form during infiltration, and no significant entrapment of air bubbles occurred (Figure 4.5B).

Soil air

In addition to analyzing samples of seepage water, we measured the composition of gases in samples of soil air. Application of excess air models implies that the con-

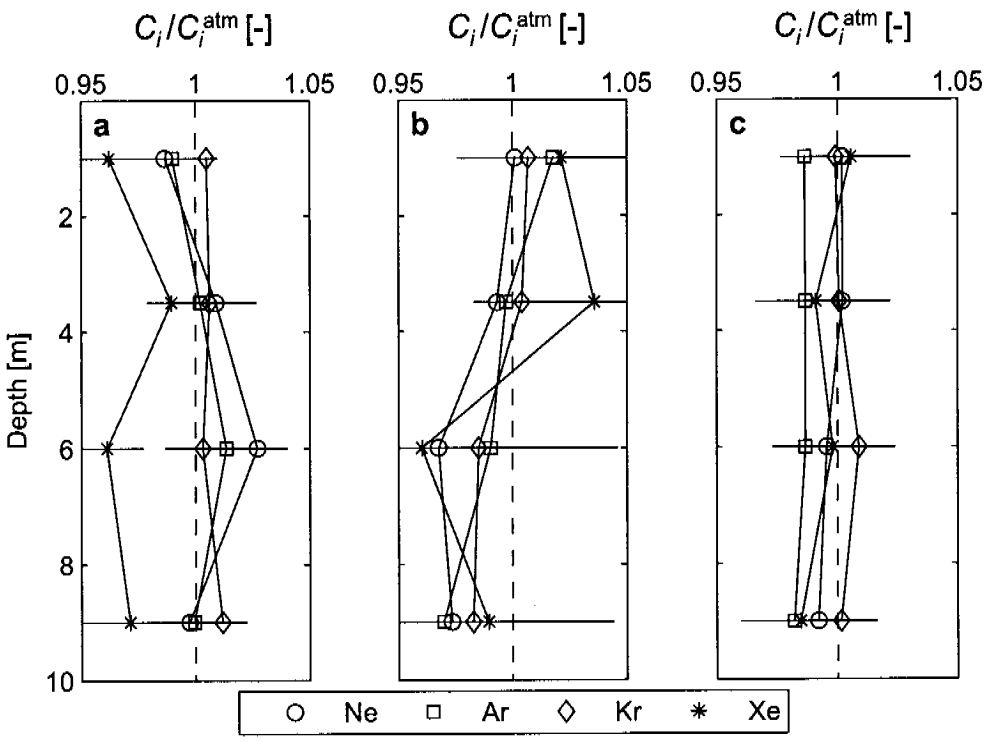

Figure 4.9: Noble gases in the soil air at the Munich site (a: November 3, 2004; b: December 3, 2004; c: March 7, 2005). All noble gas concentrations (C_i) are normalized to the relevant atmospheric concentrations (C_i^{atm}). Profile b was sampled immediately after the sprinkling experiments. The error bars represent 1σ-errors.

centrations of the noble gases in soil air are identical to those in atmospheric air. The soil air samples were analyzed in order to verify this assumption. Samples were taken at depths of 1, 3.5, 6, and 9 m. The measurements show that the noble gas concentrations at all depths indeed correspond to those of free atmospheric air (Figure 4.9). In addition, no significant differences could be observed between the profile sampled immediately after the sprinkling experiments and the reference profiles. The assumption that the concentrations of the noble gases Ne, Ar, Kr, and Xe in the soil air are equivalent to those in atmospheric air is therefore appropriate.

Groundwater

Additionally, we obtained two samples of shallow groundwater from an observation well situated close to the shaft. The noble gas concentrations in both samples were in atmospheric solubility equilibrium (Figure 4.10). The groundwater samples therefore support the findings gained from the sprinkling experiments. Hence, both lines of evidence suggest that little or no excess air is produced during infiltration into the local aquifer system.

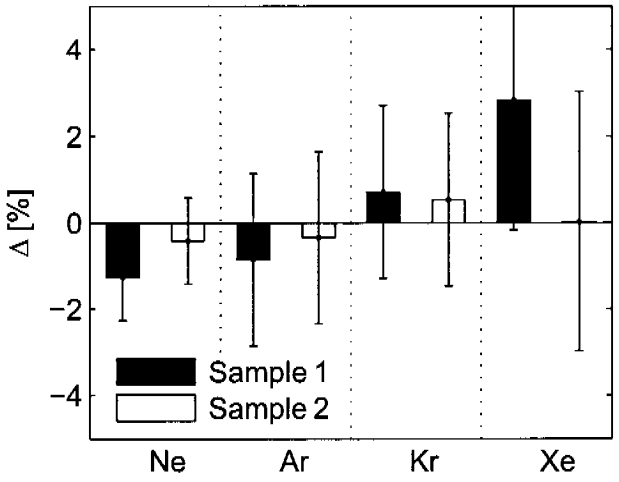

Figure 4.10: Relative saturations of the noble gases dissolved in the groundwater samples at the Munich site with respect to their respective atmospheric solubility equilibria. Both samples are in atmospheric solubility equilibrium within analytical uncertainty. The error bars represent 1σ-errors.

4.5 Conclusions

The results of the sprinkling experiments at the Schlüssberg and Munich sites add further evidence supporting the hypothesis that the formation of excess air depends on the infiltration mechanism and soil characteristics.

The fine-grained sediments of the Schlüssberg field site were partly saturated during the sprinkling experiment, forming perched water lenses due to the reduced hydraulic permeability at the moraine surface. Air bubbles were entrapped in the soil matrix by the infiltrating water (Figure 4.5A). The captured air bubbles were partly dissolved in the surrounding water, producing excess air owing to an increase in pressure – probably in both hydrostatic and surface-tension pressures – with respect to the free atmosphere. The strongly fractionated excess air component in the water samples indicates the presence of large volumes of entrapped air which were dissolved in the water only to a small extent.

By contrast, the results from the Munich experiment show that virtually no air could be entrapped by the water infiltrating into the highly permeable, coarse sands and gravels (Figure 4.5B), and that noble gas concentrations were in local equilibrium with free soil air. The absence of excess air in the infiltrating water suggests that the soil air was connected to the free atmosphere, and that gas exchange occurred at atmospheric pressure rather than at increased hydrostatic pressure between a finite entrapped air volume and the surrounding water phase, as was observed at the Schlüssberg site. There are no small pores in the coarse gravel that would allow the capillary pressure to become relevant for the solubility equilibrium.

Importantly, the NGTs, which increase with depth, clearly indicate the occurrence

of gas exchange between the infiltrating water and the soil air, with the dissolved noble gas concentrations reaching equilibrium at atmospheric pressure conditions and reflecting the in-situ soil temperature. This finding is of significant importance for the use of dissolved atmospheric noble gases as a proxy for paleotemperatures, as it provides an experimental evidence supporting the assumption that NGTs are identical to (past) soil temperatures.

The field experiments conducted imply the existence of a strong functional dependence of both gas exchange and excess air formation on soil properties during the infiltration process. However, infiltration dynamics could also have a significant impact on the formation of excess air. For example, the influence of the infiltration rate – normalized to the hydraulic properties of the sediments – should therefore be assessed in future studies.

This study has focused on gas exchange and the formation of excess air during the infiltration process within the unsaturated zone. However, excess air can also be formed as a result of air being trapped by a rise in the groundwater table, caused either by local infiltration or by pressure transmission. Furthermore, other aspects of gas/water partitioning in porous media which play only a minor role in the current study – e.g., the role of capillary pressure in the unsaturated zone (see Mercury et al., 2004) – still remain unexplained and would require further field experiments to be conducted.

Acknowledgements. We would like to thank Christian Holzner and Helena Amaral for their help during the field work in Munich, and Markus Hofer and Nora Graser for analyzing the soil air samples. Thanks are also due to Associate Editor Bernard Marty, Axel Suckow, Chris Ballentine, and an anonymous reviewer for their valuable and constructive reviews which helped to improve our manuscript. This work was supported by the Swiss National Science Foundation (project no. 200020-107489/1).

Part III

Case studies using environmental tracers

Chapter 5

Noble gas temperatures and the mean annual soil temperature in a shallow aquifer in Michigan

This chapter (5.2-5.3) has been published in *Geophysical Research Letters* (Klump et al., 2006a).

Preface

The field experiment in Munich (see chapter 4) showed that the NGT is identical to the soil temperature at the time of infiltration. This finding is of great importance for using noble gases as a proxy for paleotemperature. In fact, the assumption that the NGT is identical to the mean annual soil temperature is often implicitly made, though not always justified. The experimental data from Munich also indicate that the noble gas temperature is not identical to the mean annual soil temperature because the experiment was conducted in December, when the temperature in the shallow subsurface is significantly lower than the mean annual soil temperature. Such an offset of NGT from the mean annual soil temperature was observed in groundwater samples from an aquifer in Michigan. Based on the results of the field experiment in Munich, an alternative explanation can be found for the noble gas data from Michigan.

5.1 Introduction

Hall et al. (2005) analyzed water samples from the shallow Glacial Drift aquifer located in Ann Arbor, southern Michigan (Figure 5.1). They found all NGTs to be consistently lower than the mean annual air temperature of 9.1 °C, although this is identical to the mean annual soil temperature as indicated by measured groundwater temperatures. Furthermore, all samples contain significant excesses of both He isotopes ^{3}He and ^{4}He, which, from the authors' point of view, allegedly contradicts the observation that the groundwater responds quickly to the infiltration of snow melt wa-

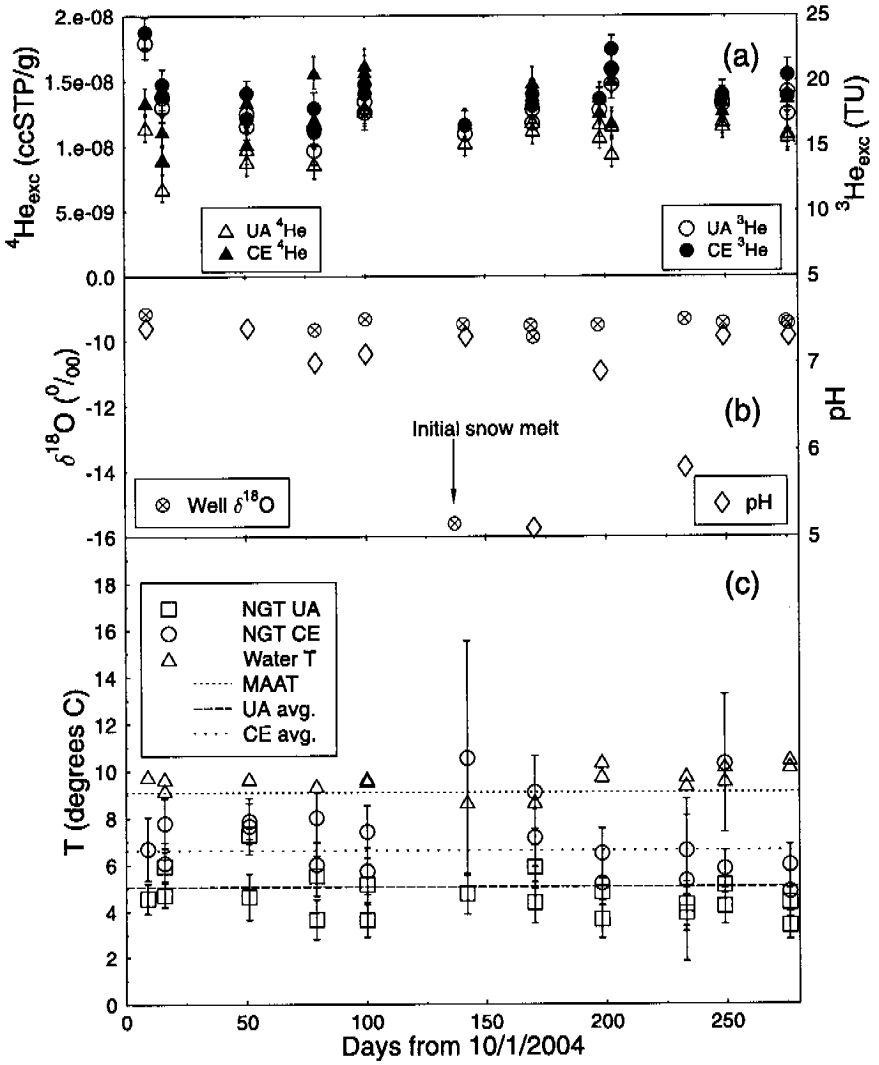

Figure 5.1: Noble gas and stable isotope data from the shallow aquifer in Michigan (from Hall et al., 2005). (a) He excess; (b) $\delta^{18}O$, pH; (c) NGTs and measured groundwater temperature. All error bars represent 1σ errors.

ter, as is suggested by low values of $\delta^{18}O$ and pH (Figure 5.1b). The authors provide several hypotheses to explain the observed temperature offset and He excess but could not find a conclusive solution to the problem.

The main hypotheses of Hall et al. (2005) can be summarized as follows:

- **NGT offset.** The partial loss of excess air by diffusion predicted by the PR model (Stute et al., 1995b) might explain at least part of the observed offset of the NGTs. A drop in relative humidity in the unsaturated zone would cause an increase in the local noble gas solubility, as proposed by the capillary pressure model of Mercury et al. (2004). An increase in noble gas partial pressures in the unsaturated zone due to oxygen consumption without an equivalent increase in CO_2 would also lead to lower apparent NGTs.

- **He excess.** Hall et al. (2005) assume that the groundwater is very young for the reasons discussed above. They therefore conclude that the partial pressures of ^{3}He and ^{4}He must be greater in the unsaturated zone than in atmospheric air. They analyzed He concentrations in ice and found it to be enriched in ^{4}He, which might explain some of the assumed ^{4}He excess in the unsaturated zone as a result of the infiltration of melted ice at the end of the winter. However, the low concentrations of Ar, Kr, and Xe would tend to increase the apparent NGT, which is the opposite of what was observed. Furthermore, the excess of ^{3}He cannot be explained by the melting-ice hypothesis and is attributed by the authors to origin from ^{3}H decay.

In our opinion, the interpretation provided by Hall et al. (2005) is incomplete and debatable in many points. The field experiments in Munich have shown that the NGT is identical to the in-situ soil temperature at the time of infiltration, and the NGT has therefore not necessarily to correspond to the mean annual soil or air temperatures. We believe that there are more natural and more convincing explanations for the data of Hall et al. (2005) which are explored below.

5.2 Discussion

Hall et al. (2005) present a comprehensive, stimulating and controversial set of noble gas data from a shallow, unconfined, sandy aquifer in Ann Arbor, Michigan. This data set comprises a time series of about 270 days starting in October 2004. The authors determined the noble gas temperature (NGT) from the measured noble gas concentrations. NGTs were found to be consistently lower than the mean annual air temperature (MAAT) of 9.1°C, whereas the MAAT agrees with the measured in-situ groundwater temperature. Because of this agreement, we can assume that the mean annual soil temperature (MAST) corresponds closely to the MAAT. Hall et al. (2005) developed several concepts to explain the deviation between the NGT and MAAT. However, they could not find a conclusive solution to the problem and conclude that further studies are needed to assess and identify the relevant mechanisms.

Here we show that NGT and MAST do not need to be equal. We will present additional hypotheses which we consider to give reasonable and convincing explanations for the data, and which were not explored by Hall et al. (2005).

5.2.1 Noble gas temperatures and mean annual soil temperature

In a strict, physical sense, the NGT, which is derived from the concentrations of dissolved atmospheric noble gases, is identical to the water temperature that prevailed during the last gas/water partitioning. In groundwater, this corresponds to the temperature at which gas exchange occurred at the groundwater table during recharge. In many cases, the thickness of the unsaturated zone exceeds several meters. In these cases, the soil temperature at the groundwater table shows little seasonal variation and

corresponds closely to the MAAT (Stute and Schlosser, 1993), unless the land cover introduces a systematic offset between MAST/NGT and MAAT (Stute and Sonntag, 1992). In the case of a shallow unsaturated zone, however, the seasonal temperature fluctuation at the groundwater table can amount to several Kelvin. Assuming a typical thermal diffusivity for sandy soils of $D_{\mathrm{th}} = 0.1\ \mathrm{m^2 d^{-1}}$, temperature variations detectable by variations in noble gas concentrations are present down to soil depths of about 10 m (e.g., Hillel, 2003; Stute and Schlosser, 1993), i.e., the annual amplitude of soil temperature variation is about 8°C at 2 m depth, 3°C at 5 m depth, and 1°C at 10 m depth.

The NGT of groundwater samples therefore represents a mean of the changing soil temperature weighted by the recharge rate. As a result, the NGT would be lower than the MAAT (or MAST) if recharge occurs predominantly during the cold season (e.g., Beyerle et al., 1999a).

Land cover has to be excluded as an explanation for the observed differences between NGTs and MAAT, because the measured groundwater temperature is virtually identical to the MAAT. The geometrical information on the sampling well of Hall et al. (2005) is ambiguous (depth of well, depth of groundwater table, position of screen). Furthermore, no information is given on the thickness of the unsaturated zone within the catchment area of the well, or on the local recharge rate and its seasonal variability. However, groundwater-level data available from the Michigan Groundwater Mapping Project (http://gwmap.rsgis.msu.edu) show that the thickness of the unsaturated zone in the vicinity of the sampling well is partly less than 5 to 10 m.

Well hydrographs from shallow aquifers in Michigan (http://nwis.waterdata.usgs.gov) show a recurrent annual rise in the groundwater tables from autumn until spring, with a maximum during spring. After this rise, groundwater levels drop back to a minimum in autumn. The groundwater table rise during winter and spring indicates that most of the recharge occurs during the cold season, when soil temperature in the shallow subsurface is significantly lower than the MAAT. In fact, the stable isotope data presented by Hall et al. (2005) show a considerable recharge component during snow melt as all samples indicate a mixture of $\gtrsim$30% melt water and $\lesssim$70% rain water.

The seasonality of groundwater recharge is further indicated by the seasonal variation in the excess air component (Figure 5.2). Since the formation of excess air is usually closely connected to groundwater recharge, and groundwater table fluctuations (Holocher et al., 2002), the strong excess air variation indicates a pronounced seasonality of local recharge.

In summary, the above discussion shows that the NGT at the study site can indeed be expected to be lower than MAAT and MAST due to its weighting by the recharge rate, which is highest during the cold season. Furthermore, the possibility of a deviation between NGT and MAAT or MAST is further demonstrated by recent field experiments. We analyzed the noble gas concentrations of seepage water sampled from a shallow unsaturated zone (Klump et al., 2007). The NGTs of these samples correspond closely to the in-situ soil temperatures at the date of sampling.

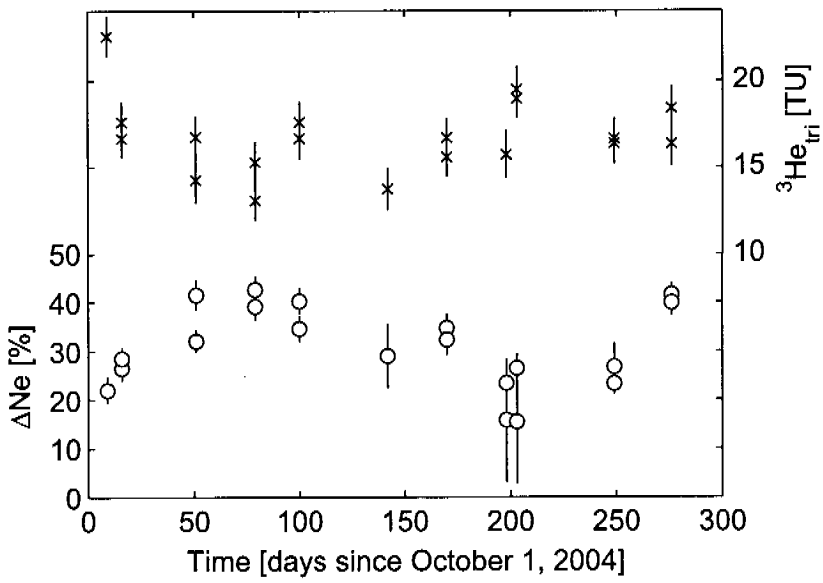

Figure 5.2: Ne excess with respect to the atmospheric equilibrium concentration (ΔNe) and $^3He_{tri}$ as a function of time. ΔNe, which reflects the excess air component in the groundwater, and $^3He_{tri}$ were estimated from the reprocessed data of Hall et al. (2005) using the closed-system equilibration model of Aeschbach-Hertig et al. (2000). ΔNe shows a significant seasonal variability, indicating local seasonality of recharge. $^3He_{tri}$ seems to follow a similar seasonal variation.

The soil temperature, however, shows a seasonal variation, and the NGTs therefore differed significantly from MAAT and MAST. To us, the weighting of the NGT by the recharge rate therefore seems a reasonable and natural explanation for the difference in the NGT and the MAAT or MAST observed by Hall et al. (2005).

5.2.2 Helium excess

Similarly, we would like to present a more natural explanation for the ^{3}He and ^{4}He results found by Hall et al. (2005). The authors observed ^{3}He and ^{4}He excesses in all groundwater samples and concluded that the partial pressures of both He isotopes in the soil air close to the groundwater table must exceed those in the free atmosphere. From the amount of He excess, the authors estimate that the soil air at the groundwater table remains out of atmospheric equilibrium for years to decades. However, a simple estimate of the characteristic diffusion length of He in porous media calls this conclusion into question. The diffusion length of He is $x = \sqrt{2Dt}$ (Einstein, 1905), where $D = D_0 \cdot \varepsilon^{4/3}$ is the effective He diffusivity in the unsaturated zone (Millington, 1959), $D_0 = 6 \cdot 10^{-5} \mathrm{m^2 s^{-1}}$ is the He diffusivity in free air, and $\varepsilon = 0.4$ is a typical value for the gas-filled porosity. For an unsaturated-zone depth of less than 20 m (i.e. $x < 20\,\mathrm{m}$), the characteristic time scale t of diffusive He exchange between atmosphere and groundwater is therefore less than about 4 months. Although groundwater

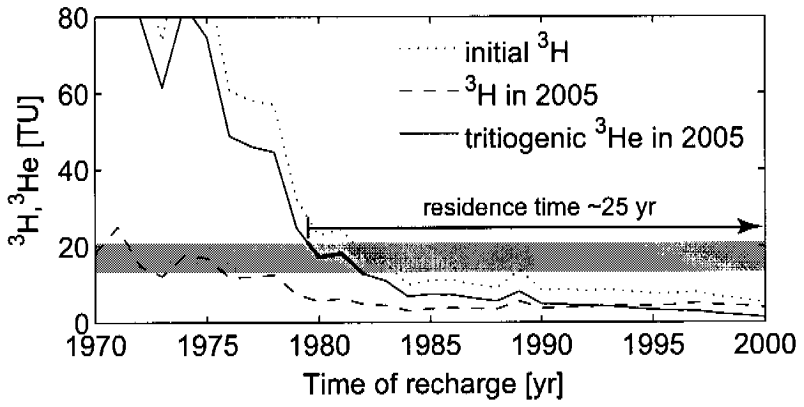

Figure 5.3: Atmospheric ^{3}H input, remaining ^{3}H due to decay, and accumulated tritiogenic ^{3}He in groundwater relative to the time of recharge. The figure shows the ^{3}H input function for Chicago, which has been extended by correlation with the ^{3}H input function for Vienna (data available at http://isohis.iaea.org). The gray bar indicates the range of the ^{3}He excess in the data of Hall et al. (2005) due to ^{3}H decay, calculated using the closed-system equilibration model of Aeschbach-Hertig et al. (2000).

that has accumulated considerable amounts of radiogenic He may act in principle as a source of radiogenic He in the unsaturated zone, the fast diffusion in the gas phase with respect to that in groundwater ($D_{\text{soil air}} \gg D_{\text{water}}$) will prevent any observable increase in the partial pressure of He in shallow unsaturated zones. Hence, the He partial pressure at the groundwater table is unlikely to remain out of equilibrium with the atmosphere on time scales of years to decades as put forward by Hall et al. (2005).

Hall et al. (2005) assert that the accumulated amount of radiogenic ^{4}He suggests a groundwater residence time of about 30 years. From our point of view, the observed amounts of accumulated tritiogenic ^{3}He can also be consistently understood in terms of groundwater residence time. Although no ^{3}H measurements in the groundwater at the study site are available, the atmospheric ^{3}H input and the ^{3}He excess can be used to estimate the groundwater residence time at ~25 years (Figure 5.3).

Also, Hall et al. (2005) argue that the sample taken immediately following a major snow melting event shows the influx of modern water reflected by low values of δ^{18}O and δ^2H. Hall et al. (2005) further claim that this is in disagreement with the significant and constant He excess observed in all samples. They therefore conclude that "these gases are not in equilibrium with the atmosphere". However, we disagree on this conclusion because the sample with low stable isotope values was taken on February 15, and Hall et al. (2005) do not provide any He data from this date. Instead, the next sample with available He data was taken on February 20 showing a similar amount of He excess as all other samples. This is not surprising as the stable isotope sample taken on February 19 also shows δ^{18}O and δ^2H values that are heavier than those of the sample from February 15 and similar to all other samples, again.

It has to be noted that all samples represent a mixture of waters with different residence times, even the one sample which was taken immediately following a snow

melting event and which might indicate a significant portion of very young groundwater. This applies especially to wells with large screen lengths of several meters because mixing predominantly occurs in the well and not within the aquifer. The fast diffusion of He in the unsaturated zone, the agreement of radiogenic ^{4}He and tritiogenic ^{3}He in terms of groundwater residence time, and the incomplete He data set challenge the explanation put forward by Hall et al. (2005) that the soil air might be enriched in He.

5.3 Conclusions

The hypotheses of He enrichment and O_2 depletion, as well as the negative pressure model, could be assessed directly by analyzing the composition and relative humidity of the soil air. Hall et al. (2005) report that all noble gas isotope ratios, with the exception of He, are identical to those in the free atmosphere. This contradicts the diffusion model. If this model was applicable, the isotope ratios should be fractionated, i.e., the groundwater should be depleted in the lighter isotopes of these elements due to their larger diffusivities (relative deviations from the atmospheric equilibrium values: 0.7 – 3% for ^{20}Ne/^{22}Ne, 0.2 – 1.4% for ^{40}Ar/^{36}Ar). Typical measurement errors for Ne and Ar isotope ratios are less than 0.5% and fractionation should therefore be observable in the data. Otherwise the diffusion model has to be rejected.

Hall et al. (2005) present a stimulating set of noble gas concentrations in groundwater that touches on crucial issues of gas/water partitioning in porous media. However, we believe that the hypotheses provided by the authors to elucidate the differences between NGTs and MAAT, as well as the observed He excess, are incomplete and debatable. In our point of view, seasonally variable groundwater recharge and groundwater mixing (in the well) provide a more realistic and physically more appropriate framework to explain the data.

Chapter 6

Pleistocene groundwater dynamics in Wisconsin derived from noble gas, ^{14}C, and stable isotope data

Preface

As mentioned in section 2.5, excess air can be viewed as a potential proxy for paleo-recharge conditions. This is especially true for Pleistocene groundwater from aquifers which were ice covered during the last ice age, because climatic and hydraulic conditions can be assumed to have changed dramatically in response to glaciation. Groundwater from a deep aquifer in southern Wisconsin covers a range in residence time from modern to late Pleistocene, and has recorded changes in paleo-environmental conditions during this period of time.

6.1 Introduction

Because the deep sandstone aquifer of southeastern Wisconsin represents a very important regional water resource, a number of groundwater studies have been conducted to investigate this aquifer (Weaver and Bahr, 1991a,b; Young, 1992; Grundl and Cape, 2006). Previous groundwater flow modeling (Feinstein et al., 2005a,b), isotopic studies (Perry et al., 1982) and some unpublished ^{14}C data indicate that the groundwater in portions of this aquifer is very old, extending into the late Pleistocene. Since the area was glaciated during the last ice advance (e.g., Mickelson and Colgan, 2004; Colgan et al., 2003), the groundwater flow field must have changed dramatically in response to the ice advance and ice retreat. However precise data on groundwater residence times or on the paleo-flow field and recharge conditions are not available. Noble gases provide a high precision tool needed to reconstruct paleo-environmental conditions and can provide - together with ^{14}C dating and stable isotope information - a clear insight into paleo-conditions.

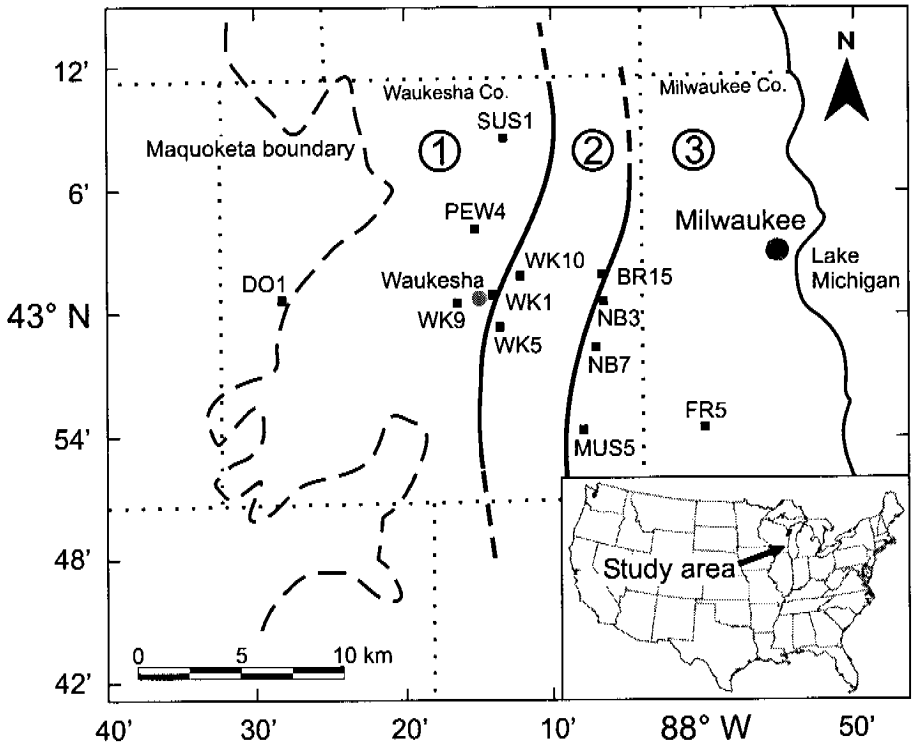

Figure 6.1: Map of the study area including sampling locations. The aquifer investigated is confined east of the Maquoketa boundary and semi-confined west of it. The solid lines demarcate the portions of the aquifer containing groundwater which infiltrated during the Holocene (1), during last glacial maximum (LGM) (2), and pre-LGM (3).

6.2 Hydrogeologic conditions

This study investigates the deep sandstone aquifer within Waukesha and Milwaukee counties in southeastern Wisconsin (Figure 6.1). The deep sandstone aquifer consists of Cambrian to Ordovician transgressive-regressive marine sedimentary rocks, predominantly sandstones with some minor dolomite strata (Young, 1992; Feinstein et al., 2005a,b). The essentially impermeable Pre-Cambrian basement rocks act as the basal boundary of the aquifer. All units within the aquifer dip eastward towards the Michigan Basin and southward towards the Illinois Basin. The deep aquifer is overlain by a shallow, unconfined aquifer and, in most of the study area, by the aquitard of the Maquoketa and Sinnippee Formations. The Maquoketa aquitard thins as the western edge is approached and its confining capability diminishes. West of the Maquoketa boundary the shallow and the deep sandstone aquifers are hydraulically connected (Siegel, 1990; Weaver and Bahr, 1991b).

Recharge to the deep aquifer is concentrated west of the Maquoketa boundary where it is unconfined. Small, local flow cells dominate the flow regime to the west of the Maquoketa boundary and water is freely exchanged between the deep sandstone aquifer and the overlying aquifer and surface water. The aquifer transitions to confined conditions east of the Maquoketa boundary and the flow regime changes

markedly to a system of uniform, lateral flow toward Lake Michigan which serves as the regional sink for groundwater flow (Feinstein et al., 2005a). This study is limited to the confined portion of the deep aquifer. The aquifer is a regionally important source of drinking water and as production has steadily increased during the last 100 years, a cone of depression 160 meters deep has developed in east central Waukesha county. Under present conditions, groundwater in the area no longer flows towards Lake Michigan, but instead flows radially towards the cone of depression.

6.3 Methods

In the study area, a total of 12 wells were sampled for noble gases, stable isotope and ^{14}C analyses (Figure 6.1; Tables 6.1, 6.2, 6.3). Not all wells were sampled for each parameter. ^{14}C data for four wells were obtained from D. I. Siegel (unpublished data, pers. comm.). The water samples for noble gas analyses were taken from the wellhead tap, filled in copper tubes and pinched to make a gas-tight seal. Care was taken to insure that no entrained bubbles remained in the sample. Noble gas abundances of He, Ne, Ar, Kr, Xe and the isotope ratios $^{3}He/^{4}He$, $^{20}Ne/^{22}Ne$, $^{36}Ar/^{40}Ar$ were measured by noble gas mass spectrometry and standard experimental protocols (Beyerle et al., 2000). The samples for stable isotope analysis were collected in polyethylene bottles and analyzed by mass spectrometry at the Stable Isotope Laboratory of the University of Bern. ^{14}C samples were collected in 50 L bottles, adjusted to pH 10 with NaOH and precipitated by addition of $BaCl_2$. Excess supernatant was decanted off to a volume of 1 L. The 1 L samples were prepared and measured by the Radiocarbon Laboratory of the University of Bern.

The use of noble gases as environmental tracers, and their interpretation in terms of NGT, and excess air amount and fractionation are described in detail in chapter 2.

6.4 Results and discussion

The NGTs vary between 1.4 °C (WK10) and 8.1 °C (DO1), indicating that some groundwater recharge occurred under distinctly colder climatic conditions than at present. The modern mean annual air temperature within the study area of about 8.5 °C (data available at http://www.noaa.gov) is reflected only by sample DO1 which is located in the recharge area west of the Maquoketa boundary. All other samples show lower NGTs. Figure 6.2A shows that the NGT is lowest in the central part of the study area, suggesting that this water infiltrated during the last glacial period. Flow distance from point of recharge in Figure 6.2 was obtained from the numerical model of Feinstein et al. (2005a,b). Samples taken from further east infiltrated before the last glacial maximum (LGM) under slightly warmer, but still colder climatic conditions than today.

The Pleistocene origin of these groundwater samples was confirmed by corrected ^{14}C ages which were calculated by averaging the results of different correction models

Table 6.1: Sampling locations and tracer data of the groundwater samples from Wisconsin. The model parameters NGT (noble gas temperature), A (initial amount of entrapped air), and F (fractionation factor) were calculated using the closed-system equilibration model of (Aeschbach-Hertig et al., 2000). The uncertainties of these model parameters are determined from the covariance matrix in the least squares fitting algorithm (Aeschbach-Hertig et al., 1999). The parameters derived from the inverse modeling were then used to calculate the Ne excess and hence the ΔNe as the difference between the measured total Ne and the calculated equilibrium fraction.

Sample	Flow dist. [km]	Longitude	Latitude	NGT [°C]	ΔNe [%]	A [cm^3_{STP}/g]	F [-]
BR15	21	88 6' 42.0" W	43 1' 40.5" N	2.9±0.5	72.4±4.7	21.6±3.2	0.35±0.04
DO1	-1	88 28' 20.2" W	43 0' 47.2" N	8.1±0.4	12.5±1.8	1.3±6.0	0.00±0.00
FR5	39	88 0' 2.8" W	42 54' 6.2" N	3.4±0.4	73.8±3.7	13.4±2.1	0.21±0.06
MUS5	28	88 8' 12.6" W	42 54' 6.0" N	4.1±0.6	20.1±2.5	28.6±13.9	0.77±0.04
NB3	23	88 6' 41.2" W	43 0' 23.8" N	3.3±0.6	34.8±3.1	25.1±7.1	0.62±0.04
NB7	26	88 7' 13.4" W	42 58' 10.2" N	2.6±0.2	37.9±0.3	14.7±1.6	0.51±0.02
PEW4	8	88 15' 14.8" W	43 4' 8.1" N	3.5±0.5	30.6±2.9	10.8±4.6	0.51±0.11
SUS1	13	88 13' 8.5" W	43 8' 34.4" N	4.5±0.6	30.0±2.9	22.0±7.3	0.65±0.05
WK10	15	88 12' 11.2" W	43 1' 43.6" N	1.4±0.5	72.0±4.6	16.9±2.8	0.29±0.05
WK5	18	88 13' 40.2" W	42 59' 13.6" N	2.3±0.5	45.7±2.7	30.4±5.7	0.57±0.03
WK9	13	88 16' 30.6" W	43 0' 27.5" N	5.5±0.5	28.3±2.2	12.7±4.7	0.58±0.08
WK1	14	88 14' 6.1" W	43 0' 50.2" N			n.d.	

Table 6.2: Stable isotope and radiocarbon data for the groundwater samples. The ^{14}C ages and errors are average values and 1-σ errors determined making use of three different correction models for calculating the initial activity A_0 of radiocarbon (Fontes and Garnier, 1979; Pearson and White, 1967; Tamers, 1967). It is important to note that all models yield very similar values for A_0.

Sample	$\delta^{18}O$ [‰]	$\delta^{2}H$ [‰]	^{14}C [pmC]	$\delta^{13}C$ [‰]	A_0 [pmC]	^{14}C age [yr]
BR15	-11.3	-77.3		n.d.		
DO1	-9.3	-62.1	38.2±0.2	-10.4±0.2	49±5	2065±828
FR5	-9.4	-63.3	1.8±0.1	-11.4±0.2	52±1	27851±478
MUS5	-8.6	-57.1		n.d.		
NB3	-10.3	-71.3	0.07*±0.2	-11.8±0.2	54±1	54974±23619
NB7	-9.9	-67.3	1.5±0.1	-11.7±0.2	54±1	29606±583
PEW4	-10.9	-75.8		n.d.		
SUS1	-10.8	-74.1		n.d.		
WK10	-12.4	-87.8	4.4±0.1	-11.3±0.2	52±1	20403±245
WK5	-11.9	-83.3	7.0*±0.2	-11.2±0.2	52±2	16534±371
WK9	-9.6	-65.5	25.4*±0.2	-11.8±0.2	54±1	6277±150
WK1	n.d.		18.9*±0.2	-10.7±0.2	51±5	8274±780

*unpublished data from D. I. Siegel (pers. comm.)

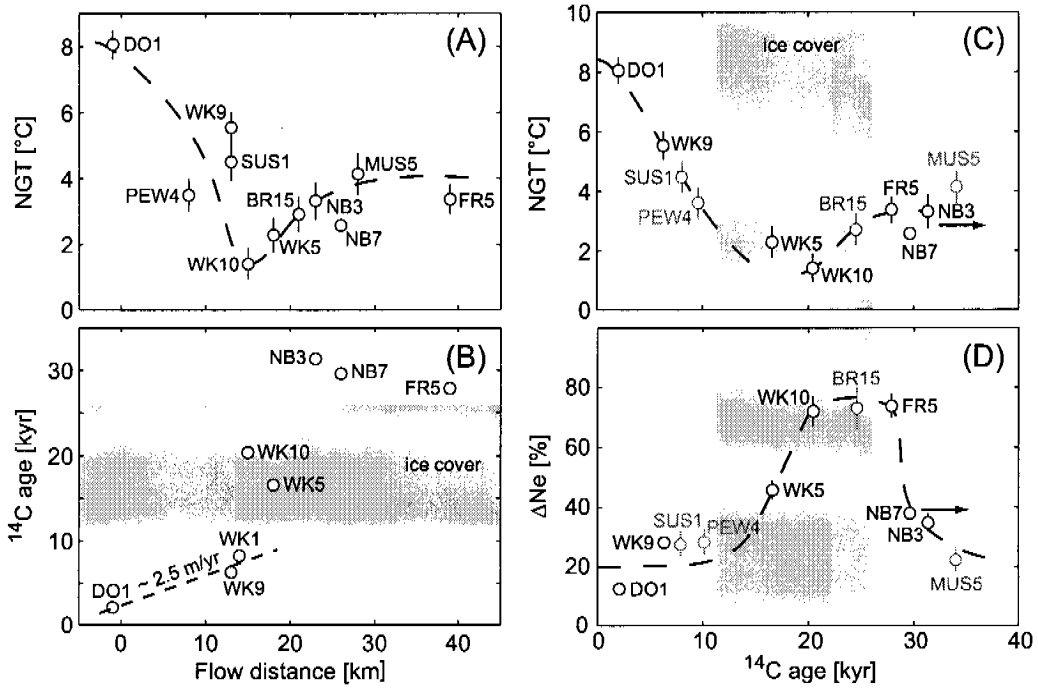

Figure 6.2: (A): NGT vs. flow distance from the point of recharge. (B): ^{14}C age vs. flow distance. The interruption in recharge occurs between WK1/WK9 and NB3/NB7. WK5 and WK10 were probably recharged during short periods of ice retreat.(C): NGTs vs. ^{14}C ages. Samples printed in gray were not ^{14}C dated and their ages were estimated from their NGTs and positions in the flow field, according to the temperature curve reconstructed from NGTs of dated samples (dashed line). (D): ΔNe vs. ^{14}C age. Variations in the amount of excess air (ΔNe) indicate changes in recharge dynamics shortly before and at the beginning of glaciation of the study area. The gray-printed samples were not ^{14}C dated and added to the plot according to the age estimate described in the text and shown in (C).

Table 6.3: Noble gas concentrations and isotope ratios of the groundwater samples. All concentrations are given in [cm^3_{STP}/g]. Overall measurement errors of the noble gas concentrations are about ±1 % for He, Ne, and Ar, ±2 % for Kr, and Xe, and <0.5 % for the isotope ratios.

Sample	He $[10^{-6}]$	Ne $[10^{-7}]$	Ar $[10^{-4}]$	Kr $[10^{-7}]$	Xe $[10^{-8}]$	$^3He/^4He$ $[10^{-8}]$	$^{22}Ne/^{20}Ne$	$^{40}Ar/^{36}Ar$
BR15	8.31	3.66	5.62	1.25	1.79	6.43	0.1021	295.9
DO1	0.167	2.26	4.06	0.954	1.41	52.1	0.1020	295.4
FR5	5.09	3.67	5.37	1.21	1.73	7.20	0.1021	296.0
MUS5	1.22	2.51	4.78	1.12	1.65	10.8	0.1021	295.4
NB3	7.11	2.85	5.11	1.18	1.72	6.30	0.1022	296.0
NB7	4.04	2.93	5.12	1.19	1.75	6.62	0.1023	295.6
PEW4	6.15	2.75	4.86	1.13	1.69	6.53	0.1021	295.3
SUS1	4.50	2.71	4.86	1.12	1.65	6.99	0.1022	295.9
WK10	6.52	3.71	5.70	1.29	1.86	6.92	0.1022	295.5
WK5	4.14	3.11	5.48	1.26	1.81	7.26	0.1021	295.8
WK9	2.38	2.64	4.62	1.07	1.56	7.26	0.1021	295.4
WK1					n.d.			

(see Table 6.2). The ^{14}C data confirm that samples WK5 and WK10, which exhibit the lowest NGTs, have an age of about 17 and 20 kyr BP (Figure 6.2C), respectively. It is during this time, from about 12-26 kyr BP, that the ice sheets of the Michigan and Green Bay Lobes covered the area (Colgan et al., 2003; Mickelson and Colgan, 2004). The samples NB3, NB7 and FR5, taken east of WK10, are ^{14}C dated prior to the LGM at about 28 (FR5), 30 (NB7) and >31 kyr BP (NB3) under slightly warmer climatic conditions. A minimum age for NB3 is given because this well has very little ^{14}C activity (0.07±0.2 pmC) and is at the edge of reliable ^{14}C dating. Samples DO1, WK1 and WK9, located west of WK10, have ^{14}C ages of 2.1 (DO1), 8.3 (WK1) and 6.3 kyr BP (WK9) – long after the retreat of the Laurentide ice sheet.

The ^{14}C dated samples along with their NGTs can be used to reconstruct a paleo-soil temperature curve during the late Pleistocene and Holocene (Figure 6.2C). By the use of this soil temperature curve, NGTs – together with the position of the samples in the flow field – can be used as a rough proxy for residence time for those samples that were not ^{14}C dated.

The stable isotopic composition of water contains similar information on the source of groundwater. All stable isotope samples plot close to the global meteoric water line (Figure 6.3), indicating that the groundwater originated from meteoric water and has not undergone significant isotope exchange with the aquifer matrix.

Samples during and after the LGM follow the global $\delta^{18}O$-temperature relationship and match the noble gas temperatures very well (round symbols in Figure 6.4A). This is evidence that temperatures derived from stable isotopes and noble gases during this period of time yield essentially identical paleotemperatures. Groundwater recharged during the LGM cannot be pure glacial meltwater because pure meltwater

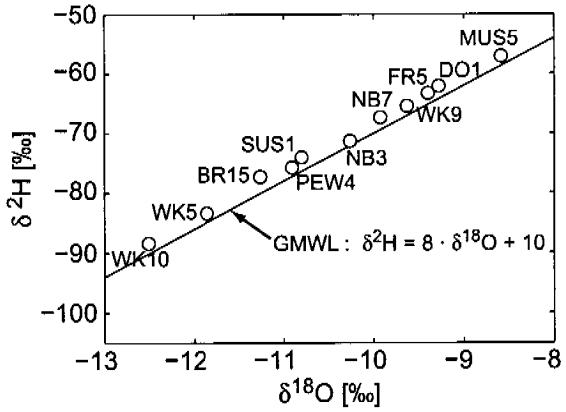

Figure 6.3: Stable isotopic composition of the groundwater samples. All samples plot close to the global meteoric water line (GMWL; Craig, 1961).

of the Laurentide ice sheet would have $\delta^{18}O$ values as low as -30 to -35 ‰ (Clark et al., 2000, and references therein), well below our minimum $\delta^{18}O$ value of -12.5 ‰. The easternmost samples FR5, NB3, NB7, and MUS5, which are older than the LGM, plot above the global $\delta^{18}O$-temperature relationship (square symbols in Figure 6.4A). The $\delta^{18}O$ values in these wells are too heavy with respect to the corresponding NGTs. Previous authors have made similar observations in North America, and have attributed the enriched $\delta^{18}O$ values to a change in atmospheric circulation patterns, particularly to an increase in the influence of the Gulf of Mexico moisture source which is known to be enriched in $\delta^{18}O$ (Plummer, 1993; Amundson et al., 1996; Ma et al., 2004).

Wells within the Waukesha (WK) and New Berlin (NB) well fields are located close to each other (Figure 6.1). With respect to the modern flow field, however, the ^{14}C ages are very different - much more than would be expected from the short flow distances involved. Figure 6.2B shows three distinct portions of the flow field. The youngest portion (DO1, WK1, WK9) records the modern flow field in which the rate of groundwater flow (~2.5 m/yr) matches rates obtained using the numerical model of Feinstein et al. (2005b). The oldest portion (NB3, NB7 and FR5) is only ~8 km further downgradient yet was recharged ~20 kyr earlier - before the area was covered with ice. The probable reason for this ~20 kyr interruption in groundwater recharge is the ice cover that existed throughout the area from about 12 to 26 kyr BP.

The intermediate portion is represented by WK5 and WK10, both of which lie in the middle of the time gap. $\delta^{18}O$ data indicate that water in these wells is not derived from glacial meltwater, but rather originated as meteoric water. Therefore, recharge events during the LGM may have occurred during small periods of ice retreat. The ^{14}C ages of WK5 and WK10 could also result from dispersive mixing of groundwater which infiltrated shortly before and after the LGM (Beyerle et al., 1998).

The amount of excess air – expressed as the relative Ne supersaturation with respect to the atmospheric equilibrium (ΔNe) – reveals two groups of water samples

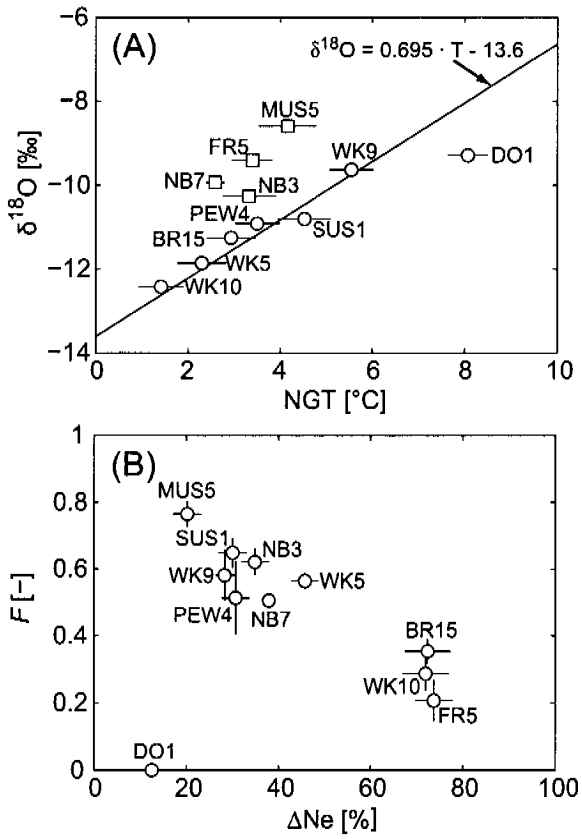

Figure 6.4: (A): δ^{18}O vs. NGT. Samples from during and after ice cover (circles) follow the global δ^{18}O-temperature (T) relationship (Dansgaard, 1964). Pre-ice cover samples (squares) show evidence of enrichment in δ^{18}O. (B): Fractionation factor (F) vs. excess air (ΔNe). The strong correlation between amount of excess air and fractionation is indicated.

(Figures 6.2D and 6.4B). The first group (WK10, BR15, and FR5) is characterized by ΔNe values of about 75 % with low fractionation factors and groundwater ages of 20-28 kyr BP. All other samples contain between 20 to 50 % ΔNe, are much more fractionated and infiltrated either after the LGM or earlier than 28 kyr BP. One can speculate that the large amounts of excess air found in the samples WK10, BR15, and FR5 are the result of changes of the regional hydraulic conditions, due to an increase in groundwater table fluctuations during recharge or to progression of the ice sheet. The remaining samples were recharged under conditions similar to today with moderate groundwater table fluctuations. The observed amounts of excess air are further evidence, in addition to the $\delta^{18}O$ data, that none of the groundwater samples are pure glacial meltwater which is known to contain as much as several hundred percent ΔNe (Vaikmäe et al., 2001).

The fractionation factor F should be correlated with the hydrostatic pressure, and hence with the amount of excess air, because high pressure leads to a more complete dissolution of the trapped gas phase (Kipfer et al., 2002). All samples, except for DO1, show this clear negative correlation between the amount of excess air and its fractionation (Figure 6.4B). Our data make a strong case that the observed changes in the size and fractionation of the excess air component can be interpreted in terms of changes in hydraulic conditions during groundwater recharge.

6.5 Conclusions

The data presented suggest a soil cooling of about 6.5 to 7 °C during the last glacial period relative to the modern soil temperature. Similar estimates of -5 to -7 °C for the glacial cooling have been made for paleogroundwater in North America (Clark et al., 1997, 1998; Stute et al., 1992, 1995a; Ma et al., 2004), and Europe (Andrews and Lee, 1979; Rudolph et al., 1984; Stute and Deak, 1989; Beyerle et al., 1998). Aeschbach-Hertig et al. (2002b) found a temperature difference between LGM and Holocene of 9 °C for the Aquia aquifer in Maryland. This considerably larger temperature difference is because the Aquia aquifer was 250 km from to the maximal extent of the Laurentide ice sheet (Aeschbach-Hertig et al., 2002b). In contrast, our study site was ice covered during the LGM, but shows a LGM-modern temperature difference of only 6.5 to 7 °C. This smaller temperature drop in our study area is probably caused by the lack of recharge during the coldest period when the area was ice covered.

The soil temperature prior to glaciation of the study area was about 3 °C, and recharge conditions were similar to those after glaciation as indicated by similar amounts of excess air. Furthermore, stable isotopes indicate a stronger influence of an enriched moisture source prior to glaciation, probably from the Gulf of Mexico.

Recharge dynamics seem to change before/when the area became ice covered and shortly before the NGT dropped to the minimum at about 20 kyr BP. This change in recharge dynamics is shown by an increase in the amount of excess air, suggesting, for example, increasing groundwater table fluctuations. No evidence of subglacial meltwater infiltration as proposed by Ma et al. (2004) for an aquifer in Michigan could

be found, because neither isotopically strongly depleted water nor any water with large ΔNe content could be found in our study area. The combination of ^{14}C ages, ΔNe and stable isotope data indicate groundwater recharge is driven by precipitation and not by infiltration of (glacial) meltwater during the last 40 kyr. The environmental tracer data of this study suggest a similar discontinuous recharge regime as found for Pleistocene groundwater in Europe where glaciation also interrupted groundwater recharge (Andrews and Lee, 1979; Beyerle et al., 1998). The observed decrease in amounts of excess air during and after glaciation of the area indicates that recharge dynamics changed quickly to present day conditions after ice retreat.

The environmental tracer results presented here have the potential to be used as tools to not only investigate aquifer dynamics, but also to validate existing groundwater models, to improve the conceptual framework for further modeling, to constrain glacier/aquifer interactions, and to elucidate paleoclimate changes.

Chapter 7

Groundwater dynamics and arsenic mobilization in Bangladesh assessed using noble gases and tritium

This chapter, except for section 7.2.5, has been published in *Environmental Science and Technology* (Klump et al., 2006b).

Preface

Beside the formation of excess air as a result of the dissolution of entrapped air within the quasi-saturated zone, secondary gas loss into an initially noble gas-free gas phase is a further aspect of gas exchange in groundwater. Such degassing, which is known to occur in very reducing aquifers, crucially hampers the use of dissolved noble gases as tracers for groundwater residence time. Groundwater from an aquifer in Bangladesh that is contaminated with naturally occurring arsenic is known to be partly degassed. Nevertheless, the groundwater could be dated using noble gases and tritium, by applying a simple, yet effective correction method to the degassed samples.

Abstract

The contamination of groundwater by geogenic arsenic is the cause of major health problems in south and southeast Asia. Various hypotheses proposing that As is mobilized by the reduction of iron (oxy)hydroxides are now under discussion. One important and controversial question concerns the possibility that As contamination might be related to the extraction of groundwater for irrigation purposes. If As were mobilized by the inflow of re-infiltrating irrigation water rich in labile organic carbon, As-contaminated groundwater would have been recharged after the introduction of groundwater irrigation 20-40 yr ago. We used environmental tracer data and conceptual groundwater flow and transport modeling to study the effects of groundwater pumping and to assess the role of re-infiltrated irrigation water in the mobilization of

As. Both the tracer data and the model results suggest that pumping induces convergent groundwater flow to the depth of extraction and causes shallow, young groundwater to mix with deep, old groundwater. The As concentrations are greatest at a depth of 30 m where these two groundwater bodies come into contact and mix. There, within the mixing zone, groundwater age significantly exceeds 30 yr, indicating that recharge of most of the contaminated water occurred before groundwater irrigation became established in Bangladesh. Hence, at least at our study site, the results call into question the validity of the hypothesis that re-infiltrated irrigation water is the direct cause of As mobilization. However, the tracer data suggest that at our site hydraulic changes due to groundwater extraction for irrigation might be related to the mobilization of As.

7.1 Introduction

Groundwater contamination by geogenic As is a widespread problem in south and southeast Asia. One of the most severely affected countries is Bangladesh (Chowdhury et al., 2000; Karim, 2000). The alluvial aquifers of the Ganges, Brahmaputra, and Megna river floodplains are intensively used for water supply. Tube wells have been installed since the 1970s in order to provide pathogen-free drinking water instead of the biologically contaminated surface water used before. The As concentrations in groundwater from about a third of the recently installed 6 to 10 million drinking water wells exceed the Bangladesh standard of 50 μg/L (WHO standard is 10 μg/L). Millions of people are threatened by arsenicosis and increasing cancer rates (Kinniburgh and Smedley, 2001; Yu et al., 2003).

From a geochemical point of view, the principal chemical mechanisms of As mobilization are understood on a conceptual level, whereas the processes resulting in the erratic, patchy distributions of As contaminations in Bangladesh are still unknown. Different hypotheses have recently been formulated, proposing different spatial and hydrogeochemical origins of As in groundwater. Most authors assume that As is mobilized by reduction of iron (oxy)hydroxides (e.g., Kinniburgh and Smedley, 2001; Nickson et al., 1998; Harvey et al., 2002; McArthur et al., 2004; Zheng et al., 2004). Despite the geochemical studies, coupling of As contamination with groundwater hydraulics was never rigorously addressed. Up to now, little work has been done to evaluate groundwater hydrology in relation to the origin and distribution of As contamination.

In rural Bangladesh, groundwater is extracted for irrigation from the same aquifers that are used for drinking water production, and pumping volumes for irrigation are by far larger than those for drinking water. The impact of water extraction for irrigation on groundwater flow and As mobilization is controversially discussed. Some researchers argue that irrigation pumping has had little effect on groundwater flow (Aggarwal et al., 2003), whereas others argue that pumping has significantly affected flow patterns (Harvey et al., 2002, 2003). It is conceivable that pumping could either increase or decrease As levels.

Arsenic levels could be increased by the transport of organic carbon (C_{org}) into regions of the aquifer where C_{org} mobilizes As, or simply by transporting As from regions with high aqueous As concentrations. It has been speculated that C_{org} may come (i) directly from surface waters (permanent ponds and rivers) which receive large inputs of organic waste (agricultural and anthropogenic), (ii) from sediments beneath these recharge areas, or (iii) from irrigated rice fields (Harvey et al., 2002, 2005). The third of these scenarios assumes irrigated paddy fields being local sources of re-infiltrated irrigation water rich in labile C_{org}, which causes the mobilization of As in the sediments. The subsequent transport of the As-contaminated groundwater produces an As plume, resulting in the observed bell-shape of the vertical profile of the As concentration (hypothesis A, Figure 7.1A). Other papers assume that irrigation pumping may decrease As concentrations by flushing As from the system (e.g., McArthur et al. (2004), hypothesis B, Figure 7.1B), a process that may explain why irrigation wells at our site have lower As concentrations on average than drinking water wells (Harvey et al., 2003). Pumping could also lower As concentrations by increasing the oxic recharge that immobilizes As. However, at our field site dissolved oxygen concentrations are <0.35 mg/L throughout the depth profile (Swartz et al., 2004). In this paper, we suggest that irrigation pumping has caused younger and older water bodies to come into contact and mix. Mixing of the two groundwater bodies may mobilize As.

Information on groundwater hydrology - e.g., on groundwater residence times - is necessary to review hypotheses for As mobilization. Any conceptual model assuming that As is mobilized by water that was recharged after groundwater irrigation started (e.g., hypothesis A) requires that As-contaminated water be younger than the irrigation; i.e., the residence time of the groundwater must be less than the time span of irrigation. Hypothesis B also implies lowering of the residence time of the shallow groundwater. However, note that this does not necessarily mean that the water has to be younger than the time span of groundwater irrigation as it is required for hypothesis A. Unfortunately, no historical data are available on when groundwater irrigation was introduced at our field site. However, according to national estimates, groundwater irrigation has been common practice in Bangladesh since the 1970s (Harvey et al., 2005). Some groundwater samples from Bangladesh that contain elevated concentrations of As are older than 50 yr (Zheng et al., 2004; Dowling et al., 2002; van Geen et al., 2003). This clearly indicates that this As has not been mobilized by water that entered the aquifer during the last 50 yr, unless these waters have been recycled as re-infiltrated irrigation water, a possibility which we explore below. However, it remains open whether hydraulic changes due to groundwater pumping may affect As mobilization. We applied environmental tracer analyses and conceptual groundwater modeling to assess whether groundwater dynamics, especially the water extraction for irrigation, may affect As mobilization in Bangladesh. Our work provides quantitative information on the time-scales of groundwater transport that is relevant to the distribution of As in the aquifer.

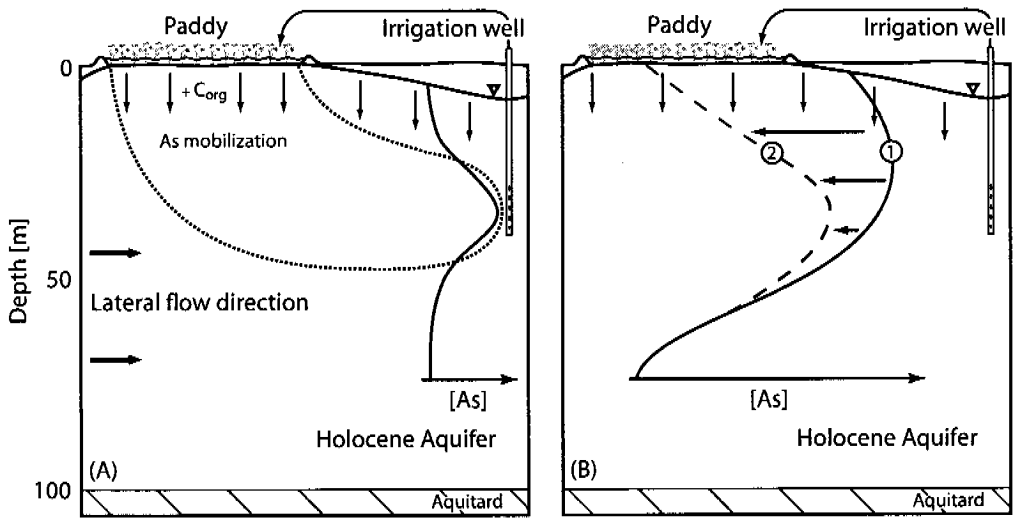

Figure 7.1: Schematic cross-sections illustrating hypotheses A and B, which both link the distribution of As in the aquifer to groundwater pumping for irrigation purposes. Hypothesis A proposes that As is mobilized by re-infiltrated irrigation water which has high concentrations of young organic carbon. Hypothesis B proposes that the decrease in groundwater residence time in the upper part of the Holocene aquifer causes As to be flushed out of it. The pumping of large water volumes increases the rate of groundwater renewal, and hence the pronounced peak-shape of profile (2) develops from profile (1). Both hypotheses provide a conceptual explanation for the peak-shaped vertical As concentration profile observed at our field site (see text), as well as at other field sites throughout the Bengal Basin (Kinniburgh and Smedley, 2001; McArthur et al., 2004, 2001). Note that hypotheses A and B are not mutually exclusive.

7.2 Methods

7.2.1 Field site

Our study site is located in the small village of Bejgaon, near the village of Sreenagar in the rural Munshiganj district of Bangladesh, 30 km south of Dhaka and 7 km north of the Ganges River (for a detailed description of the study site see Swartz et al. (2004)). As is typical for southern Bangladesh, the local groundwater system consists of two aquifers. At our site, 21 groundwater observation wells tapping the upper, Holocene, aquifer were installed in an area of about 100 m^2. Each well is completed at a distinct depth (screen length: 1.5 m for shallow wells <30 m, 3 m for deep wells >30 m), so that the entire well-field covers a depth range from 4.6 to 107 m. At the surface, the upper aquifer is covered by a 3.5 m thick clay layer. This layer of low permeability is unsaturated to a depth of about 2 m during the maximum water drawdown during the dry season. The upper aquifer, which is used for local drinking water supply and irrigation, consists of intercalated sands and silty sands of gray and grayish-green color. It is about 100 m thick and hydraulically disconnected from the lower, Pleistocene, aquifer by a 40-m thick aquitard of marine clay. The Pleistocene aquifer consists of light brown to orange sands and As concentrations are low in this

aquifer. In the following, our study concentrates on the upper, Holocene, aquifer which is strongly contaminated by geogenic As (Swartz et al., 2004). The hydraulic heads of the upper and lower aquifers differ by several centimeters (Harvey et al., 2005).

The field site is located about 500 m east of a small river, about 200 m away from the closest irrigation wells and there are two ponds right next to the field site (Figure 3B in Harvey et al. (2006); the density of irrigation wells is about 5 wells per km^2). About two thirds of the area in the vicinity of our site is irrigated for rice cultivation. The irrigation season starts in January and ends in late April. The flooding season, due to the monsoon rains and the rise of the Ganges, extends from June to October. Because dry season rice cultivation requires about 1 m of irrigation annually, a corresponding amount of groundwater is extracted from the upper aquifer. In addition, there is a much smaller, not irrigated fall season rice crop.

The hydrology and hydrochemistry of the study site (including the $\delta^{18}O$ and As data used here) have been well characterized (Harvey et al., 2002, 2005; Swartz et al., 2004). The vertical As profile shows a distinct concentration maximum of more than 600 μg/L As at a depth of about 30 m (Figure 7.2). The solid-phase As concentrations are about uniform throughout the entire depth profile of the aquifer sediments with higher concentrations in the clayish aquitards (Harvey et al., 2002).

Ponds provide much of the groundwater recharge (Harvey et al., 2006). Under natural conditions - i.e., without anthropogenic water extraction - the groundwater is expected to discharge towards rivers. Irrigation, however, strongly modifies groundwater flow, so that in the seasonal average pumping becomes the dominant groundwater sink (Harvey et al., 2006).

7.2.2 Analytical methods

In January 2004, 17 wells were sampled along a vertical transect for noble gas and tritium (^3H) analysis (Table 7.1). After purging the wells, the samples were taken using a submersible pump. To avoid degassing of the groundwater due to bubble formation during sampling, the water was pumped at high rates to maintain high pressure. No gas bubbles were observed during groundwater sampling. The samples for noble gas and ^3H analysis were filled into copper tubes and sealed gas-tight using pinch-off clamps. All samples were analyzed for noble gas concentrations and the isotope ratios $^3He/^4He$, $^{20}Ne/^{22}Ne$ and $^{36}Ar/^{40}Ar$ using noble gas mass spectrometry in the Noble Gas Laboratory at ETH Zürich (Beyerle et al., 2000). ^3H concentrations were determined by the ^3He-ingrowth method using a high-sensitivity compressor-source noble gas mass spectrometer (Beyerle et al., 2000; Baur, 1999). In the field, temperature and electrical conductivity were measured using a WTW LF 330 probe during sampling.

Table 7.1: Noble gas and ^{3}H concentrations. The overall measurement errors (1σ errors) are $\pm 1\%$ for He and Ne, $\pm 0.7\%$ for R_{He}, $\pm 0.3\%$ for R_{Ne}, and $\pm 0.2\%$ for R_{Ar}. The absolute errors of ^{3}H are specified individually.

Depth [m]	He[a] [10^{-8}]	Ne[a] [10^{-7}]	R_{He}[b] [10^{-6}]	R_{Ne}[c] [-]	R_{Ar}[d] [10^{-3}]	^{3}H [TU]	$^3He_{tri}$ [TU]	τ[e] [yr]	$^4He_{ter}$[a] [10^{-9}]
9	4.59	1.87	1.47	9.77	3.374	5.02±0.16	1.8±0.6	5±2	-1.3±0.7
14	4.93	1.94	3.85	9.77	3.380	9.23±0.27	61.9±15.5	36±4	0.3±0.6
18	6.12	2.33	5.97	9.78	3.374	18.5±0.5	142±36	39±4	1.0±0.8
24	5.74	1.98	5.60	9.78	3.368	n.d.[f]	127±32	n.d.[f]	9.0±2.3
24	5.73	2.03	5.24	9.79	3.373	12.4±0.4	116±29	42±4	7.4±2.0
30	6.63	2.49	2.04	9.77	3.374	2.22±0.13	23.4±5.9	44±4	1.9±1.0
30	6.76	2.62	1.41	9.76	3.374	n.d.[f]	0.9±0.6	n.d.[f]	-1.1±0.9
30	6.73	2.53	2.17	9.78	3.373	1.96±0.10	28.2±7.1	49±4	1.7±0.9
30	6.93	2.66	1.98	9.76	3.380	1.82±0.12	20.9±5.3	45±4	-0.6±0.9
38	5.36	1.73	1.35	9.79	3.368	n.d.[f]	7.0±1.8	n.d.[f]	13.5±3.4
38	5.43	1.75	1.36	9.78	3.377	0.12±0.08	7.4±1.9	74±12	13.5±3.4
46	5.24	1.67	1.30	9.77	3.383	0.01±0.09	6.1±1.6	>50	14.1±3.6
46	5.16	1.64	1.30	9.80	3.376	0.01±0.07	6.0±1.6	>50	14.1±3.6
61	7.97	2.22	1.24	9.83	3.380	n.d.[f]	10.3±2.7	n.d.[f]	28.4±7.2
61	5.40	1.67	1.14	9.78	3.379	0.04±0.08	2.6±0.8	>50	16.1±4.1
76	6.27	1.97	1.12	9.78	3.376	0.03±0.08	0.9±0.6	>50	16.0±4.1
107	4.88	1.40	1.03	9.77	3.381	0.00±0.07	2.4±0.7	>50	19.4±4.9

[a] Noble gas concentrations are given in cm^3_{STP}
[b] $^3He/^4He$, [c] $^{20}Ne/^{22}Ne$, [d] $^{36}Ar/^{40}Ar$
[e] $^3H/^3He$-age
[f] not determined

7.2.3 Environmental tracers

Noble gases dissolved in groundwater are widely used as chemically inert tracers in subsurface hydrology in order to study groundwater transport and gas/water partitioning (see e.g., Kipfer et al. (2002); Cook and Herczeg (2000) for reviews). Atmospheric noble gases enter the groundwater by gas exchange within the unsaturated zone. The solubility equilibrium concentration is given by the environmental conditions (water temperature, air pressure, salinity) prevailing during infiltration. In addition, the dissolution of entrapped air bubbles below the groundwater table yields a supersaturation of atmospheric gases with respect to the equilibrium concentration ("excess air"; Heaton and Vogel, 1981). Besides noble gases of atmospheric origin, most groundwater samples also contain radiogenic noble gases; e.g., tritiogenic ^{3}He and ^{4}He produced by U and Th decay. These non-atmospheric components provide information on groundwater age. Tritium, the radioactive hydrogen isotope ^{3}H (half-life $\tau_{1/2} = 4500$ d), has a natural atmospheric background concentration of about 5 TU (Craig and Lal (1961); 1 tritium unit equals 1 ^{3}H atom in 10^{18} ^{1}H atoms). It decays to its stable daughter isotope $^3He_{tri}$ (tritiogenic ^{3}He). In recent waters, ^{3}H originates mainly from the atmospheric thermonuclear bomb tests conducted during the 1950s

and 1960s, with subsequent incorporation of ^{3}H into the water cycle by oxidation. The maximum ^{3}H concentration of up to several thousand TU (in the northern hemisphere) occurred in 1963/64, and formed the so-called "bomb peak".

7.2.4 Groundwater dating

In cases where the local atmospheric ^{3}H input function is known, ^{3}H can be used to date the groundwater by comparing the measured ^{3}H concentrations with the input function corrected for decay relative to the time of sampling. Furthermore, ^{3}H can be used to distinguish between pre-bomb groundwater (with virtually no ^{3}H), which infiltrated before ~1955, from water containing significant amounts of (bomb-derived) ^{3}H indicating infiltration less than 50 yr ago. The atmospheric ^{3}H input function, which needs to be known for groundwater dating by ^{3}H, shows significant spatial variation at local and global scales. Since the local input function for southern Bangladesh is unknown, we used an input function for Dhaka (Stute, 2001) that was reconstructed from known ^{3}H time series in south and southeast Asia.

In addition to the information gained from the ^{3}H input function, the ^{3}H/^{3}He dating method, which is based on the "clock" inherent in the radioactive decay of ^{3}H to ^{3}He, can be used to determine groundwater ages. The ^{3}H/^{3}He age τ is calculated from the following equation (e.g., Schlosser et al., 1988):

$$\tau = \frac{\tau_{1/2}}{\ln(2)} \ln\left(1 + \frac{[^3\mathrm{He}_{\mathrm{tri}}]}{[^3\mathrm{H}]}\right) \tag{7.1}$$

where $[^3\mathrm{He}_{\mathrm{tri}}]$ and $[^3\mathrm{H}]$ are the concentrations of tritiogenic ^{3}He and ^{3}H in the water sample, respectively. The $^3\mathrm{He}_{\mathrm{tri}}$ component can be determined by the following equation (Kipfer et al., 2002; Schlosser et al., 1989):

$$\begin{aligned}[^3\mathrm{He}_{\mathrm{tri}}] = [^4\mathrm{He}_{\mathrm{tot}}] \left(\left(\frac{^3\mathrm{He}}{^4\mathrm{He}}\right)_{\mathrm{tot}} - \left(\frac{^3\mathrm{He}}{^4\mathrm{He}}\right)_{\mathrm{ter}}\right) - [^4\mathrm{He}_{\mathrm{equ}}] \cdot \\ \left(\left(\frac{^3\mathrm{He}}{^4\mathrm{He}}\right)_{\mathrm{equ}} - \left(\frac{^3\mathrm{He}}{^4\mathrm{He}}\right)_{\mathrm{ter}}\right) - \left(\frac{\mathrm{He}}{\mathrm{Ne}}\right)_{\mathrm{exc}} \cdot \\ ([\mathrm{Ne}_{\mathrm{tot}}] - [\mathrm{Ne}_{\mathrm{equ}}]) \left(\left(\frac{^3\mathrm{He}}{^4\mathrm{He}}\right)_{\mathrm{exc}} - \left(\frac{^3\mathrm{He}}{^4\mathrm{He}}\right)_{\mathrm{ter}}\right)\end{aligned} \tag{7.2}$$

where $[^4\mathrm{He}_{\mathrm{tot}}]$ is the measured ^{4}He concentration, $(^3\mathrm{He}/^4\mathrm{He})_{\mathrm{tot}}$ is the measured ^{3}He/^{4}He ratio, $(^3\mathrm{He}/^4\mathrm{He})_{\mathrm{ter}}$ is the ^{3}He/^{4}He ratio of terrigenic He, i.e., He emanating from solid earth. As the sediments in Bangladesh mainly originate from crustal rocks, a value of $(2 \pm 1) \cdot 10^{-8}$ was used for $(^3\mathrm{He}/^4\mathrm{He})_{\mathrm{ter}}$, which represents the expected production ratio in crustal rocks (Mamyrin and Tolstikhin, 1984). $[^4\mathrm{He}_{\mathrm{equ}}]$ is the atmospheric equilibrium ^{4}He concentration, $(^3\mathrm{He}/^4\mathrm{He})_{\mathrm{equ}}$ $(= 1.36 \cdot 10^{-6})$ is the atmospheric equilibrium ^{3}He/^{4}He ratio in water, $(\mathrm{He/Ne})_{\mathrm{exc}}$ $(= 0.288)$ is the He/Ne ratio of the excess

air component assuming unfractionated excess air, and $(^3He/^4He)_{exc}$ $(= 1.38 \cdot 10^{-6})$ is the $^3He/^4He$ ratio of the excess air component (for detailed discussion see Kipfer et al., 2002).

Commonly, the concentration of $^4He_{ter}$ can be used at least as a qualitative indication of groundwater age on time scales of ~100 yr or more. The release of $^4He_{ter}$ from the aquifer matrix (and deeper crust or mantle) into the groundwater yields a relationship between the groundwater residence time and the accumulated $^4He_{ter}$. The $^4He_{ter}$ concentration is determined by the following equation (e.g., Schlosser et al., 1989):

$$\left[^4He_{ter}\right] = \left[^4He_{tot}\right] - \left[^4He_{equ}\right] - \left(\left[Ne_{tot}\right] - \left[Ne_{equ}\right]\right)\left(\frac{He}{Ne}\right)_{exc} \tag{7.3}$$

7.2.5 Dispersive effects

In order to evaluate the influence of dispersive transport on the ^3H signal and $^3H/^3He$ ages, the 1-D advection-dispersion equations for ^3H and $^3He_{tri}$ has been solved numerically:

$$\frac{\partial\left[^3H\right]}{\partial t} = D_L\frac{\partial^2\left[^3H\right]}{\partial x^2} - v\frac{\partial\left[^3H\right]}{\partial x} - \lambda\left[^3H\right] \tag{7.4}$$

$$\frac{\partial\left[^3He_{tri}\right]}{\partial t} = D_L\frac{\partial^2\left[^3He_{tri}\right]}{\partial x^2} - v\frac{\partial\left[^3He_{tri}\right]}{\partial x} + \lambda\left[^3H\right] \tag{7.5}$$

where D_L is the longitudinal dispersion coefficient, x is the spatial coordinate in flow direction and v is the flow velocity. We discretize equations (7.4) and (7.5) by the finite volume method, applying upstream differentiation of the advective term. Numerical dispersion is controlled by fine spatial discretization (1500 cells). The resulting system of ordinary differential equations is integrated numerically by the Matlab routine ode15s (Shampine and Reichelt, 1997). The boundary conditions are given by:

$$\left[^3H\right](x = 0, t) = \left[^3H\right]_0(t) \tag{7.6}$$

$$\left[^3He_{tri}\right](x = 0, t) = 0 \tag{7.7}$$

where $\left[^3H\right]_0(t)$ is the atmospheric input of ^3H.

The initial concentration distribution was calculated by the steady-state solutions of equations (7.4) and (7.5) (Solomon and Sudicky, 1991), because the (natural) atmospheric ^3H concentration ($\left[^3H\right]_0^{nat}$) can be assumed to be constant prior to 1955:

$$\left[^3H\right](x, t < 1955) = \left[^3H\right]_0^{nat}\exp(\gamma x), \quad \gamma = \frac{v}{2D_L} - \left(\frac{\lambda + v^2/4D_L}{D_L}\right)^{1/2} \tag{7.8}$$

$$\left[^3\mathrm{He_{tri}}\right](x,t<1955) = \left[^3\mathrm{H}\right]_0^{\mathrm{nat}} - \left[^3\mathrm{H}\right](x,t<1955) \tag{7.9}$$

Note that the solutions of the equations (7.4) and (7.5) only depend on the dimensionless parameter $\xi = v^2(D_L\lambda)^{-1} = v(\alpha\lambda)^{-1}$ (with $\alpha = Dv^{-1}$ being the dispersivity), which is given by the hydraulic conditions of the aquifer and the decay constant of ^{3}H. The effect of dispersive mixing on the ^{3}H concentrations and ^{3}H/^{3}He ages is further discussed in section 7.3.3 and in Figure 7.3.

7.2.6 Conceptual groundwater model

To evaluate a possible impact of water extraction due to extensive pumping, we numerically simulated different conceptual hydrological scenarios with or without water extraction. The model parameters are summarized in Table 2. We chose a 3-D model domain reflecting the typical capture zone of an irrigation well in the area, which is determined by the distance of the wells and the thickness of the aquifer (length = 400 m, width = 400 m, height = 120 m). The domain is discretized in 200×200×120 cells. Groundwater flow was modeled by a cell-centered finite volume method, using a conjugate gradient solver with algebraic multigrid preconditioning for the solution of the linear system of equations (Stüben, 2001). The vertical hydraulic conductivity distribution was determined by pump tests at our field site (Harvey et al., 2005). The bottom and the vertical sides of the model domain are no-flow boundaries. We computed residence times by a semi-analytical particle tracking method, neglecting dispersion (Pollock, 1988). Because the simulations cover time spans of several decades, seasonal fluctuations of hydrological boundary conditions are averaged out and mean annual values are used for recharge and pumping rates. This results in quasi-steady state simulations of groundwater flow.

We analyzed three conceptually different scenarios. (i) The non-irrigation scenario is modeled with a fixed hydraulic head at the top left edge of the model domain, representing the river, and a uniform flow boundary at the top of the model domain with a recharge rate of 0.25 m/yr that was determined by hydrological budget modeling (Harvey et al., 2006). (ii) In the permanent irrigation scenario, a pumping well (screened from 20–30 m depth, with a pumping rate of 20 L/s during the irrigation season) is situated in the center of the model domain and at the top a fixed hydraulic head is assumed. As indicated by hydrological budget modeling (Harvey et al., 2006), river ex- and infiltration cancel out in the annual average so that the river was neglected as special boundary section in our modeling exercise. Groundwater flow and mixing characteristics changed in the 1970s, as groundwater extraction for irrigation greatly increased across the country (Harvey et al., 2005). (iii) The third scenario, which assumes a rapid change from the non-irrigation regime to the irrigation regime 30 yr ago, was implemented by a combination of the non-irrigation and permanent irrigation scenarios described above. The results of the scenario calculations will be discussed below.

Table 7.2: Model parameters of the conceptual groundwater model.

Hydraulic Conductivity Profile[a]

Depth [m]	K_{hor} [10^{-4} m/s]	Depth [m]	K_{hor} [10^{-4} m/s]	Depth [m]	K_{hor} [10^{-4} m/s]
0–3	0.01	16–21	3.40	40–52	2.10
3–6	0.50	21–26	0.70	52–68	3.80
6–11	0.60	26–32	1.20	68–90	2.35
11–16	2.40	32–40	1.75	90–120	0.75

Anisotropy factor K_{vert}/K_{hor}: 0.1[b]
Porosity: 0.3[b]
Well screening: 20–30 m below surface[c]
Dimensions of model domain (L×W×H): 400×400×120 m
Discretization: 200×200×120 cells

Boundary Conditions

Scenario	Top face	Top left edge (river)	Bottom/sides	Pumping rate
A	Recharge: 0.25 m/yr[d]	Fixed head	No flow	No well
B	Fixed head	No impact[e]	No flow	20 L/s[f]
C	Switch from A to B 30 yr before sampling			

[a]Determined by pumping tests in the monitoring wells (Harvey et al., 2005)
[b]Typical value for sand deposits
[c]Typical value in the study area
[d]Estimated annual average before beginning of pumping (Harvey et al., 2006)
[e]River in- and exfiltration cancel in the annual average (Harvey et al., 2006)
[f]Annual average (Harvey et al., 2006)

7.3 Results and discussion

7.3.1 Electrical conductivity and $\delta^{18}O$

Figure 7.2 shows the vertical profiles of electrical conductivity and $\delta^{18}O$. Two different groundwater bodies can be distinguished. The shallow groundwater down to a depth of 20–30 m is characterized by low electrical conductivity and low $\delta^{18}O$ values. With increasing depth, both electrical conductivity and $\delta^{18}O$ decrease slightly. The deeper groundwater (depth >30 m) shows high electrical conductivity and high $\delta^{18}O$ values. Both tracer profiles suggest that there are two geochemically different groundwater bodies which mix at 30 m depth.

7.3.2 Noble gases and tritium

The measured noble gas concentrations suggest a slight degassing of the groundwater samples. This is indicated, for instance, by some samples with Ne concentrations below the solubility equilibrium value. In case of degassing controlled by diffusion, e.g., in the case of bubble formation due to pressure decrease during sampling, diffusion kinetics would result in a decrease in the $^{3}He/^{4}He$, $^{20}Ne/^{22}Ne$ and $^{36}Ar/^{40}Ar$ ratios in the water due to the higher diffusivity of the lighter isotopes ("Rayleigh fractionation"; Nagao et al., 1979; Brennwald et al., 2005). Whereas the isotope ratio of He is affected by radiogenic He production, the isotope ratios of Ne and Ar correspond closely to the atmospheric equilibrium value, thus excluding any strong,

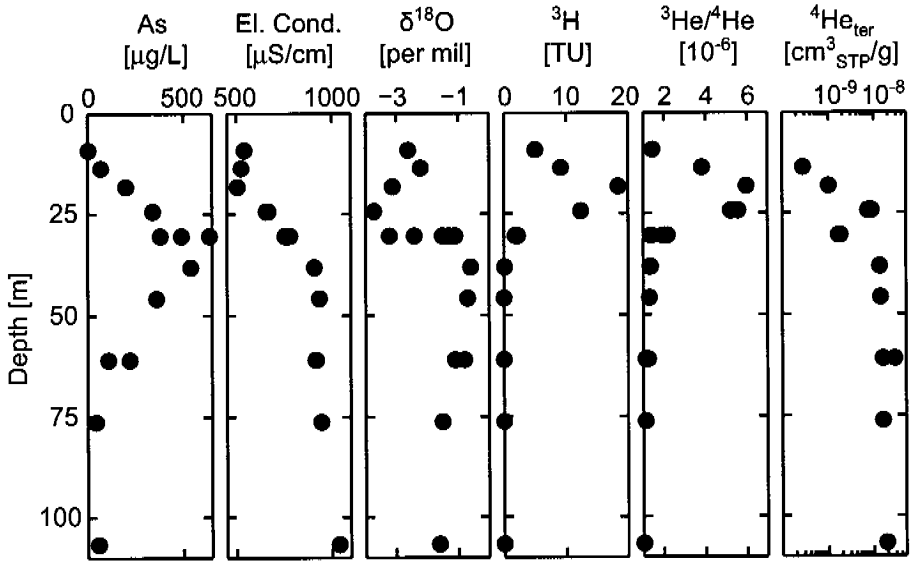

Figure 7.2: Depth profiles of As (12), electrical conductivity, $\delta^{18}O$ (11), ^3H, $^3He/^4He$ and $^4He_{ter}$ in the groundwater at the study site. In the vicinity of the study site, groundwater is typically pumped from depths of about 30 m. The ^3H concentration profile we present here qualitatively matches the ^3H profile that was measured in 2000/01 (Harvey et al., 2003) with the exception that in 2000 we found ~0.8 TU in one sample from 61 m depth. This finding could not be reproduced by the new data, which indicate virtual absence of ^3H below ~35 m.

diffusion-controlled degassing (Brennwald et al., 2005). Hence, we tend to assume that equilibrium degassing by gas stripping, e.g., due to exsolution of supersaturated CH_4 or CO_2 in surface water or groundwater, as it has been observed in other studies (e.g., Brennwald et al., 2005; Thomas et al., 2003; Purtschert et al., 2004; Holzner et al., 2004), is responsible for the degassing. However, the exact mechanism leading to the observed degassing of the groundwater remains unknown. The observed degassing pattern prohibits a statistically sound estimate of the amount and the fractionation of the excess air component based on the excess of the atmospheric noble gases (e.g., Aeschbach-Hertig et al., 1999).

As equilibrium degassing does not affect the isotope ratios, the $^3He/^4He$ ratio (Figure 7.2), which is used for the determination of $^3He_{tri}$, can be assumed to remain unaffected by degassing processes. Near the groundwater table, the measured $^3He/^4He$ ratio corresponds to the atmospheric equilibrium ratio. The $^3He/^4He$ ratio increases with depth due to strong accumulation of $^3He_{tri}$ and shows a maximum at 20 m depth, below which the $^3He/^4He$ ratio decreases again with increasing depth. Below 35 m, the $^3He/^4He$ ratio decreases slightly below the atmospheric equilibrium value as a result of the slight accumulation of $^4He_{ter}$ and the lack of large amounts of $^3He_{tri}$. The shape of the ^3H concentration profile is similar to that of the profile of the $^3He/^4He$ ratio (Figure 7.2). The ^3H concentration increases with depth and peaks with 18.5 TU at a depth of approximately 20 m. The ^3H concentration decreases below 20 m, and

below ~35 m the groundwater is virtually free of ^3H.

7.3.3 Groundwater dating

The ^3H and $^3He/^4He$ peaks at 20 m depth result from the atmospheric ^3H "bomb peak". The groundwater at this depth was therefore recharged during the early 1960s. The fact that below 35 m depth the groundwater is virtually free of ^3H indicates that this groundwater was recharged prior to the atmospheric bomb peak, and hence is at least 55 yr old.

Application of the $^3H/^3He$ dating method requires a knowledge of $^3He_{tri}$ concentrations. Degassing affects all dissolved gases, and hence principally hampers determination of the $^3He_{tri}$ concentration. As a first approximation, the $^3He_{tri}$ concentration was determined from equation (7.2) assuming no degassing (see above). The in-situ groundwater temperature of 26°C, which corresponds to the mean annual air temperature in the area, was used to calculate the atmospheric equilibrium concentrations. The excess air component was assumed to be unfractionated; i.e., to be of pure atmospheric composition. Note that such a determination of the $^3H/^3He$ age, disregarding degassing effects and assuming unfractionated excess air, yields a lower limit for the $^3H/^3He$ age, because both the correction for degassing and the assumption of fractionated excess air would increase the $^3H/^3He$ age. Correcting for fractionated instead of unfractionated excess air would not increase the $^3H/^3He$ ages significantly (<6% for samples from below 10 m depth), and therefore this scenario will not be discussed further. Comparison of the $^3H/^3He$ ages obtained (which indicate the time of recharge) and the measured ^3H concentrations with the atmospheric ^3H input function serves as a consistency check for the $^3H/^3He$ data. Figure 7.3A illustrates that the groundwater samples seem to be slightly degassed and the ^3He data can be corrected according to the procedure shown in Figure 7.3A. Assuming that samples were affected by a similar degree of degassing, the estimated $^3He_{tri}$ loss of about 20% would reduce the $^3H/^3He$ ages by at most ~4 yr. In addition, the $^3H/^3He$ ages were corrected for the deviation between $^3H/^3He$ ages and advective travel times (distance divided by flow velocity) due to dispersive effects (Figure 7.3B). After correcting of the $^3H/^3He$ ages for degassing and dispersive effects, the groundwater age profile shown in Figure 7.4 results. Overall, the corrections of the $^3H/^3He$ data are within the range of a few years at most and do not affect our interpretation of the groundwater dynamics at the study site.

Above 10 m, the groundwater age is low (<5 yr), whereas between 15 and 30 m depth, the water ages are almost constant (~40 yr). These intermediate ages are separated by sharp gradients from younger waters (above) and older waters (below). The youngest shallow water is probably recharged from the adjacent ponds. Generally, $^3H/^3He$ ages can be interpreted as mixing ages of water components with different residence times. Strictly speaking, we cannot therefore exclude the possibility that groundwater with a certain $^3H/^3He$ age might in fact be a mixture of groundwater components with different residence times. However, the sharp ^3H bomb peak (Fig-

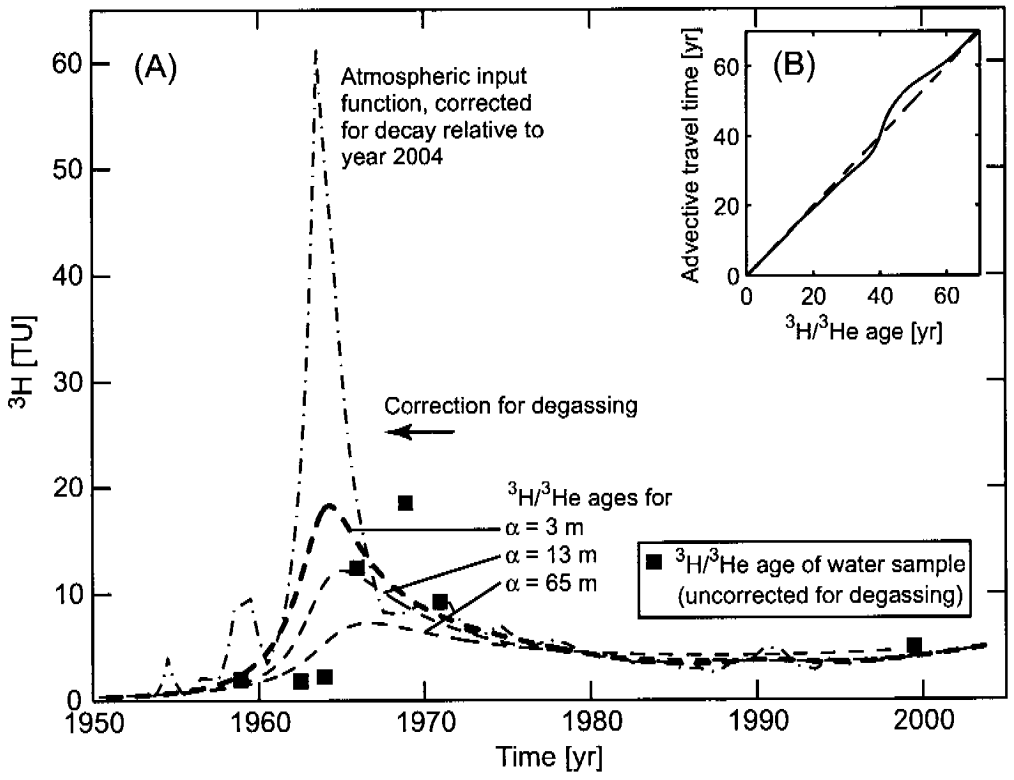

Figure 7.3: (A) Comparison of the atmospheric ^{3}H input function (Stute (2001), decay-corrected for 2004) with ^{3}H concentrations measured in the groundwater (squares). The latter are plotted along the time axis according to their calculated ^{3}H/^{3}He ages, interpreted as the time passed since the groundwater was recharged. The influence of longitudinal dispersion on the ^{3}H/^{3}He ages is shown for different dispersivities α (the ^{3}H peak is flattened and broadened due to the dispersive mixing of water components with different ^{3}H concentrations). Compared to the atmospheric ^{3}H input curve, the ^{3}H/^{3}He ages of the samples are shifted slightly toward lower ages. Most likely this indicates slight degassing of the groundwater samples, which is also indicated by the undersaturation of Ne. As indicated by the arrow, an increase in all calculated ^{3}H/^{3}He ages by the addition of an equal amount of ^{3}He would bring all groundwater samples on to the tritium input curve corrected for a dispersivity value of $\alpha = 3$ m, which is a reasonable value for the hydraulic situation existing at the field site. The required amount of additional ^{3}He corresponds to a loss of about 20% of the initial ^{3}He$_{tri}$ concentration. (B) Deviation of advective travel time from ^{3}H/^{3}He age for $\alpha = 3$ m calculated using the 1-D advection/dispersion model described above.

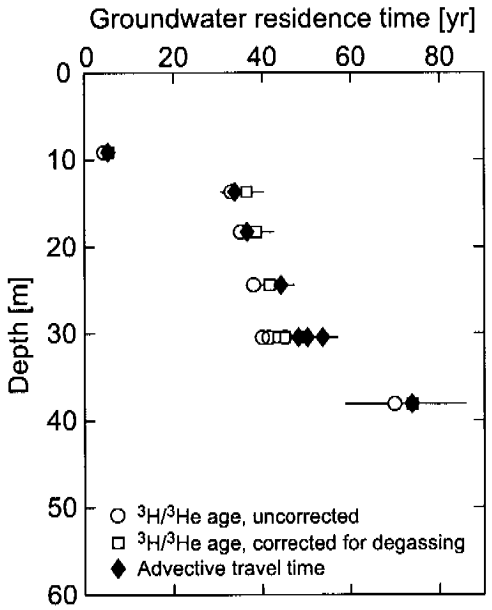

Figure 7.4: Depth profile of the $^3H/^3He$ ages of groundwater. The correction includes the effects of degassing and dispersion (see Figure 7.3).

ure 7.2) and the high ^3H concentrations of up to 18.5 TU, which are among the highest ^3H concentrations ever measured in Bangladesh groundwaters (Zheng et al., 2004; Aggarwal et al., 2003; Dowling et al., 2002), exclude strong mixing in the shallow groundwater body, because otherwise the ^3H peak would be more flattened. Since the water below 35 m is virtually free of ^3H, the exact water age of the deeper groundwater body cannot be determined using the $^3H/^3He$ method.

$^4He_{ter}$ was used as a further indicator of groundwater age. To separate out the $^4He_{ter}$ component (see equation (7.3)), a recharge temperature of 26°C and unfractionated excess air were again assumed. The loss of ^4He due to degassing is assumed to be similar to the 20% loss of ^3He, because the solubilities of ^3He and ^4He are similar and kinetic effects during degassing can be excluded (see above). The shallow groundwater contains hardly any $^4He_{ter}$ (Figure 7.2). At a depth of about 30 m the $^4He_{ter}$ concentrations increase by about one order of magnitude, indicating an abrupt increase in groundwater age. Again, this sharp gradient indicates the presence of two different groundwater bodies: young, shallow groundwater with low $^4He_{ter}$ concentrations, and old, deep groundwater with significantly larger amounts of $^4He_{ter}$. Thus, the $^4He_{ter}$ profile confirms the conclusions drawn from the electrical conductivity, $\delta^{18}O$ and ^3H. A $^4He_{ter}$ accumulation rate of $2 \cdot 10^{-11}$ $cm^3_{STP}/g_{water}/yr$ was determined for the Holocene aquifer in Laxmipur, southern Bangladesh (Dowling et al., 2003). Assuming a similar rate for our field site in Munshiganj, the estimated age of the deeper groundwater is in the range of several centuries.

In conclusion, the environmental tracer data suggest the presence of a young, shal-

low groundwater body that contains bomb-derived ^{3}H, indicating ages of less than ~55 yr, and of an old, deep groundwater body which is virtually ^{3}H-free and has accumulated significant amounts of $^{4}He_{ter}$. The latter isotope indicates that the deep groundwater seems to have characteristic renewal times of several hundred years. The two groundwater components, which are also characterized by their different mineralization and $\delta^{18}O$ signatures, are in contact and mix at about 30 m – at the same depth at which the As concentration profile peaks.

This conclusion is consistent with radiocarbon ages from our field site (Harvey et al., 2002). Dissolved inorganic carbon (DIC) has bomb-level ^{14}C at a depth of 20 m, indicating groundwater younger than 50 yr. In contrast, DIC radiocarbon ages at a depth of 30 m are in the range of about 500 to 800 yr, and are hence consistent with a strong increase in groundwater age between 20 and 30 m depth, and with the dissolution of carbon from the sediments. Furthermore, hydraulic head measurements from the field site directly indicate convergent groundwater flow at a depth of ~30 m (Harvey et al., 2005). To summarize, the available ^{14}C data and hydraulic measurements are in line with our interpretation that at 30 m depth, groundwater recharged during the last 5 decades is mixed with much older groundwater from below.

7.3.4 Conceptual groundwater model

To give a possible explanation of the observed distribution of groundwater ages, we simulated different generic hydrological scenarios, illustrating how water extraction for irrigation qualitatively influences groundwater flow and residence times (Figure 7.5). Note that irrigation significantly decreases residence times down to the depth of the well screen, as also proposed by hypothesis B (see above), and pulls up old water towards the well. The 30-yr irrigation scenario (Figure 7.5B) shows old groundwater being drawn back from the upwelling zone close to the discharging river, which results in a stepwise increase in residence time at about 30 m in the zone between the well and the river (Figure 7.5D, curve C). In contrast, note that the stepwise increase at 20 m depth in the non-irrigation scenario (Figure 7.5D, curve A) reflects the abrupt change in the hydraulic conductivity at this depth. The age profile of the 30-yr irrigation scenario agrees qualitatively with the results from the tracer data (see Figures 7.2 and 7.4).

In conclusion, the environmental tracer data and the modeling results provide important information on temporal and spatial groundwater dynamics (i.e., groundwater mixing and groundwater residence times), and indicate a possible relationship between As mobilization and the groundwater dynamics within the aquifer investigated. The extraction of large water volumes to irrigate the paddy fields causes a strong reduction in the residence time of the shallow groundwater body. Furthermore, it provokes convergent groundwater flow to the depth of extraction and induces mixing between the overlying and underlying groundwater layers.

Interestingly, As concentrations peak at the same depth (30 m) at which young, shallow groundwater mixes with old, deep groundwater. However, the $^{3}H/^{3}He$ data

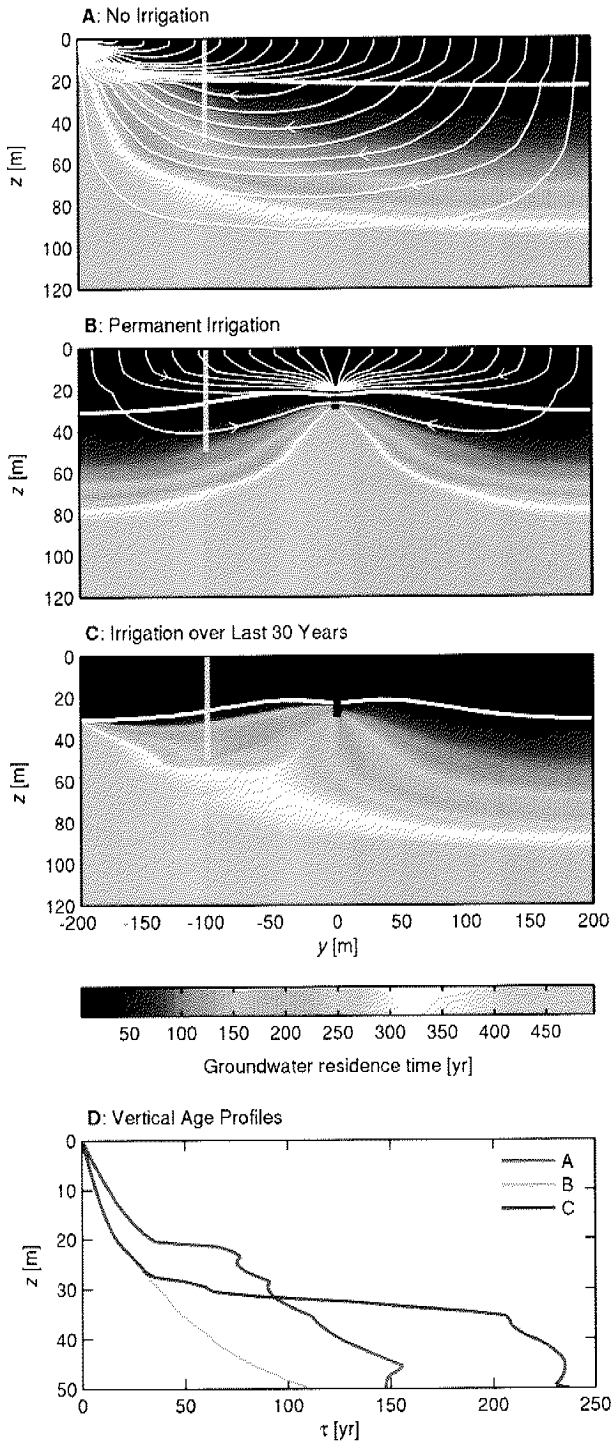

Figure 7.5: (A–C): Vertical cross-sections through the center of the 3-D model domain, showing groundwater residence times calculated by a particle-tracking algorithm for the non-irrigation (A), permanent irrigation (B) and the 30-yr irrigation (C) scenarios (y: horizontal coordinate, z: vertical coordinate). The thin white lines represent streamlines of the steady-state scenarios (A, B). The arrows indicate the direction of groundwater flow. The thick white line is the 30-yr isochrone. The black lines in B and C show a pumping well, screened from 20 to 30 m depth, situated in the center of the model domain. In A and C, the river is located at the top left-hand edge of the model domain. The gray line in A, B and C marks the position of the vertical age profiles shown in D.

clearly show that most of the As-rich groundwater is older than groundwater irrigation, which underwent a great increase across the country in the 1970s. This conclusion is especially evident with regard to the depth of the ^{3}H peak, which lies ~5–10 m above the maximum As concentration (see Figure 7.2). Furthermore, the As-contaminated groundwater below 35 m is virtually ^{3}H-free, and was therefore recharged before 1955. Thus, for the groundwater below 35 m, the tracer data calls into question the validity of hypothesis A, which assumes that re-infiltrated irrigation water drives the As mobilization. Above 35 m depth, the contribution of a small admixture of recently re-infiltrated irrigation water to As mobilization cannot strictly be excluded. However, the tracer data do not indicate the presence of re-infiltrated irrigation water at depths below ~15 m; hence, the contribution of re-infiltrated irrigation water to the As contamination is likely to be of minor importance.

However, there might be a second explanation for groundwater with a ^{3}H/^{3}He age of approximately 40 yr that agrees with hypothesis A. A significant proportion of groundwater recharge at our field site is re-infiltrated irrigation water (Harvey et al., 2006), and because re-infiltrated irrigation water is recycled groundwater, it may have low ^{3}H concentrations. Irrigation wells at our site withdraw water from 30 m or deeper, where we find low ^{3}H concentrations. Thus, given the measured ^{3}H concentrations, it is possible that groundwater below 30 m at our site contains re-infiltrated irrigation water. However, this scenario requires that at least two other conditions must be met. Firstly, the re-infiltrated irrigation water would have to follow a preferential flow path beneath the more slowly moving water that infiltrated before the atmospheric 3H bomb peak in 1963/64. At our field site, the hydraulic conductivity increases to a maximum at ~60 m depth beneath a low-conductivity layer of silty sediment at 24 m (Harvey et al., 2005). If the hydraulic conductivity profile at our site is representative on the regional scale and the high-conductivity layer is connected to the surface, possible preferential flow paths of re-infiltrated irrigation water cannot be excluded, although the tracer data do not indicate such a scenario.

The second necessary condition is that significant precipitation cannot mix with re-infiltrated irrigation water. During the irrigation season there is very little rain, and after the irrigation season the aquifer is primarily recharged from ponds and rivers (Harvey et al., 2006). Therefore, recharge from rice fields may lack a significant admixture of modern precipitation.

However, the interpretation that the deeper water has a significantly larger residence time than the shallower water seems to be more reasonable in hydrological and physical terms, and is able to give a consistent explanation of the tracer data. As a result, we conclude that re-infiltrated irrigation water from the rice fields does not contribute significantly to the As contamination at our field site – at least at depths greater than ~15 m, where the ^{3}H peak is an unambiguous time marker. However, other surface waters (ponds, rivers) still represent possible sources of recharging water rich in labile C_{org} that may drive the As mobilization (Harvey et al., 2002, 2005). The tracer data presented in this paper do not allow the impact of ponds and rivers to be assessed. Importantly, we are able to constrain scenarios that assume recharging

surface waters to be the primary cause of As mobilization by excluding re-infiltrated irrigation water as a factor of major importance.

To scrutinize, geochemically, a possible link between As release and the mixing of shallow and deep groundwater due to pumping, further studies, especially near operating irrigation wells, would be necessary. Such investigations might yield further information on the link between the geochemistry of As and the hydrodynamics of the Bangladesh aquifers. In addition, high-resolution profiles of groundwater age from other As-contaminated sites could be of great help in pinning down the relationships between As contamination and groundwater age.

Acknowledgments

We thank O. Leupin (Eawag), R. Beckie and M. Bolton (University of British Columbia), P. Oates (MIT), and M. F. Ahmed, M. A. Ali and the team from BUET for their help in logistics and field work. Thanks are also due to H. Amaral and C. Holzner (Eawag) for their help in lab work, D. M. Livingstone (Eawag) for editing assistance, and five anonymous reviewers for their helpful comments about our work. This work was supported by grants from the Swiss National Science Foundation (Project no. 200020-107489/1) and the Alliance for Global Sustainability.

Chapter 8

Synthesis and outlook

The reasons why excess air is an important issue in groundwater hydrology are manifold. In addition to the interpretation of environmental tracer data – e.g., noble gases, SF_6, and chlorofluorocarbons – where measured concentrations must be reliably corrected for the excess air component, excess air itself is a possible proxy for paleo-environmental conditions, as has been shown in the paleogroundwater study in Wisconsin. A necessary prerequisite for the use of excess air as a tracer for paleo-recharge conditions is a sound understanding of the physical processes governing its formation.

The results of the laboratory and field experiments, in combination with numerical investigations, confirm the validity of the conceptual model of the formation of excess air as being the result of the dissolution of entrapped air in quasi-saturated porous media. Moreover, the laboratory and field experiments, which are broadly based on the experimental and theoretical findings of Holocher et al. (2002, 2003), yield further insights into the physical processes controlling bubble-mediated gas exchange in porous media. Kinetic effects on the dissolution of entrapped air turned out to be only important at very large water flow velocities, and are most likely negligible in most natural systems.

Hydrostatic pressure is the main determinant of local gas equilibria, and hence controls the dissolution of entrapped air. Since the pressure gradients are fundamentally different for horizontal, vertically downward, and vertically upward flow, the timing of bubble dissolution and the evolution of the composition of both dissolved and entrapped gas are strongly affected by the direction of the flow.

The sand-column experiment, in conjunction with numerical simulations using the local equilibrium and KBD models, also revealed that apparently unfractionated excess air can be produced in the presence of a partly dissolved entrapped gas phase. This finding is of importance for the interpretation of the formation of unfractionated excess air which has originally been attributed to the complete dissolution of entrapped air. The new interpretation of the formation of apparently unfractionated excess air in the presence of partly dissolved entrapped air helps to overcome the problem that the hydrostatic pressure is usually insufficient to cause the complete dissolution of entrapped air in natural systems.

The results of the field experiments, which were the first field experiments con-

ducted to study the formation of excess air in natural systems, support the validity of the conceptual model of excess air formation. Furthermore, they suggest that soil properties such as grain-size and pore-size distribution, and hydraulic conductivity, have an influence on the formation of excess air which is favored by infiltration into and partial saturation of fine-grained sediments.

Besides hydrostatic pressure, soil temperature is also a determinant of gas exchange in the unsaturated and quasi-saturated zones. The field experiment in Munich showed that the NGT is identical to the local in-situ soil temperature at the time of infiltration which is important for the application of noble gases dissolved in groundwater as a proxy for paleo-soil temperature. Ma et al. (2004) studied a shallow aquifer in Michigan in which the NGTs differ from the mean annual soil temperature. Based on the results of the Munich experiment, further convincing explanations were proposed to find a conclusive solution to the problem in Michigan.

Although the recent work by Holocher et al. (2002, 2003) and the results presented here have contributed to obtaining a good understanding the formation of excess air in groundwater, there is still much work to be done on studying gas exchange in quasi-saturated porous media and on assessing the potential of excess air as a tracer for (paleo-)hydrological conditions. Future work could focus on the following questions:

- **What is the quantitative relationship between the amount of excess air and groundwater table fluctuations?**
  The hydrostatic pressure, which in natural aquifers is determined by fluctuations in the groundwater table, is known to be the main factor controlling the rate of dissolution of entrapped air. To use the amount of excess air as a tracer for groundwater table fluctuations, which in turn depend on climatic conditions, further studies would be needed to pin down quantitatively the relationship between the amount of excess air and the amplitude of water table fluctuations in natural, heterogeneous aquifers.

- **What determines the fractionation of excess air in natural systems?**
  Based on the results presented here, the presence of unfractionated excess air can not necessarily be attributed to the complete dissolution of entrapped air. By contrast, both fractionated and unfractionated excess air are produced during different phases of the dissolution process in the presence of an entrapped gas phase. Seepage velocity, residence time within the quasi-saturated zone, and the frequency of groundwater table fluctuations seem to determine the degree of fractionation. However, clear evidence from field studies is still lacking.

- **How do soil properties influence the formation of excess air?**
  The field experiments conducted here have shown that soil properties affect gas exchange in porous media. Further systematic studies are needed to investigate the impact of grain size, pore size, and hydraulic conductivity on gas exchange. This is important because excess air most likely depends on both climatic/recharge conditions and soil properties. To use excess air as a proxy for

paleo-environmental conditions, these two factors must be able to be separated reliably.

- **What is the impact of bubble-mediated gas transfer on the availability of O_2 and other (non-conservative) atmospheric gases dissolved in groundwater?**
  Noble gases have proved to be reliable tracers for gas exchange in quasi-saturated porous media. Since excess air formation concerns all atmospheric gases, the availability of O_2, which is an important measure of groundwater quality, is also affected by the formation of excess air. However, investigation of this issue is complicated by the non-conservative behavior of O_2. Ar is very similar to O_2 with respect to solubility and diffusivity, and could therefore be used as a conservative tracer for O_2 in groundwater. Modern analytical methods would even allow the concentrations of Ar and O_2 to be measured quasi-continuously. This would certainly yield new insights into both the formation of excess air (including short-term variations) and O_2 decay rates in groundwater.

These are just a few suggestions for potential relevant future research. Hopefully, the work described in this thesis will stimulate hydrogeologists and environmental physicists to continue working in the future in the exciting field of bubble-mediated gas exchange in quasi-saturated porous media.

Bibliography

Aeschbach-Hertig, W., Beyerle, U., Holocher, J., Peeters, F., and Kipfer, R. (2002a). Excess air in groundwater as a potential indicator of past environmental changes. In IAEA, editor, *Study of Environmental Change Using Isotope Techniques*, volume 13/P of *C&S Papers Series*, pages 174–183, Vienna. IAEA.

Aeschbach-Hertig, W., Peeters, F., Beyerle, U., and Kipfer, R. (1999). Interpretation of dissolved atmospheric noble gases in natural waters. *Water Resour. Res.*, 35(9):2779–2792.

Aeschbach-Hertig, W., Peeters, F., Beyerle, U., and Kipfer, R. (2000). Palaeotemperature reconstruction from noble gases in ground water taking into account equilibration with entrapped air. *Nature*, 405:1040–1044.

Aeschbach-Hertig, W., Stute, M., Clark, J., Reuter, R., and Schlosser, P. (2002b). A paleotemperature record derived from dissolved noble gases in groundwater of the Aquia Aquifer (Maryland, USA). *Geochim. Cosmochim. Acta*, 66(5):797–817.

Aggarwal, P. K., Basu, A. R., and Kulkarni, K. M. (2003). Comment on "Arsenic mobility and groundwater extraction in Bangladesh" (I). *Science*, 300:584d.

Amundson, R. G., Chadwick, O. A., Kendall, C., Wang, Y., and DeNiro, M. J. (1996). Isotopic evidence for shifts in atmospheric circulation patterns during the late Quaternary in mid-North America. *Geology*, 24(1):23–26.

Andrews, J. N. and Lee, D. J. (1979). Inert gases in groundwater from the Bunter Sandstone of England as indicators of age and palaeoclimatic trends. *J. Hydrol.*, 41(3-4):233–252.

Ballentine, C. J. and Hall, C. M. (1999). Determining paleotemperature and other variables by using an error-weighted, nonlinear inversion of noble gas concentrations in water. *Geochim. Cosmochim. Acta*, 63(16):2315–2336.

Baur, H. (1999). A noble-gas mass spectrometer compressor source with two orders of magnitude improvement in sensitivity. In *American Geophysical Union, Fall Meeting*, volume 80 of *EOS, Trans. Am. Geophys. Union*, page F1118, San Francisco. American Geophysical Union.

Beyerle, U., Aeschbach-Hertig, W., Hofer, M., Imboden, D. M., Baur, H., and Kipfer, R. (1999a). Infiltration of river water to a shallow aquifer investigated with $^{3}H/^{3}He$, noble gases and CFCs. *J. Hydrol.*, 220(3-4):169–185.

Beyerle, U., Aeschbach-Hertig, W., Imboden, D. M., Baur, H., Graf, T., and Kipfer, R. (2000). A mass spectrometric system for the analysis of noble gases and tritium from water samples. *Environ. Sci. Technol.*, 34(10):2042–2050.

Beyerle, U., Aeschbach-Hertig, W., Peeters, F., Kipfer, R., Purtschert, R., Lehmann, B., Loosli, H., and Love, A. (1999b). Noble gas data from the Great Artesian Basin provide a temperature record of Australia on time scales of 10^5 years. In *Isotope techniques in water resources development and management*, volume IAEA-SM-361/25, pages 57–58, Vienna. IAEA.

Beyerle, U., Purtschert, R., Aeschbach-Hertig, W., Imboden, D. M., Loosli, H. H., Wieler, R., and Kipfer, R. (1998). Climate and groundwater recharge during the last glaciation in an ice-covered region. *Science*, 282:731–734.

Beyerle, U., Rüedi, J., Leuenberger, M., Aeschbach-Hertig, W., Peeters, F., Kipfer, R., and Dodo, A. (2003). Evidence for periods of wetter and cooler climate in the Sahel between 6 and 40 kyr BP derived from groundwater. *Geophys. Res. Lett.*, 30(4):1173.

Brennwald, M. S., Imboden, D. M., and Kipfer, R. (2005). Release of gas bubbles from lake sediment traced by noble gas isotopes in the sediment pore water. *Earth Planet. Sci. Lett.*, 235(1-2):31–44.

Brusseau, M. L. (1992). Rate-limited mass transfer and transport of organic solutes in porous media that contain immobile immiscible organic liquid. *Water. Resour. Res.*, 28(1):33–45.

Cecil, L. D. and Green, J. R. (2000). Radon-222. In Cook, P. and Herczeg, A. L., editors, *Environmental tracers in subsurface hydrology*, pages 175–194. Kluwer Academic Publishers, Boston, Dordrecht.

Chowdhury, U. K., Biswas, B. K., Chowdhury, T. R., Samanta, G., Mandal, B. K., Basu, G. K., Chanda, C. R., Lodh, D., Saha, K. C., Mukherjee, S. K., Roy, S., Kabir, S., Quamruzzaman, Q., and Chakraborti, D. (2000). Groundwater arsenic contamination in Bangladesh and West Bengal, India. *Environ. Health Persp.*, 108:393–397.

Cirpka, O. A. and Kitanidis, P. K. (2001). Transport of volatile compounds in porous media in the presence of a trapped gas phase. *J. Contam. Hydrol.*, 49:263–285.

Clark, I. D., Douglas, M., Raven, K., and Bottomley, D. (2000). Recharge and preservation of Laurentide glacial melt water in the Canadian Shield. *Ground Water*, 38(5):735–742.

Clark, J. F., Davisson, M. L., Hudson, G. B., and Macfarlane, P. A. (1998). Noble gases, stable isotopes, and radiocarbon as tracers of flow in the Dakota aquifer, Colorado and Kansas. *J. Hydrol.*, 211(1-4):151–167.

Clark, J. F., Stute, M., Schlosser, P., Drenkard, S., and Bonani, G. (1997). A tracer study of the Floridan aquifer in southeastern Georgia: Implications for groundwater flow and paleoclimate. *Water Resour. Res.*, 33(2):281–289.

Clever, H. L., editor (1979). *Krypton, xenon and radon-gas solubilities*, volume 2 of *Solubility data series*. Pergamon Press, Oxford.

Colgan, P. M., Mickelson, D. M., and Cutler, P. M. (2003). Glacial landsystems of the southern Laurentide ice sheet. In Evans, D., editor, *Glacial landsystems*, pages 111–142. Arnold, London.

Cook, P. G. and Herczeg, A. L., editors (2000). *Environmental tracers in subsurface hydrology*. Kluwer Academic Publishers, Boston.

Craig, H. (1961). Isotopic variations in meteoric waters. *Science*, 133(3465):1702–1703.

Craig, H. and Lal, D. (1961). The production rate of natural tritium. *Tellus*, 13(1):85–105.

Dansgaard, W. (1964). Stable isotopes in precipitation. *Tellus*, 16(4):436–463.

Dowling, C. B., Poreda, R. J., and Basu, A. R. (2003). The groundwater geochemistry of the Bengal Basin: Weathering, chemsorption, and trace metal flux to the oceans. *Geochim. Cosmochim. Acta*, 67(12):2117–2136.

Dowling, C. B., Poreda, R. J., Basu, A. R., Peters, S. L., and Aggarwal, P. K. (2002). Geochemical study of arsenic release mechanisms in the Bengal Basin groundwater. *Water Resour. Res.*, 38(9):1173.

Einstein, A. (1905). Über die von der molekularkinetischen Theorie der Wärme geforderte Bewegung von in ruhenden Flüssigkeiten suspendierten Teilchen. *Annalen der Physik*, 17:549–560.

Epstein, P. S. and Plesset, M. S. (1950). On the stability of gas bubbles in liquid-gas solutions. *J. Chem. Phys.*, 18(11):1505–1509.

Feinstein, D. T., Eaton, T. T., Hart, D. J., Krohhelski, J. T., and Bradbury, K. R. (2005a). Regional aquifer model for southeastern Wisconsin. Report 1: Data collection, conceptual model development, numerical model construction, and model calibration. Technical Report 41, Southeastern Wisconsin Regional Planning Commission, USA.

Feinstein, D. T., Hart, D. J., Krohelski, J. T., Eaton, T. T., and Bradbury, K. R. (2005b). Simulation of regional groundwater flow in southeastern Wisconsin. Report 2: Model results and interpretation. Technical Report 41, Southeastern Wisconsin Regional Planning Commission, USA.

Fontes, J.-C. and Garnier, J.-M. (1979). Determination of the initial ^{14}C activity of the total dissolved carbon: A review of the existing models and a new approach. *Water Resour. Res.*, 15(2):399–413.

Freitag, G., Großmann, J., Hoffmann, M., Merkel, B., Prömper, R., Sperling, B., Udluft, P., and Ullsperger, I. (1987). Beschaffenheit und Abfluss von Sickerwässern aus einem städtischen Siedlungsgebiet. Technical report, TU München.

Grundl, T. and Cape, M. (2006). Geochemical factors controlling radium activity in a sandstone aquifer. *Ground Water*, 44(4):518–527.

Hall, C. M., Castro, M. C., Lohmann, K. C., and Ma, L. (2005). Noble gases and stable isotopes in a shallow aquifer in southern Michigan: Implications for noble gas paleotemperature reconstructions for cool climates. *Geophys. Res. Lett.*, 32:L18404.

Harvey, C. F., Ashfaque, K. N., Yu, W., Badruzzaman, A. B. M., Ali, M. A., Oates, P. M., Michael, H. A., Neumann, R. B., Beckie, R., Islam, S., and Ahmed, M. F. (2006). Groundwater dynamics and arsenic contamination in Bangladesh. *Chem. Geol.*, 228:112–136.

Harvey, C. F., Swartz, C. H., Badruzzaman, A. B. M., Keon-Blute, N., Yu, W., Ali, M. A., Jay, J., Beckie, R., Niedan, V., Brabander, D., Oates, P. M., Ashfaque, K. N., Islam, S., Hemond, H. F., and Ahmed, M. F. (2002). Arsenic mobility and groundwater extraction in Bangladesh. *Science*, 298:1602–1606.

Harvey, C. F., Swartz, C. H., Badruzzaman, A. B. M., Keon-Blute, N., Yu, W., Ali, M. A., Jay, J., Beckie, R., Niedan, V., Brabander, D., Oates, P. M., Ashfaque, K. N., Islam, S., Hemond, H. F., and Ahmed, M. F. (2003). Response to comments on "Arsenic mobility and groundwater extraction in Bangladesh". *Science*, 300:584d.

Harvey, C. F., Swartz, C. H., Badruzzaman, A. B. M., Keon-Blute, N., Yu, W., Ali, M. A., Jay, J., Beckie, R., Niedan, V., Brabander, D., Oates, P. M., Ashfaque, K. N., Islam, S., Hemond, H. F., and Ahmed, M. F. (2005). Groundwater arsenic contamination on the Ganges Delta: biogeochemistry, hydrology, human pertubations, and human suffering on a large scale. *C. R. Geoscience*, 337:285–296.

Heaton, T. H. E. and Vogel, J. C. (1981). "Excess air" in groundwater. *J. Hydrol.*, 50:201–216.

Hillel, D. (2003). *Introduction to Environmental Soil Physics*. Elsevier, Amsterdam.

Holocher, J. (2002). *Investigations of gas exchange in quasi-saturated porous media using noble gases as conservative tracers*. Diss. ETH No. 14588, ETH Zürich.

Holocher, J., Peeters, F., Aeschbach-Hertig, W., Hofer, M., Brennwald, M., Kinzelbach, W., and Kipfer, R. (2002). Experimental investigations on the formation of excess air in quasi-saturated porous media. *Geochim. Cosmochim. Acta*, 66(23):4103–4117.

Holocher, J., Peeters, F., Aeschbach-Hertig, W., Kinzelbach, W., and Kipfer, R. (2003). Kinetic model of gas bubble dissolution in groundwater and its implications for the dissolved gas composition. *Environ. Sci. Technol.*, 37(7):1337–1343.

Holzner, C. P., Amaral, H., Brennwald, M. S., Klump, S., and Kipfer, R. (2004). Assessment of methane emission from bubble plumes in the Black Sea by noble gases. *Geochim. Cosmochim. Acta*, 11S:A323.

Imboden, D. M. (1977). Natural radon as a limnological tracer for the study of vertical and horizontal eddy diffusion. In IAEA, editor, *Isotopes in lake studies*, pages 213–218, Vienna. IAEA.

Imboden, D. M. and Emerson, S. (1978). Natural radon and phosphorus as limnologic tracers: Horizontal and vertical eddy diffusion in Greifensee. *Limnol. Oceanogr.*, 23(1):77–90.

Imboden, D. M. and Joller, T. (1984). Turbulent mixing in the hypolimnion of Baldeggersee (Switzerland) traced by natural radon-222. *Limnol. Oceanogr.*, 29(4):831–844.

Jähne, B., Heinz, G., and Dietrich, W. (1987). Measurement of the diffusion coefficients of sparingly soluble gases in water. *J. Geophys. Res.*, 92(C10):10767–10776.

Karim, M. M. (2000). Arsenic in groundwater and health problems in Bangladesh. *Water Res.*, 34:304–310.

Kienzler, P. and Naef, F. (2007). Subsurface storm flow formation at different hillslopes and implications for the "old water paradox". *Hydrol. Process.*, in press.

Kinniburgh, D. G. and Smedley, P. L. (2001). *Arsenic contamination of groundwater in Bangladesh.* British Geological Survey Technical Report WC/00/19. British Geological Survey, Keyworth.

Kipfer, R., Aeschbach-Hertig, W., Peeters, F., and Stute, M. (2002). Noble gases in lakes and ground waters. In Porcelli, D., Ballentine, C., and Wieler, R., editors, *Noble gases in geochemistry and cosmochemistry*, volume 47 of *Rev. Mineral. Geochem.*, pages 615–700. Mineralogical Society of America, Geochemical Society.

Klump, S., Brennwald, M. S., and Kipfer, R. (2006a). Comment on "Noble gases and stable isotopes in a shallow aquifer in southern Michigan: Implications for noble gas paleotemperature reconstructions for cool climates" by Chris M. Hall et al. *Geophys. Res. Lett.*, 33:L24403.

Klump, S., Kipfer, R., Cirpka, O. A., Harvey, C. F., Brennwald, M. S., Ashfaque, K. N., Badruzzaman, A. B. M., Hug, S. J., and Imboden, D. M. (2006b). Groundwater dynamics and arsenic mobilization in Bangladesh assessed using noble gases and tritium. *Environ. Sci. Technol.*, 40(1):243–250.

Klump, S., Tomonaga, Y., Kienzler, P., Kinzelbach, W. Baumann, T., Imboden, D. M., and Kipfer, R. (2007). Field experiments yield new insights into gas exchange and excess air formation in natural porous media. *Geochim. Cosmochim. Acta*, 71(6):1385–1397.

Kreft, A. and Zuber, A. (1978). On the physical meaning of the dispersion equation and its solutions for different initial and boundary conditions. *Chem. Engng. Sci.*, 33:1471–1480.

Kühnhardt, M. (1994). *Untersuchungen zur Dispersion von polyzyklischen aromatischen Kohlenwasserstoffen (PAHs) in der ungesättigten Zone eines fluvioglazialen Schotters.* PhD thesis, TU München.

Kulongoski, J. T., Hilton, D. R., and Selaolo, E. T. (2004). Climate variability in the Botswana Kalahari from late Pleistocene to the present day. *Geophys. Res. Lett.*, 31:L10204.

Lagarias, J. C., Reeds, J. A., Wright, M. H., and Wright, P. (1998). Convergence properties of the Nelder-Mead Simplex Method in low dimensions. *SIAM J. Optim.*, 9(1):112–147.

Lucas, L. L. and Unterweger, M. P. (2000). Comprehensive review and critical evaluation of the half-life of tritium. *J. Res. Natl. Inst. Stand. Technol.*, 105(4):541–549.

Ma, L., Castro, M. C., and Hall, C. M. (2004). A late Pleistocene-Holocene noble gas paleotemperature record in southern Michigan. *Geophys. Res. Lett.*, 31(23):L23204.

Mamyrin, B. A. and Tolstikhin, I. N. (1984). *Helium isotopes in nature*, volume 3 of *Developments in Geochemistry*. Elsevier, Amsterdam, Oxford, New York, Tokyo.

Manning, A. H., Solomon, D. K., and Sheldon, A. L. (2003). Applications of a total dissolved gas pressure probe in ground water studies. *Ground Water*, 41(4):440–448.

Mazor, E. (1972). Paleotemperatures and other hydrological parameters deduced from gases dissolved in groundwaters, Jordan Rift Valley, Israel. *Geochim. Cosmochim. Acta*, 36(12):1321–1336.

McArthur, J. M., Banerjee, D. M., Hudson-Edwards, K. A., Mishra, R., Purohit, R., Ravenscroft, P., Cronin, A., Howarth, R. J., Chatterjee, A., Talukder, T., Lowry, D., Houghton, S., and Chadha, D. K. (2004). Natural organic matter in sedimentary basins and its relation to arsenic in anoxic ground water: the example of West Bengal and its worldwide implications. *Appl. Geochem.*, 19:1255–1293.

McArthur, J. M., Ravenscroft, P., Safiulla, S., and Thirlwall, M. F. (2001). Arsenic in groundwater: Testing pollution mechanisms for sedimentary aquifers in Bangladesh. *Water Resour. Res.*, 37(1):109–117.

Mercury, L., Pinti, D. L., and Zeyen, H. (2004). The effect of the negative pressure of capillary water on atmospheric noble gas solubility in ground water and palaeotemperature reconstruction. *Earth Planet. Sci. Lett.*, 223:147–161.

Merkel, B., Nemeth, G., Udluft, P., and Grimmeisen, W. (1982). Hydrogeologische und hydrochemische Untersuchungen in der ungesättigten Zone eines Kiesgrundwasserleiters. Teil 1: Entwicklung und Erstellung eines begehbaren Probenahmeschachtes zur Boden-, Wasser- und Luftuntersuchung. *Z. Wasser-Abwasser-Forsch.*, 15:191–195.

Merkel, T. C., Bondar, V. I., Nagai, K., Freeman, B. D., and Pinnau, I. (2000). Gas sorption, diffusion, and permeation in poly(dimethylsiloxane). *J. Ploym. Sci. Part B: Polym. Phys.*, 38:415–434.

Mickelson, D. M. and Colgan, P. M. (2004). The southern Laurentide ice sheet. *Devel. Quat. Sci.*, 1:1–16.

Millington, R. J. (1959). Gas diffusion in porous media. *Science*, 130:100–102.

Nagao, K., Takaoka, N., and Matsabayashi, O. (1979). Isotopic anomalies of rare gases in the Nigorikawa geothermal area, Hokkaido, Japan. *Earth Planet. Sci. Lett.*, 44(1):82–90.

Nickson, R., McArthur, J. M., Burgess, W., Ahmed, K. M., Ravenscroft, P., and Rahman, M. (1998). Arsenic poisoning of Bangladesh groundwater. *Nature*, 395:338.

Oana, S. (1957). Bestimmung von Argon in besonderem Hinblick auf gelöste Gase in natürlichen Gewässern. *J. Earth Sci. Nagoya Univ.*, 5:103–124.

Oberrauch, F. (2003). Experimentelle Quantifizierung von Pre-Event Water. Diploma thesis, Universität für Bodenkultur, Vienna.

Ozima, M. and Podosek, F. A. (1983). *Noble gas geochemistry*. Cambridge University Press, Cambridge, London, New York.

Pearson, F. J. and White, D. E. (1967). Carbon-14 ages and flow rates of water in Carrizo Sand, Atascosa County, Texas. *Water. Resour. Res.*, 3(1):251–261.

Perry, E. C., Grundl, T. J., and Gilkeson, R. H. (1982). H, O, S isotopic study of the groundwater in the Cambro-Ordovician aquifer system of northern Illinois. In Perry, E. C. and Montgomery, C., editors, *Isotopic studies of hydrologic processes*, pages 35–44. NIU Press, DeKalb, Illinois.

Plummer, L. N. (1993). Stable isotope enrichment in paleowaters of the southeast Atlantic Coastal Plain, United States. *Science*, 262:2016–2020.

Pollock, D. W. (1988). Semianalytical computation of path lines for finite-difference models. *Ground Water*, 26(6):743–750.

Purtschert, R., van Breukelen, B. M., Suckow, A., and Hofer, M. (2004). Estimation of groundwater flow velocities in a landfill leachate plume using ^{85}Kr measurements. *Geochim. Cosmochim. Acta*, 11S:A494.

Rudolph, J., Rath, H. K., and Sonntag, C. (1984). Noble gases and stable isotopes in ^{14}C-dated palaeowaters from central Europe and the Sahara. In IAEA, editor, *Isotope Hydrology 1983*, volume IAEA-SM-270/17, pages 467–477, Vienna. IAEA.

Schlosser, P., Stute, M., Dörr, C., Sonntag, C., and Münnich, K. O. (1988). Tritium/^{3}He-dating of shallow groundwater. *Earth Planet. Sci. Lett.*, 89(3-4):353–362.

Schlosser, P., Stute, M., Sonntag, C., and Münnich, K. O. (1989). Tritiogenic ^{3}He in shallow groundwater. *Earth Planet. Sci. Lett.*, 94(3-4):245–256.

Schwarzenbach, R. P., Gschwend, P. M., and Imboden, D. M. (2003). *Environmental Organic Chemistry*. John Wiley and Sons, New York.

Shampine, L. F. and Reichelt, M. W. (1997). The MATLAB ODE Suite. *SIAM J. Sci. Comput.*, 18:1–22.

Siegel, D. I. (1990). Sulfur isotope evidence for regional recharge of saline water during continental glaciation, north-central United States. *Geology*, 18:1054–1056.

Solomon, D. K. and Sudicky, E. A. (1991). Tritium and helium 3 isotope ratios for direct estimation of spatial variations in groundwater recharge. *Water Resour. Res.*, 27(9):2309–2319.

Stüben, K. A. (2001). A review of algebraic multigrid. *J. Comput. Appl. Math.*, 128(1-2):281–309.

Stute, M. (2001). Tritium (^{3}H) in precipitation in Bangladesh. In Jacks, G., Bhattacharya, P., and Khan, A. A., editors, *Groundwater arsenic contamination in the Bengal Delta Plain of Bangladesh*, KTH-Dhaka University Seminar, pages 109–117, Dhaka. Royal Institute of Technology, Stockholm.

Stute, M., Clark, J., Schlosser, P., and Broecker, W. (1995a). A 30,000 yr continental paleotemperature record derived from noble gases dissolved in groundwater from the San Juan Basin, New Mexico. *Quatern. Res.*, 43:209–220.

Stute, M. and Deak, J. (1989). Environmental isotope study (^{14}C, ^{13}C, ^{18}O, D, noble gases) on deep groundwater circulation systems in Hungary with reference to paleoclimate. *Radiocarbon*, 31(3):902–918.

Stute, M., Forster, M., Frischkorn, H., Serejo, A., Clark, J. F., Schlosser, P., Broecker, W. S., and Bonani, G. (1995b). Cooling of tropical Brazil (5 °C) during the Last Glacial Maximum. *Science*, 269:379–383.

Stute, M. and Schlosser, P. (1993). Principles and applications of the noble gas paleothermometer. In Swart, P. K., Lohmann, K. C., McKenzie, J., and Savin, S., editors, *Climate Change in Continental Isotopic Records*, volume 78 of *AGU Geophysical Monograph Series*, pages 89–100. American Geophysical Union, Washington, DC.

Stute, M., Schlosser, P., Clark, J. F., and Broecker, W. S. (1992). Paleotemperatures in the Southwestern United States derived from noble gases in ground water. *Science*, 256:1000–1003.

Stute, M. and Sonntag, C. (1992). Paleotemperatures derived from noble gases dissolved in groundwater and in relation to soil temperature. In *Isotopes of noble gases as tracers in environmental studies*, pages 111–122, Vienna. IAEA.

Stute, M. and Talma, A. S. (1998). Glacial temperatures and moisture transport regimes reconstructed from noble gases and δ^{18}O, Stampriet Aquifer, Namibia. In *Isotope techniques in the study of environmental change*, pages 307–318, Vienna. IAEA.

Swartz, C. H., Keon-Blute, N., Badruzzaman, A. B. M., Ali, A., Brabander, D., Jay, J., Besancon, J., Islam, S., Hemond, H. F., and Harvey, C. F. (2004). Mobility of arsenic in a Bangladesh aquifer: Inferences from geochemical profiles, leaching data, and mineralogical characterization. *Geochim. Cosmochim. Acta*, 68(22):4539–4557.

Tamers, M. A. (1967). Radiocarbon ages of groundwater in an arid zone unconfined aquifer. In *Isotope Techniques in the Hydrological Cycle*, AGU Monograph 11, pages 143–152.

Thomas, J. M., Hudson, G. B., Stute, M., and Clark, J. F. (2003). Noble gas loss may indicate groundwater flow across flow barriers in southern Nevada. *Environ. Geol.*, 43(5):568–579.

Torgersen, T., Clarke, W. B., and Jenkins, W. J. (1979). The tritium/helium-3 method in hydrology. In IAEA, editor, *Isotope Hydrology 1978*, pages 917–930, Vienna. IAEA.

Torgersen, T., Top, Z., Clarke, W. B., Jenkins, W. J., and Broecker, W. (1977). A new method for physical limnology–tritium-helium-3 ages – results for Lakes Erie, Huron and Ontario. *Limnol. Oceanogr.*, 22(2):181–193.

Vaikmäe, R., Vallner, L., Loosli, H. H., Blaser, P. C., and Juillard, M. (2001). Palaeogroundwater of glacial origin in the Cambrian-Vendian aquifer of northern Estonia. In Edmunds, W. M. and Milne, C. J., editors, *Palaeowaters in Coastal Europe: evolution of groundwater since the late Pleistocene*, volume 189 of *Geol. Soc. Special Publication*, pages 17–22. Geological Society of London, London.

van Geen, A., Zheng, Y., Stute, M., and Ahmed, K. M. (2003). Comment on "Arsenic mobility and groundwater extraction in Bangladesh" (II). *Science*, 300:584d.

Weaver, T. R. and Bahr, J. M. (1991a). Geochemical evolution in the Cambrian-Ordovician sandstone aquifer, eastern Wisconsin: 1. major ion and radionuclide distribution. *Ground Water*, 29(3):350–356.

Weaver, T. R. and Bahr, J. M. (1991b). Geochemical evolution in the Cambrian-Ordovician sandstone aquifer, eastern Wisconsin: 2. correlation between flow paths and ground water chemistry. *Ground Water*, 29(4):510–515.

Weiss, R. F. (1970). The solubility of nitrogen, oxygen and argon in water and seawater. *Deep-Sea Res.*, 17(4):721–735.

Weiss, R. F. (1971). Solubility of helium and neon in water and seawater. *J. Chem. Eng. Data*, 16(2):235–241.

Weiss, R. F. and Kyser, T. K. (1978). Solubility of krypton in water and seawater. *J. Chem. Eng. Data*, 23(1):69–72.

Wilson, G. B. and McNeill, G. W. (1997). Noble gas recharge temperatures and the excess air component. *Appl. Geochem.*, 12(6):747–762.

Young, H. L. (1992). Summary of groundwater hydrology of the Cambro-Ordovician aquifer system in the northern Midwest, United States. *United States Geological Survey Professional Paper*, 1405-A:55 pp.

Yu, W., Harvey, C., and Harvey, C. F. (2003). Arsenic in groundwater in Bangladesh: A geostatistical and epidemiological framework for evaluating health effects and potential remedies. *Water Resour. Res.*, 39(6):1146.

Zheng, Y., Stute, M., van Geen, A., Gavrieli, I., Dhar, R., Simpson, H. J., Schlosser, P., and Ahmed, K. M. (2004). Redox control of arsenic mobilization in Bangladesh groundwater. *Appl. Geochem.*, 19:210–214.

Curriculum Vitae

Stephan Rüdiger Klump

March 17, 1977	Born in Limburg/Lahn, Germany
1983–1985	Primary school in Limburg, Germany
1985–1987	Primary school in Hadamar, Germany
1987–1996	High school in Hadamar, Germany School-leaving exam (Abitur)
1996–1997	Civil service
1997–2003	Studies in geology Clausthal University of Technology, Germany
2003	Diploma in geology (Dipl.-Geol.) Clausthal University of Technology, Germany
2003–2007	PhD student and research assistant in the Department of Environmental Sciences of the Swiss Federal Institute of Technology Zurich (ETH), Zürich and in the Department of Water Resources and Drinking Water of the Swiss Federal Institute of Aquatic Science and Technology (Eawag), Dübendorf.